Fuzzy Logic Based Online Adaptation of Current and Speed Controllers for Improved Performance of IPMSM Drive

by

Ronald Shourav Rebeiro

A thesis submitted in partial fulfilment of the requirement for Masters of Science in

Control Engineering

at

Lakehead University

Thunder Bay, Ontario

September 2010

Abstract

Precise torque and speed control of electric motors is a key issue in industries for variable speed drives (VSD). Over the years the induction motors have been widely utilized in industries for VSD applications. However, induction motor has some significant drawbacks like low efficiency, lagging power factor, asynchronous speed, low torque density etc. Nowadays the interior permanent magnet synchronous motor (IPMSM) is becoming popular for high performance variable speed drive (HPVSD) due to its high torque-current ratio, large power-weight ratio, high efficiency, high power factor, low noise and robustness as compared to conventional induction and other ac motors. Smooth torque response, fast and precise speed response, quick recovery of torque and speed from any disturbance and parameter insensitivity, robustness in variable speed domain and maintenance free operations are the main concerns for HPVSD.

This work proposes a closed loop vector control of an IPMSM drive incorporating two separate fuzzy logic controllers (FLCs). Among them one FLC is designed to minimize the developed torque ripple by varying online the hysteresis band of the PWM current controller. Another Sugeno type FLC is used to tune the gains of a proportional-integral (PI) controller where the PI controller actually serves as the primary speed controller. Thus, the limitations of traditional PI controllers will be avoided and the performance of the drive system can be improved. A flux controller is also incorporated in such a way that both torque and flux of the motor can be controlled while maintaining current and voltage constraints. The flux controller is designed based on maximum-torque-per-ampere (MTPA) operation below the rated speed and flux weakening

operation above the rated speed. Thus, the proposed drive extends the operating speed limits for the motor and enables the effective use of the reluctance torque.

In order to verify the performance of the proposed IPMSM drive, first a simulation model is developed using Matlab/Simulink. Then the complete IPMSM drive has been implemented in real-time using digital signal processor (DSP) controller board DS1104 for a laboratory 5 HP motor. The effectiveness of the proposed drive is verified both in simulation and experiment at different operating conditions. In this regard, a performance comparison of the proposed FLC based tuned PI and adapted hysteresis controllers based drive with the conventional PI and fixed bandwidth hysteresis controllers based drive is provided. These comparison results demonstrate the better dynamic response in torque and speed for the proposed IPMSM drive over a wide speed range.

Acknowledgement

I would like to take this opportunity to acknowledge and thank those persons who have helped me in different ways during my research preparation and academic course-work in Lakehead University. Firstly I would like to express my utmost gratitude and appreciation to my thesis supervisor Dr. M. N. Uddin, without whose proper guidance and supervision this work might not be accomplished at all. Also his immense encouragement and motivation was vital throughout this program. I am also thankful to Dr. A. Tayebi for his valuable suggestions in my graduate seminar which encouraged me to improve the work afterwards. I specially thank Mr. B. Misner and Mr. W. Paju for providing me important technical assistance a few times. At this moment, I also recall my teachers in my undergraduate university BUET, who mentored me in my early years and inspired me to greater achievements. Particularly I would like to mention Dr. Md. Ali who greatly motivated me to higher studies.

I would like to acknowledge the assistance from my fellow graduate students and people from Thunder Bay who gave me moral support. I specially thank my labmate Mr. Md. Hafeez with whom I shared many healthy and motivational discussions.

Finally I express my utmost gratitude to my parents, Mr. Denis Rebeiro and Mrs. Elizabeth Rebeiro, and my siblings with their spouses who are always the prime source of motivation in my life. I also acknowledge the encouragement and moral support from my friends and relatives.

Contents

List of Symbols

i_a, i_b, i_c	actual a-b-c phase currents
v_a, v_b, v_c	actual a-b-c phase voltages
$v_{d,}$ v_d^r	d-axis voltage
$v_{q,}$ v_q^r	q-axis voltage
$i_{d,}$ i_d^r	d-axis current
$i_{q,}$ i_q^r	q-axis current
i_d*	command d-axis current
i_q*	command q-axis current
V_a	maximum phase voltage amplitude
I_a	maximum line current amplitude
r_s	per phase stator resistance
L_d	d-axis inductance
L_q	q-axis inductance
L_l	leakage inductance
L_{md}	d-axis magnetizing inductance
L_{mq}	q-axis magnetizing inductance
ω_s	stator angular frequency
ω_r	actual motor speed
ω_r*	command motor speed
Θ_r	rotor position
P	number of pole pairs

P_{phase}	motor developed power per phase
P_d	total developed motor power
T_e	developed electromagnetic torque
T_L	load torque
J	rotor inertia constant
B_m	friction damping coefficient
ψ_m	magnetic flux linkage
V_B	DC bus voltage for the inverter
e	error between actual and command speed
Δe	change of speed error
d_{iq}	error between actual and command q-axis current
H_u	fixed upper hysteresis band limit
H_l	fixed lower hysteresis band limit
Δh	incremental hysteresis band limit
K_p	proportional gain of PI controller
K_i	integral gain of PI controller
a	proportional gain multiplying factor
b	integral gain multiplying factor

List of Acronyms

ANN	Artificial neural network
BLDC	Brushless DC
DSP	Digital signal processor
DTC	Direct torque control
FBFN	Fuzzy basis function network
FLC	Fuzzy logic controller
FW	Flux weakening
GA	Genetic algorithm
GTO	Gate Turn-Off Thyristor
HB	Hysteresis band
HPVSD	High performance variable speed drive
HVDC	High voltage direct current
IGBT	Insulated-gate bipolar transistor
IM	Induction motor
IPMSM	Interior Permanent Magnet Synchronous Motor
MRAC	Model Reference Adaptive Controller
MTPA	Maximum torque per ampere
NFC	Neuro-fuzzy controller
PI	Proportional Integral
PID	Proportional Integral Derivative
PM	Permanent Magnet

PMSM	Permanent Magnet Synchronous Motor
PWM	Pulse Width Modulation
RBFN	Radial basis function network
SM	Synchronous motor
SMC	Sliding Mode Control
SPMSM	Surface mounted Permanent Magnet Synchronous Motor
SPST	Single pole single throw
SRM	Switched Reluctance Motor
VSD	Variable Speed Drive
VSI	Voltage Source Inverter

Chapter 1

Introduction

1.1 Electric Motors

The invention and consequent improvements of different electric motors is one of the most significant success points of modern science history. Apparently the modern civilization would not have flourished in the 20th century in the same conquering way as we observe today but for the growth and use of electric motors in every aspect of science and technology. Most common people might say that they do not see an electric motor everyday like they do a light bulb or telephone just because of the fact that electric motors are seamlessly integrated in many household appliances, as well as industries, such that they are sometimes difficult to recognize. Very common examples of household appliances incorporating electric motors are microwave oven, washing machine, dryer, refrigerator, air conditioner etc. Electric motors act as the workhorses for almost every industry like paper mills, cement factories, petroleum industry, plastic industry, automotive industry, mining and drilling companies, robotics, automation etc. Basically an electric motor uses electrical energy to produce mechanical energy, typically through the interaction of magnetic fields and current-carrying conductors as explained by Lorentz force law. They may be powered up by direct current or alternating current depending on their structure and today they consume more than half of all electrical energy produced.

1.1.1 Brief History

Michael Faraday demonstrated the conversion of electrical energy into mechanical energy by electromagnetic means for the first time in 1821. In his experiment, he showed that a free-hanging wire, dipped into a pool of mercury, rotated around a permanent magnet when a current was passed through the wire [1]. In 1828 Hungarian inventor Anyos Jedlik demonstrated the first electromagnetic rotating device which contained the three main components of practical direct current motors: stator, rotor and commutator. There were some other refinements too around that time but they were demonstration devices only and unsuitable for practical applications due to their primitive construction.

The first commutator-type DC motor capable of taking significant loads was invented by British scientist William Sturgeon in 1832 which was then followed by DC motor built and patented by American inventor couple Emily and Thomas Davenport in 1837 [1]. But these motors had the critical drawback of high cost of zinc electrodes required in the primary battery, and therefore they were commercially unsuccessful.

The modern DC motor was invented by accident in 1873 when Belgian electrical engineer Zenobe Gramme connected his invented dynamo to another similar unit, driving it as a motor. The Gramme machine was also the first industrially successful electric motor. In 1886 “Father of Electric Traction” Frank J. Sprague invented the first practical non-sparking DC motor suitable for variable speed and load conditions, which he subsequently used to develop the first electric trolley and electric elevator systems. The first practicable AC motor (initial brushless induction motor) was invented by Nikola Tesla in 1887, and he continued his works on it in the following years in George

Westinghouse's company [2]. This invention of induction motor is a breakthrough in electric motor history as AC motors are more robust, efficient and effective than previously introduced DC motors. Introduction of Tesla's motor from 1887 onwards also initiated what is sometimes referred to as the "Second Industrial Revolution", making possible both the efficient generation and long distance distribution of electrical energy using Tesla's another invention, the polyphase alternating current transmission system [2].

1.2 Classification of Electric Motor

Electric motors are mainly classified as DC and AC types. The detailed classification is shown in Fig. 1.1. The relevant and significant types will be discussed in the following sub-sections.

1.2.1 DC Motor

A brushed DC motor uses internal commutation to create an oscillating AC current from DC source. The stator or field is either a wound or permanent magnet type. The rotor or armature consists of one or more coils of wire wound around a shaft and the DC source is connected to the rotor coil through the commutator and the brushes, causing the current to flow in the armature and thereby producing electromagnetism effect. The commutator actually causes the current direction in the coils to be reversed as the rotor turns in order to keep the magnetic poles of the rotor from ever fully aligning with the magnetic poles of the stator, such that the rotor keeps rotating indefinitely as long as electric power is applied and is sufficient enough to sustain load torque, friction and other

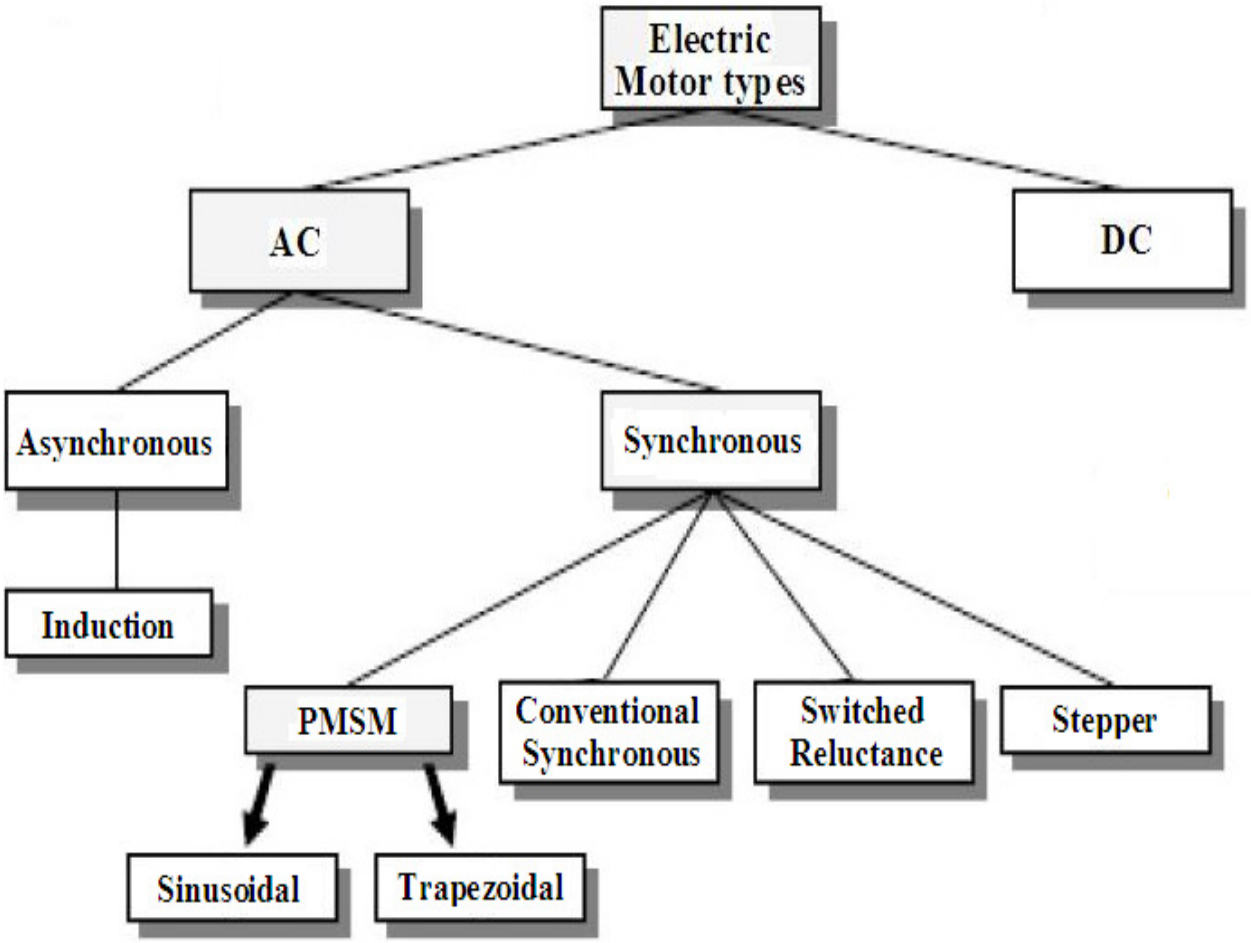

Figure 1.1: General classification of electric motors.

losses. Separately excited DC motor has the advantage of easy control method but has high initial cost and high maintenance (commutator) cost [3, 4].

1.2.2 Induction Motor

An induction motor is an asynchronous AC motor where power is supplied directly to the stator and then the power is transferred to the rotating part by means of electromagnetic induction. The rotor can be a wound one or squirrel-cage type where conductive bars are set into grooves and connected together at both ends by shorting rings

forming a cage-like shape. From the analogy of their working principles, an induction can be also referred as a rotating transformer because the stator is essentially the primary side of the transformer and the rotor is the moving secondary side. Induction motors are robust, durable and least expensive, and that's why they are widely used in industrial drives [3-5].

1.2.3 Synchronous Motor

A conventional synchronous motor works with similar induction principle except that the rotor is excited by an external DC field so as to ensure that it has zero slip under normal operating conditions. Slip rings and brushes are required to conduct current to the rotor. Once the rotor starts running at near synchronous speed then the rotor field is excited externally, and thereby allowing the rotor poles to be aligned with the magnetic stator poles and move at the same speed with rotating magnetic field. Hence the name is synchronous motor [3-5].

1.2.4 Permanent Magnet Synchronous Motor

A permanent magnet synchronous motor (PMSM) is a variation of synchronous motor where the field excitation is provided by permanent magnets contained in the rotor. Thus, in contrast with conventional synchronous motor, external power supply with field winding, slip ring and brushes are not required. This also eliminates the power loss due to excitation winding. Recent improvement and popularity of PMSMs is directly related to the success achieved in high-energy permanent magnet materials. Rare earth magnetic materials and their alloys such as neodymium-boron-iron (Nd-B-Fe), samarium-cobalt

(Sm-Co), aluminium-nickel-cobalt (Al-Ni-Co) etc. have a high residual and coercive force than the ferrite materials. But they are also very expensive and so they are usually used for high performance variable speed drives (HPVSD) where high torque to inertia ratio is a demanding feature [6-8].

Based on the permanent magnets' positions within the rotor, PMSM can be of several types which are discussed below [7, 8].

(a) Surface mounted type (SPMSM):

In this type, the permanent magnets are mounted on the surface of the rotor and are typically glued to the rotor with a non-conducting material. It is a non-salient type motor ($L_q = L_d$), and therefore it can only utilize the developed torque and not the reluctance torque. It has a large air gap which weakens the armature reaction effect. So its operation is restricted to low speed and constant torque region. Its cross-sectional view is shown in Fig. 1.2(a).

(b) Inset type PMSM:

In this type, the permanent magnets are fully or partially inset into the rotor core and are typically glued directly or banded with a non-conducting material inside the rotor. Its cross-sectional view is shown in Fig. 1.2(b). It has smaller and relatively smoother air gap than SPMSM. This type is also not suitable for high speed applications.

(c) Interior type permanent magnet synchronous motor (IPMSM):

As shown in Fig. 1.2(c), the permanent magnets are embedded in the interior of rotor core of IPMSM. This is the most recent method of attaching the permanent magnet and this structure type overcomes the inherent drawbacks of the other two types because of its narrower and smoother air gap. This is a salient type motor ($L_q > L_d$), which gives

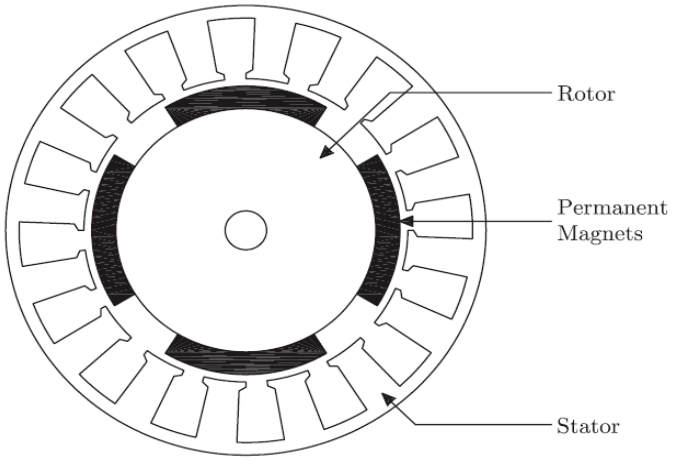

(a)

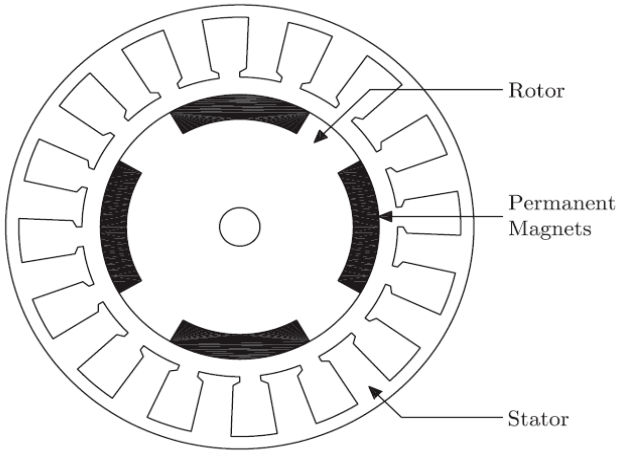

(b)

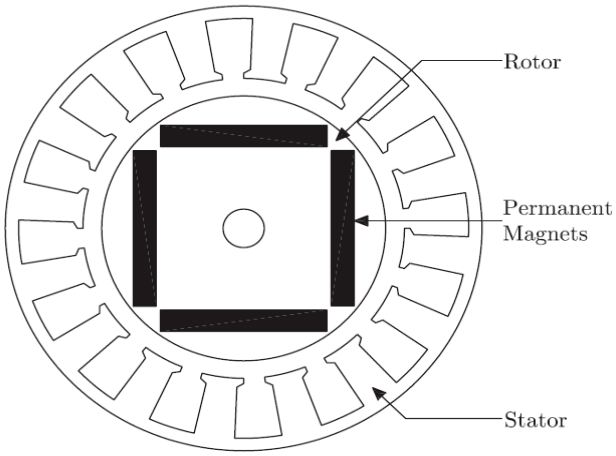

(c)

Figure 1.2: Cross-sectional views of different type of permanent magnet synchronous motors, (a) Surface mounted type (SPMSM), (b) Inset type, (c) Interior type (IPMSM).

provision of many advantageous features. This motor type is chosen as the working model of this research work and this choice is discussed and justified in the next section.

1.3 Choice of Motor

Among the commercially used electric motors, DC motor, particularly separately excited DC motor, requires the simplest control strategy because of the decoupled nature of its field and armature quantities. So the flux and torque of the DC motor can be controlled separately and hence the control task is very easy. That's why it was widely used in variable speed drive (VSD) applications for a long time. But DC motor has critical disadvantages such as low torque density, low power-weight ratio, limited speed range of operation, power loss in field circuit, lack of robustness, frequent maintenance requirement, high cost due to brushes and commutators. On the contrary, fast and precise speed response, quick recovery of speed from any disturbances and parameter insensitivity, robustness in variable speed domain and maintenance free operations are the main concerns for HPVSD applications. So, induction motors and synchronous motors were introduced by researchers in HPVSD applications in order to overcome the aforementioned drawbacks of DC motor. Induction motor (IM) is very popular and widely used in various industry applications because of certain advantages over DC motor like low cost, robustness in structure and power supply connection, low maintenance requirement etc. But IM has some inherent limitations that researchers cannot ignore when performance rather than cost is the top priority. IM always has to operate at a lagging power factor as the rotor current is induced from the stator side. Besides it always runs at lower than synchronous speed and that is why rotor quantities'

calculations depend on slip speed. Moreover, real-time implementation of IM drive requires sophisticated modeling and estimation of machine parameters.

The disadvantages of DC motor and IM encouraged further extensive research on synchronous motor (SM) in HPVSD applications. An SM's control algorithm is less complex because it rotates at synchronous speed and thereby eliminates slip power loss. But again conventional SM has some disadvantages like additional external DC power supply requirement, presence of slip rings and brushes at the rotor side. PMSMs provide a very good solution in this case by eliminating extra power supply, slip rings, brushes and power loss due to excitation. It is already proved that PMSM provides more torque density and operates at higher efficiency than IM, and the inverter size is also greatly reduced within speed range below and above rated speed [9].

The IPMSM is lighter and more robust than the other PMSM types because of its compact rotor structure. There is no copper wear on the rotor and so it does not have the problem of excessive shaft heating. Because of its smooth rotor surface and narrower air gap, the noise level of IPMSM is much lower than that of IM and other PMSMs. IPMSM is a salient type motor which means its q-axis inductance (L_q) is larger than the d-axis inductance (L_d). This saliency gives the provision of utilizing reluctance torque, and applying flux weakening operation and thereby enabling the motor operation above rated speed in constant power region. By applying closed loop vector control for IPMSM drive and using Park's transformation method [10], it is possible to decouple the flux and torque controlling components of IPMSM quantities. Thus the motor behaves like a separately excited DC motor while maintaining general advantages of AC motor over DC motor. The detail of the vector control method is discussed in chapter 2.

In summary, IPMSM, which has been selected as the working model of this research work, is better suited to HPVSD applications in a wide speed range than its counterparts, and thereby proving its selection as a wise option as per knowledge and concern of the author.

1.4 Literature Review

Dynamics and control of ac motor drives are complicated and their complexity increases with high quality performance requirements in variable speed and load conditions. So researchers were encouraged to implement their HPVSD using advanced power electronics technology. The demand for control of electric power for electric motor drive systems and industrial controls existed for many years, and evolutionary advancements have been achieved in power semiconductor and microprocessor technologies on the design of electric motor drives over the last few decades. Scalar control like open loop volts/Hz control has been used popularly in low performance drives because of its simplicity but it is not a good choice for high performance drives because of its poor transient response, limitation in torque control and sensitivity to disturbances. So closed loop vector control is chosen in this work which is the sophisticated method for HPVSD.

The controllers used in motor drives research works can be broadly categorized into three types such as: (a) fixed gain types, (b) adaptive types, (c) artificial intelligent types. Over the years, many research works have been reported incorporating these controllers in motor area and other research areas. Relevant research works have been briefly discussed below in subsections 1.4.1, 1.4.2 and 1.4.3. Combination of these

controllers in hybrid or tuned approach is discussed in subsection 1.4.4. Another important aspect of this research work is the hysteresis band adaptation of PWM current controllers which is also employed in some research areas other than motor drives. These research works are also discussed in subsection 1.4.5.

1.4.1 Fixed Gain Controllers

Microprocessor based control and implementation of inverter fed PMSM drives are presented by T. H. Liu et al. [12], and B.K. Bose, P.M. Szczesny [13]. In [12], a method was proposed to improve the hysteresis current controller performance at low speed by utilizing freewheeling period. But overall performance is degraded as the average torque is reduced in this work. In [13], the operational region is divided into a constant-torque region and a high-speed field-weakening constant-power region. For controlling purpose in constant-torque region, the vector or field-oriented control technique is used with the direct axis aligned to the stator flux. PI controller is used to generate command d-q axes currents to control the speed of the motor. But this controller is sensitive to parameter variations and load disturbance and also the microcontroller based computer aided control system used here is relatively costly for simple PI controller implementation. Besides, it cannot deliver good performance in a wide range of speed. The same author [14] implemented a high performance inverter fed IPMSM drive using closed loop torque control method and feedback torque estimation. Though the proposed drive incorporated both constant torque and constant power regions, dynamic speed performance was not justified as only fixed speed performance was investigated. Some works have been reported on modelling, simulation and analysis of

controllers for vector controlled PMSM drive using state space model by Pillay and Krishnan [15-18]. In these works, transient and steady state performance were investigated as well as the performance of hysteresis and ramp comparator controllers. The authors have used linear PMSM model, i.e. forcing i_d equal to zero, to design PID type speed controller. But reluctance torque cannot be utilized and flux cannot be properly controlled without i_d. Besides, the drive performance is sensitive to parameter variation and dynamic conditions because of PID controller. So the performances of those drives have been limited to certain range of speed.

However, Jahns [19] proposed a flux weakening operation of IPMSM to examine drive performance over an extended speed range. In this method, d-axis rotor current is calculated from available phase currents and d-axis reference current. Jahns and Macminn [20] described another control technique to improve the performance of current regulators operating in the stationary reference frame. Speed-dependent back EMF and inductive voltage drops are compensated such that steady-state current errors are cancelled at all speeds until current regulator saturation limits are reached. But this technique is not applicable for a very wide range speed and the overall performance is not very satisfactory. Jahns et al. [21] proposed an adjustable IPMSM speed drive based on controlling the torque component of stator current. In this work, the author considered the effect of rotor configuration and current regulator saturation. But the method cannot provide a smooth transition from the constant torque mode to the constant power mode while the motor is in operation. Morimoto et al [22] proposed a work to control the speed of IPMSM over a wide range of speed. Current and voltage constraints for different operating regions were analyzed, and field weakening controller for high speed was

developed. Compensation was also made for magnetic saturation and demagnetization effect of permanent magnet to achieve high torque and high efficiency operation within maximum voltage and current limit of the inverter and the motor. To cancel the effect of saturation, the command i_d is generated by calculating the d-q axes inductances. But the speed controller is a fixed gain PI controller which is not suitable for HPVSD. Some other investigations of PMSM drive performance have also been reported while the flux weakening method is employed [23-25].

Radwan et al. [26] have proposed a hybrid current controller for IPMSM drive where they have employed ramp current controller for low speed operation and hysteresis current controller for high speed operation. The controller operates very well with stability but again it is sensitive to parameter variations, load variations etc. due to PI controller as speed controller. A similar work has been reported by M. Kadjoudj et al. [27]. Mademlis and Agelidis [28] proposed an IPMSM drive while dividing the operating region into three divisions: constant torque region with maximum torque to current ratio, voltage and current limited region and voltage limited region. The command i_d was determined based on the operating region and the command i_q was determined via a PI controller and a current limiter. The controller performance is sensitive to parameter changes and load disturbance. Moreover, the ripple in i_q affects the i_d too, which further increases the developed torque ripple. Chang et. al. [29] proposed a Hall-effect current sensor based IPMSM drive with a sensor-less approach to eliminate the cost of encoder. Flux control was not considered and transient performance is also not very good in this work.

1.4.2 Adaptive Controllers

Various linear and nonlinear adaptive controllers have been reported for IPMSM drive. In [30], Choy et al. developed a model reference adaptive controller (MRAC) for position control of servo PMSM drive. In this method, the drive forces the response to follow the output of the reference model regardless of the drive parameter changes. The output of the system is then compared to a desired response from a reference model, and the control parameters are updated based on this error. In this case, MRAC is used in the outer loop and a PI controller is used in the inner loop. Steady state error of the PI controller is used to compensate the chattering problem due to discontinuous control inputs. However this still does not completely solve the chattering problem. Sozer and Torrey [31] proposed an adaptive flux weakening control of PMSM drive where the d-axis current is adjusted using direct MRAC. However, the performance of the controller was tested in limited condition. Namudri and Sen [32] proposed a sliding mode controller (SMC) for a self-controlled synchronous motor. The drive system employs a phase controlled chopper and GTO inverter to provide torque-producing current component. Due to frequency limitation of GTO, this method is not suitable for HPVSD. In [33], Consoli and Antonio proposed a DSP based vector control of IPMSM drive using another SMC for torque control, and also tested the performance above the rated speed using flux weakening technique. The effect of constant acceleration, constant speed and constant deceleration were considered for designing SMC and variable bandwidth was used to reduce the chattering problem. But the drive was not proved in real-time.

Sepe and Lang [34] have proposed a discrete time observer based adaptive control for PMSM without the use of speed sensors. But this method is sensitive to inertial

mismatch and estimation of motor speed requires high gains in the presence of this inertial mismatch. This also results in noise amplification in the system which leads to poor performance. In [35], an adaptive uncertainty observer is employed with a conventional PI controller for position control of a PMSM. This method is robust but it has not been applied for speed control. Brock et al. [36] combined SMC with fuzzy logic rules to reduce chattering problem and steady state error, whereas Zhang and Li [37] combined SMC with MRAC.

1.4.3 Artificial Intelligent Controllers

Due to many advantageous features, recently the intelligent controllers like fuzzy logic controller (FLC), artificial neural network (ANN) and neuro-fuzzy controllers (NFC) have achieved particular attention of researchers for designing high performance IPMSM drive systems. Among these, FLC is the simplest and most convenient for IPMSM speed control. Particularly, FLC is good in handling nonlinear complex systems that can be controlled by a human operator without much knowledge of the system structure. Tang and Xu [38] designed a direct FLC and an adaptive FLC which is based on MRAC. The direct FLC normalizing gains are designed for limited range and conditions only. This paper also did not show any experimental result. Uddin and Rahman [39] have proposed an FLC based IPMSM drive to achieve highest torque sensitivity. The speed error and the rate of change of speed error were input variables and the torque producing current component i_q was the output variable of that FLC. But this controller suffers significant torque ripple. Butt et al. [40] worked on FLC based MTPA speed controller where command torque was derived to calculate command d-q axes

currents. But the command torque had ripples which exerted high ripple in speed output. So it was not suitable for real time implementation. Uddin et. al [41] have developed a genetic algorithm (GA) based FLC for the IPMSM drive. They minimized the number of membership functions for low computational burden of FLC. A performance index, J was tuned for the parameter of their proposed GA based FLC such that it resulted in small settling time, negligible steady state error and overshoots. The tuning parameters were adjusted offline. Due to high computational burden of GA, it is very difficult to apply GA in real time. Moreover, the control requirements of IPMSM drive under significant uncertainty and disturbance cannot be satisfied for all operating points. In [42], authors proposed an FLC for switched reluctance motor which has only one input obtained from speed error, while the FLC output is integrated to produce the torque reference. This controller is not robust as it deals only with error and it gives high ripple too.

Some researchers used ANN in motor drive systems to achieve the characteristics of adaptive controllers by utilizing its inherent nonlinear input-output mapping feature. In [43], the authors proposed an ANN based adaptive controller for IPMSM drive where an ANN model was derived as the inverse dynamic model of IPMSM. But it is difficult to get the training data required for adapting ANN parameters to get the desired performance at different conditions. In [44], Rahman and Hoque proposed another ANN controller for PMSM drive. In that work, they used offline and online training to tune weights and biases of the ANN but this controller did not ensure the stability in all operating regions. Besides, this controller needs a lot of computation. The authors proposed a high efficiency ANN controller for IPMSM drive in [45]. But the torque component current is controlled by a PI controller and so it suffers from the drawbacks of

PI controllers. Only the flux is controlled by an ANN controller but it is difficult to calculate the desired flux component current as it depends on parameters and operating conditions. This needs a lot of computation in real-time. In [46], Mobarakeh et al. proposed a self-organizing ANN controller for speed and torque control of PMSM. Both rotor position sensor and sensor-less approach were considered but torque ripple analysis was ignored.

Researchers also tried advanced intelligent controller NFC in motor drives, which is the combination of FLC and ANN controllers. The NFC utilizes the transparent, linguistic representation of FLC with the learning ability of ANN. In [47], a fuzzy basis function network (FBFN) based NFC is proposed to tune the parameters of a PI controller. In the optimization process, a performance index is developed to reflect the minimum speed deviation, settling time and zero steady-state error. But the weights and centres were trained offline in order to avoid computational burden and so the controller cannot adjust with dynamic changes. C. T. Lin [48] proposed a new structure and parameter learning scheme for ac NFC based system but the drawbacks of this scheme are that it is suitable only for offline operation and a large amount of data is required in advance of the implementation. F. Lin et.al [49] proposed a self-constructing NFC for PMSM drive but it is not suitable for real time implementation because of high computational burden.

1.4.4 Hybrid and Tuned Controllers

There are also some interesting works reported regarding hybrid and tuned speed controllers which also have motivated the author to work in this area. In these works,

researchers either use different type of controllers in a hybrid controller model or tune PI controller parameters to make the most use of different type controllers' advantageous features. Chiaberge et al. [50] provided elaborated discussion on features and advantages of different paradigms like PI, FLC, GA, NFC etc. for different systems and proposed, with the theory of finite state automation, integration of these methods in a manner depending on required performance and characteristics of the system. Vlachos et al. [51] proposed GA based auto-tuning approach of multiloop PI controllers for multivariable processes which can handle arbitrary performance objectives in time domain for different system outputs. But in its presented form, it can only be used for offline tuning due to large number of closed loop tests involved. Radial base function network (RBFN) is applied for nonlinear PI parameters adjustment in [52] and the scheme is verified by a numerical example.

Hybrid or tuned controllers are employed by researchers in other research areas to achieve specific objectives which are particularly interesting. X. Zhou et al. [53] employed relay controller to automate tuning procedure for contact-mode atomic force microscope PI controller during different scanning speed operations. They achieved the objective to sustain a constant cantilever deflection, but sample and set point factors were not discussed. PI controllers tuning with fuzzy systems for fuel flow rate and water feed rate control of a benchmark drum-boiler model is proposed in [54]. Drum pressure and drum water level were the controlled output in this case. Routray et al. [55] designed fuzzy logic based tuning method of PI controller for the rectifier side current regulator and the inverter side gamma controller in a high voltage direct current (HVDC) system. Current error, gamma error and their respective derivatives were used as principal signals

to adjust the PI controller gains. Some other interesting works were also studied where fuzzy tuned PI controllers were used to regulate frequency deviation in a two-area electrically interconnected power system [56], for hydro power plant governor control in order to track frequency variation as well as provide good response to load disturbance [57], to improve temperature control performance in a variable capacity heat pump [58].

Hybrid or tuned controllers were also tried by motor drives researchers in different works. A self-tuning method for PI speed controller of a PMSM drive system was proposed by Tursini et al. [59]. The method is derived from the analysis of the speed step response of the drive system and transplants the binary search algorithm to the tuning of PI gains. But the computation burden is high in this work. A similar tuning method is reported by S. Lee [60] to estimate PMSM model parameters R_a, L_a and K_e. His idea was to tune the PI controller to cancel the pole of motor transfer function with a controller zero and estimate motor parameters from tuned PI gains. A composite control strategy for PMSM drive is implemented in [61] by automatic switching between PI control and fuzzy logic control. But this approach is complicated with too many fuzzy rules. Fuzzy logic scheme for online tuning of PI controller parameters for linear PMSM is proposed in [62] for better tracking and disturbance rejection performance. In this work, the speed error and the rate of change of error were used as inputs to tune the controller gains. But due to the linear model used, the range of operation was limited and also torque ripple analysis was ignored. Similar tuning approach was tried by researchers in case of series connected DC motor drives [63], induction motor [64], DC servomotor [65], brushless DC motor [66, 67] and power-split hybrid electric vehicle [68].

1.4.5 Hysteresis Band Adaptation

Hysteresis band current control with pulse width modulation (PWM) strategy is widely used in power electronics research area. Some interesting works have been reported where the authors actually controlled and adapted the upper and lower hysteresis band limits, rather using their fixed base values, in order to attain certain research goals. Adaptive hysteresis band modulation strategy for a three-phase inverter is proposed in [69] as a basis of developing a new sampling based PWM strategy, where the constant width of hysteresis band was adapted as a function of maximum amplitude of a reference function. F. Liu and A. Maswood [70] presented a microprocessor based implementation of variable hysteresis band input current control technique for a three-phase three-level unity power factor rectifier. In this case, the hysteresis band is controlled with the variation of rectifier input voltage and output DC link voltage to achieve constant switching frequency at different conditions. Its advantages are its simplicity, good response to load variation and nearly sinusoidal current at the input side. An adaptive hysteresis current control algorithm is developed in [71] in application with photovoltaic grid connected inverter to ensure the synchronization of power grid voltage and injected inverter current, thereby ensuring unity power factor. Here hysteresis band is dynamically modified based on electrical parameters as switching frequency, grid voltage and slope of reference current. A similar algorithm is used by Kale and Ozdemir [72] for an active power filter to determine appropriate switching signals so as to eliminate harmonics and to compensate reactive power of three-phase rectifier. For active power filter, another fuzzy logic based hysteresis band current control method is proposed in [73], in order to limit maximum switching frequency within inverter limits and to reduce analog circuitry.

In this case, the hysteresis bandwidth was modified with respect to value of error current and rate of change of error. Similarly, Cecati et al. [74] proposed a different fuzzy logic based adaptive hysteresis current controller to be used with three-phase inverter, where the appropriate switching pattern is chosen dynamically on the basis of preset fuzzy rules.

Hysteresis band adaptation approach also encouraged researchers of motor drives but primarily this idea is integrated with direct torque control (DTC) technique. Sahoo et al. [75] developed a torque ripple minimization algorithm for switched reluctance motor (SRM) by designing an iteratively learning hysteresis current controller which is able to track the modulated phase current. But its problem is that the current values corrections have to be done exactly at the sampling point and speed has to be kept constant to ensure data updating at sampling points. So its dynamic response is poor and it is difficult to retain motor stability while the method improves current tracking. Benhadria et al. [76] proposed another adaptive hysteresis current controller for torque ripple reduction of SRM fed from a half-bridge asymmetrical inverter. But it was usable only at low speeds as 1000rpm. Many relevant works have been reported for DTC based IM drives such as [77-79]. In [77], the effect of flux and torque hysteresis bands on inverter switching loss, harmonic loss and torque ripple were investigated, and then a relevant cost function is defined and minimized in order to find the optimum limits of hysteresis bands. In [78], the hysteresis band is adapted online with the variation of applied voltage vectors, whereas a fuzzy logic based DTC technique is proposed in [79] to replace conventional hysteresis controller and look-up table. But in all these works, only torque performance was emphasized and dynamic speed performance was completely overlooked.

1.5 Research Motivation & Objective

Although IPMSM possesses many inherent advantageous features, its precise speed and torque control has always been a challenge for researchers due to nonlinear coupling among its winding currents and the rotor speed as well as the nonlinearity present in the electromagnetic developed torque because of magnetic saturation of the rotor core [22, 80]. Initially fixed gain PI controllers were employed by researchers as speed controller of IPMSM drive system. This is mainly because PI controllers have simple control structures. However, since the motor has nonlinear properties and uncertainties caused by modeling errors and process fluctuation, it is difficult to determine suitable PI controller parameters. Motor model parameters are often required in designing controllers for real time system, but these parameters also change corresponding to the equilibrium point due to nonlinear properties. Besides, fixed gain controllers exhibit poor transient response, and so they are not suitable for HPVSD. In spite of this limitation, fixed gain PI controller has the advantage of simplest structure and very good steady state response which capture the author's interest. Adaptive controllers were also used by researchers but, as mentioned in the literature review, they have the well-known disadvantages of steady-state chattering problem and dependency on motor model parameters.

Intelligent controllers come with many advantages as their designs do not need the exact mathematical model of the system and theoretically they are capable of handling any nonlinearity of arbitrary complexity. Besides they exhibit excellent dynamic response. Among the various intelligent controllers, FLC is the simplest and better in terms of response time, insensitivity to parameter and load variations. Researchers have

also used other intelligent controllers like ANN, NFC but they were associated with undesired developed torque ripple, appropriate training data and high computational burden. Thus, one motivation of this work is to combine the advantages of both PI and FLC controllers as a hybrid speed controller, where the PI controller gains will be tuned online by an FLC.

The hysteresis band PWM strategy is the most common method to control the voltage source inverter (VSI) for IPMSM drive due to easy implementation and fast transient response. As discussed in literature review, hysteresis band adaptation technique has been successfully used in power electronics research area and in some cases DTC based IM drives for torque ripple reduction. But in all these works, dynamic speed performance of IM has not been investigated. Besides, the application of hysteresis band adaptation in IPMSM drive is still very much unexplored, which is another key motivation point of this work. So, in this work, a composite approach has been taken by combining hysteresis band adaptation with the hybrid speed controller so as to achieve satisfactory speed and torque performance both in dynamic and steady state conditions.

Another aspect of IPMSM is its ability of flux weakening which makes it possible to operate above rated speed at constant voltage and thereby also helps to reduce the harmonic losses. So without controlling the flux component, the additional advantages of IPMSM over other PM motors can not be attained. But most of the reported works took an assumption of i_d equal to zero in order to linearize the IPMSM model [15-18]. So in this work a flux controller is also considered in the proposed drive to generate the appropriate d-axis current and to utilize the reluctance torque.

1.6 Thesis Organization

The organization of the remaining chapters of this thesis is as follows. Derivation of the mathematical model of IPMSM followed in this work is described in Chapter 2 with a brief review of closed loop vector control concept. Chapter 3 explains the detailed design of the proposed controllers of this work, and then provides elaborated simulation results and comparisons to demonstrate the effectiveness of the proposed scheme. In this regard, relevant fuzzy logic theory and flux weakening theory were also discussed. Chapter 4 describes the real time implementation strategy based on DSP board DS1104 with prototype laboratory 5 HP IPMSM and also provides relevant experimental results to support the proposed scheme. Finally, a summary of this work and suggestions for future scope of work are discussed in Chapter 5. After that, all relevant references and appendices of the work are listed.

Chapter 2

Mathematical Modeling of IPMSM for Vector Control Strategy

2.1 Introduction

In this chapter, mathematical model of IPMSM is developed and explained. To simplify the mathematical model and avoid unnecessary complex calculations, it will be expressed in terms of synchronously rotating reference frame where the machine equations are not dependent on rotor position. It can be accomplished in two steps using Park's transformation equations [10, 81]. In the first step, the machine equations will be transformed from the stationary a-b-c frame into the stationary d-q frame. Then in the second step, they will be transformed from the stationary d-q frame into the synchronously rotating d^r-q^r frame. Then the model is further discussed in view of the closed loop vector control strategy of IPMSM which will be followed in the rest of the work.

2.2 Basic Closed Loop Vector Control

The basic idea of closed loop vector control of inverter fed motor is to control and use the motor feedback signals in such a way that the q-axis current provides the desired developed torque. The basic block diagram of conventional VSI fed IPMSM drive is

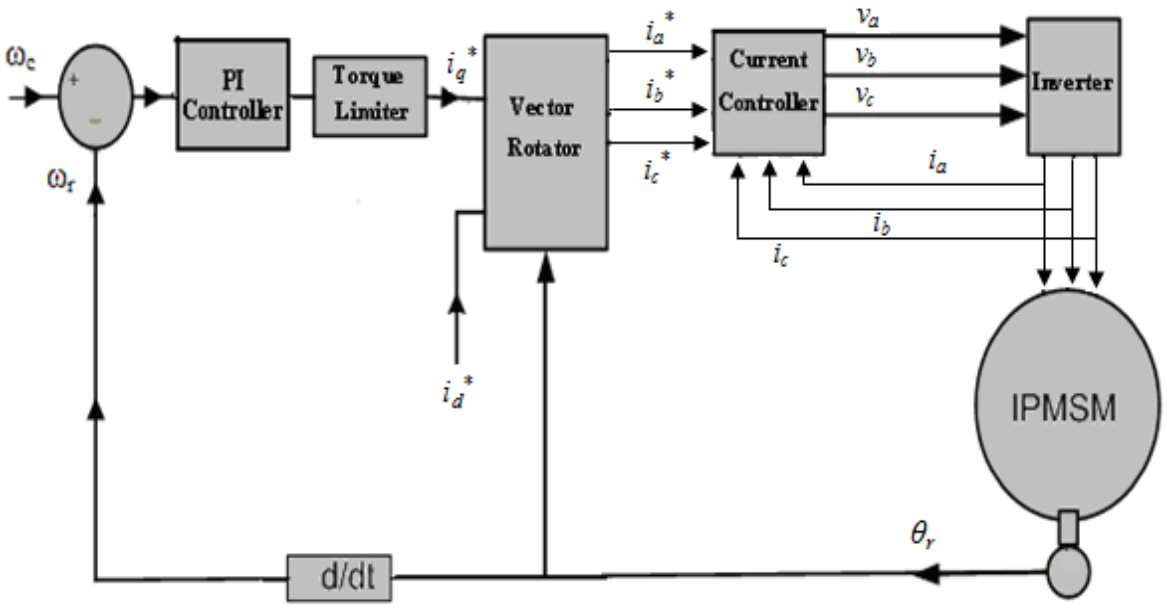

Figure 2.1: Block Diagram of Conventional PI Controlled IPMSM Vector Control. System.

shown in Fig. 2.1. The drive comprises of current controller and speed controller in the form of a conventional PI controller. The speed controller deals with the error between the command speed and the actual speed and then generates the command torque and hence the q-axis command current i_q^{r*}. The actual speed signal may come from an encoder mounted on the motor in case of sensor-based approach or from calculations in case of sensor-less approach. Conventionally the d-axis command current i_d^{r*} is set to zero to linearize the dynamic IPMSM model. Then the command phase currents i_a^*, i_b^*, i_c^* are generated from i_q^{r*}, i_d^{r*} using Park's transformation equations which will be explained in the next section.

The current controller takes actual motor phase current signals i_a, i_b, i_c and compares them with respective command phase current signals i_a^*, i_b^*, i_c^*. The current controller's objective is to force the load current to follow the command current as closely as possible and thereby forcing the motor actual speed to closely follow command

speed. Eventually the current controller generates appropriate switching signals for the inverter gates. The current controlled voltage source PWM inverter is usually preferred for IPMSM drive because of its precise control and quick response.

2.3 Mathematical Modeling of IPMSM

The flux linkages in the three phase stator winding due to permanent magnet embedded in the rotor can be given as,

$$\begin{bmatrix} \psi_{am} \\ \psi_{bm} \\ \psi_{cm} \end{bmatrix} = \psi_m \begin{bmatrix} \sin\theta_r \\ \sin(\theta_r - \frac{2\pi}{3}) \\ \sin(\theta_r + \frac{2\pi}{3}) \end{bmatrix} \tag{2.1}$$

where ψ_m is the constant flux linkage provided by the permanent magnets, θ_r is the rotor position, and ψ_{am}, ψ_{bm}, ψ_{cm} are the flux linkages in the three phase stator winding due to permanent magnet of the rotor. So total air gap flux linkages for three phases can be given as,

$$\begin{bmatrix} \psi_a \\ \psi_b \\ \psi_c \end{bmatrix} = \psi_m \begin{bmatrix} \sin\theta_r \\ \sin(\theta_r - \frac{2\pi}{3}) \\ \sin(\theta_r + \frac{2\pi}{3}) \end{bmatrix} + \begin{bmatrix} L_{aa} & M_{ab} & M_{ac} \\ M_{ba} & L_{bb} & M_{bc} \\ M_{ca} & M_{cb} & L_{cc} \end{bmatrix} \begin{bmatrix} i_a \\ i_b \\ i_c \end{bmatrix} \tag{2.2}$$

where ψ_a, ψ_b, ψ_c are the air gap flux linkages for the three phases; L_{aa}, L_{bb}, L_{cc} are the self inductances, and M_{ab}, M_{bc}, M_{ca} etc. are the mutual inductances. The phase voltage equations of the IPMSM can be defined as,

$$v_a = i_a r_a + \frac{d\psi_a}{dt} \tag{2.3}$$

$$v_b = i_b r_b + \frac{d\psi_b}{dt} \tag{2.4}$$

$$v_c = i_c r_c + \frac{d\psi_c}{dt} \tag{2.5}$$

where v_a, v_b , v_c are the three phase voltages, i_a, i_b, i_c are the three phase currents and r_a, r_b, r_c are the three phase stator resistances.

But these voltage equations depend on the flux linkage components which are function of rotor position θ_r and so the coefficients of these equations are time varying except when the motor is motionless. As discussed in the beginning, all these equations have to be transformed to the synchronously rotating rotor reference frame, where the machine equations are independent on the rotor position, using Park's transformation equations [10, 81]. The phase variables in terms of d-q-0 variables can be defined in matrix form as,

$$\begin{bmatrix} x_a \\ x_b \\ x_c \end{bmatrix} = \begin{bmatrix} \cos\theta_r & \sin\theta_r & 1 \\ \cos(\theta_r - \frac{2\pi}{3}) & \sin(\theta_r - \frac{2\pi}{3}) & 1 \\ \cos(\theta_r + \frac{2\pi}{3}) & \sin(\theta_r + \frac{2\pi}{3}) & 1 \end{bmatrix} \begin{bmatrix} x_q \\ x_d \\ x_0 \end{bmatrix} \tag{2.6}$$

The corresponding inverse relation can be given as,

$$\begin{bmatrix} x_q \\ x_d \\ x_0 \end{bmatrix} = \frac{2}{3} \begin{bmatrix} \cos\theta_r & \cos(\theta_r - \frac{2\pi}{3}) & \cos(\theta_r + \frac{2\pi}{3}) \\ \sin\theta_r & \sin(\theta_r - \frac{2\pi}{3}) & \sin(\theta_r + \frac{2\pi}{3}) \\ \frac{1}{2} & \frac{1}{2} & \frac{1}{2} \end{bmatrix} \begin{bmatrix} x_a \\ x_b \\ x_c \end{bmatrix} \tag{2.7}$$

The rotor position angle is defined as,

$$\theta_r = \int_0^t \omega_r(\tau) d\tau + \theta_r(0) \tag{2.8}$$

Both (2.6) and (2.7) are in stationary reference frame, so θ_r is only the initial rotor position $\theta_r(0)$, which is also the angle difference between the q-axis and a-phase. But x_0 does not exist for balanced three phase system and it is convenient to set initial rotor position $\theta_r(0)=0$ so that the q-axis coincides with a-phase. Considering these conditions, (2.6), (2.7) can be written as,

$$\begin{bmatrix} x_a \\ x_b \\ x_c \end{bmatrix} = \begin{bmatrix} 1 & 0 \\ -\frac{1}{2} & -\frac{\sqrt{3}}{2} \\ -\frac{1}{2} & \frac{\sqrt{3}}{2} \end{bmatrix} \begin{bmatrix} x_q \\ x_d \end{bmatrix} \tag{2.9}$$

$$\begin{bmatrix} x_q \\ x_d \end{bmatrix} = \begin{bmatrix} \frac{2}{3} & -\frac{1}{3} & -\frac{1}{3} \\ 0 & -\frac{1}{\sqrt{3}} & \frac{1}{\sqrt{3}} \end{bmatrix} \begin{bmatrix} x_a \\ x_b \\ x_c \end{bmatrix} \tag{2.10}$$

The relative position of the stationary d-q axes and the rotating d^r-q^r axes is shown in Fig. 2.2. With the help of this figure, the quantities in the stationary d-q frame can be converted to synchronously rotating d^r-q^r frame as,

$$\begin{bmatrix} x_q^r \\ x_d^r \end{bmatrix} = \begin{bmatrix} \cos\theta_r & -\sin\theta_r \\ \sin\theta_r & \cos\theta_r \end{bmatrix} \begin{bmatrix} x_q \\ x_d \end{bmatrix} \tag{2.11}$$

and its inverse relation can be defined as,

$$\begin{bmatrix} x_q \\ x_d \end{bmatrix} = \begin{bmatrix} \cos\theta_r & \sin\theta_r \\ -\sin\theta_r & \cos\theta_r \end{bmatrix} \begin{bmatrix} x_q^r \\ x_d^r \end{bmatrix} \tag{2.12}$$

Now the following assumptions are made in order to derive the d^r-q^r model:

a) The eddy current and hysteresis losses are negligible.

b) The induced emf is sinusoidal.

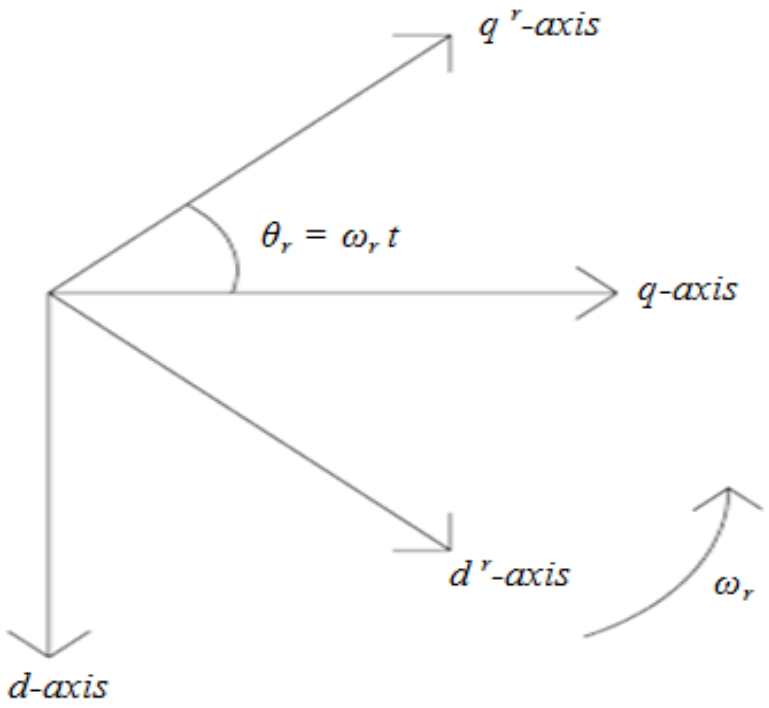

Figure 2.2: Relative position of stationary d-q axes to the synchronously rotating d^r-q^r axes.

c) The saturation is negligible.

d) The three phase stator resistances are balanced.

With these assumptions in consideration and using (2.3)-(2.5), (2.7), (2.11), the d^r-q^r axes model of IPMSM can be derived as follows,

$$v_q^r = i_q^r r_s + \frac{d\psi_q^r}{dt} + \omega_s \psi_d^r \tag{2.13}$$

$$v_d^r = i_d^r r_s + \frac{d\psi_d^r}{dt} - \omega_s \psi_q^r \tag{2.14}$$

where v_d^r, v_q^r are d-q axes voltages; i_d^r, i_q^r are d-q axes currents; ψ_d^r, ψ_q^r are d-q axes flux linkages, r_s is the stator resistance per phase, and ω_s is the stator frequency. Now it can be written,

$$\psi_q^r = L_q i_q^r \tag{2.15}$$

$$\psi_d^r = L_d i_d^r + \psi_m \tag{2.16}$$

where,
$$L_q = L_l + L_{mq} \tag{2.17}$$

$$L_d = L_l + L_{md} \tag{2.18}$$

Here L_d, L_q are d-q axes inductances; L_{md}, L_{mq} are d-q axes magnetizing inductances and L_l is the leakage inductance per phase. Relation between stator and rotor frequencies is,

$$\omega_s = P\omega_r \tag{2.19}$$

where P is the number of pole-pairs. Using (2.13)-(2.18), the motor equations can be given as,

$$v_q^r = i_q^r r_s + L_q \dot{i}_r^q + P\omega_r L_d i_d^r + P\omega_r \psi_m \tag{2.20}$$

$$v_d^r = i_d^r r_s + L_d \dot{i}_d^r - P\omega_r L_q i_q^r \tag{2.21}$$

According to (2.16)-(2.19), the d-q axes equivalent circuit diagram can be drawn as shown in Fig.2.3. Here the permanent magnet flux is represented as a constant current source I_M. Now, the total average power coming from the source (neglecting stator resistance loss) which is also the developed power per phase is given by,

$$P_{phase} = \frac{1}{2}(-P\omega_r L_q i_q^r i_d^r + P\omega_r L_d i_q^r i_d^r + P\omega_r \psi_m i_q^r) \tag{2.22}$$

The total power developed by the motor is given by,

$$P_d = \frac{3P\omega_r}{2}\{\psi_m i_q^r + (L_d - L_q) i_q^r i_d^r\} \tag{2.23}$$

So the developed electromagnetic torque is given by,

$$T_e = \frac{P_d}{\omega_r} = \frac{3P}{2}\{\psi_m i_q^r + (L_d - L_q) i_q^r i_d^r\} \tag{2.24}$$

Finally the motor dynamics can be represented by the equation,

$$T_e = T_L + B_m \omega_r + J\frac{d\omega_r}{dt} \tag{2.25}$$

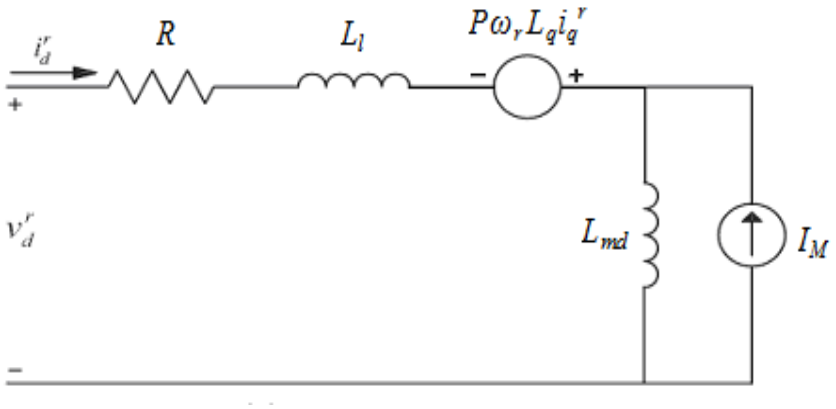

(a)

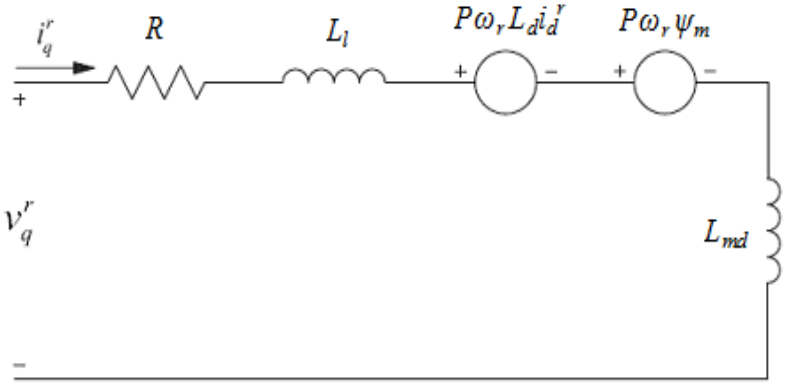

(b)

Figure 2.3: Equivalent d-q axes circuit models of IPMSM, (a) d-axis, (b) q-axis.

where T_L is the load torque (N-m), B_m is the friction damping coefficient (N-m/rad/s) and J is rotor inertia constant (kg-m^2). For dynamic simulation, these model equations can be expressed in state-space form as,

$$\frac{d}{dt}(i_q^r) = \frac{v_q^r - i_q^r r_s - P\omega_r L_d i_d^r - P\omega_r \psi_m}{L_q} \tag{2.26}$$

$$\frac{d}{dt}(i_d^r) = \frac{v_d^r - i_d^r r_s + P\omega_r L_q i_q^r}{L_d} \tag{2.27}$$

$$\frac{d\omega_r}{dt} = \frac{T_e - T_L - B_m \omega_r}{J} \tag{2.28}$$

2.4 Vector Control Strategy for IPMSM Drive

As discussed previously in Chapter 1, the closed loop vector control technique is a very effective way of controlling ac motors in HPVSD. This vector control can be applied on IPMSM drive once the machine equations are transformed from the stationary a-b-c frame to the synchronously revolving d^r-q^r frame where sinusoidal voltages act like a constant dc voltage.

We know that the developed torque in case of dc motor is,

$$T_e = K_t I_a I_f \tag{2.29}$$

where K_t is a constant, I_a is the armature current and I_f is the field current. As I_a, I_f are orthogonal and decoupled vectors, the control becomes easier for separately excited dc motor. In case of PMSMs, the first term of torque eqn. (2.24) actually represents the torque produced by the permanent magnet flux and q-axis current, and the second term represents the reluctance torque generated by the interaction of d-q axes inductances and the d-q axes currents. In case of SPMSM, $L_q \approx L_d$ and so the effect of the second term in (2.24) is negligible. Therefore, the torque equation of SPMSM becomes linear and the control task is easier. But in case of IPMSM, L_q is considerably larger than L_d. Besides, L_d, L_q values undergo significant variations in different steady state and dynamic conditions due to the excitation provided by permanent magnets, temperature change etc. Thus the nonlinear nature of the torque equation adds to the complexity of IPMSM vector control. In order to avoid these complications, most of the researchers set the command d-axis current i_d^r to zero, so that the torque eqn. (2.24) becomes linear with i_q^r and the control task becomes very easy and similar to separately excited dc motor as,

$$T_e = \frac{3P}{2}\psi_m i_q^r = K i_q^r \tag{2.30}$$

where K is a constant. But with the assumption of $i_d^r = 0$, the flux cannot be controlled in an IPMSM, and without proper flux control, motor cannot be operated above the rated speed region while maintaining voltage and current within the rated capacity of the motor and inverter. Besides, the inherent reluctance torque will be unutilized with this assumption. So in this proposed work, proper flux control has been taken into consideration so that the motor can be operated efficiently below and above the rated speed. Thus in this way, the IPMSM can be controlled like a separately excited dc motor where i_q controls torque and i_d controls flux of the IPMSM.

Using phasor notation and taking the d^r-axis as the reference axis, the steady state phase voltage V_a can be derived from steady state d^r-q^r axes voltages using (2.20) and (2.21) as,

$$V_a = v_d^r + jv_q^r = I_a r_s - \omega_s L_q i_q^r + j\omega_s L_d i_d^r + j\omega_s \psi_m \tag{2.31}$$

where the phase current,

$$I_a = i_d^r + ji_q^r \tag{2.32}$$

In case of IPMSM, the d^r-axis current is negative and it demagnetizes the main flux provided by the permanent magnets. So in order to take the absolute value of i_d^r, (2.31) can be rewritten as,

$$V_a = I_a r_s - \omega_s L_q i_q^r - j\omega_s L_d i_d^r + j\omega_s \psi_m \tag{2.33}$$

The basic vector diagram of IPMSM is shown in Fig. 2.4 based on (2.33), where the stator current can be controlled by controlling the d^r-q^r axes current components.

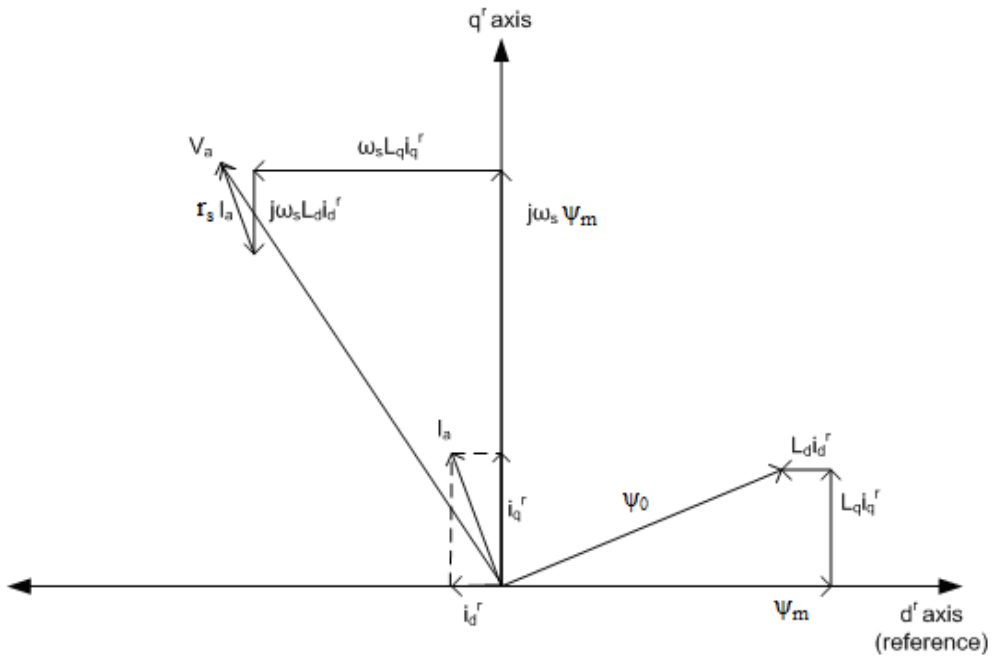

Figure 2.4: Basic vector diagram of IPMSM.

Chapter 3

Design and Development of FLC Based Tuned Hysteresis and PI Controllers with a Flux Controller

3.1 Introduction

Nowadays IPMSM is becoming popular for high performance variable speed drive (HPVSD) applications due to its high torque-current ratio, large power-weight ratio, high efficiency, high power factor, low noise and robustness [21]. Despite many advantageous features of IPMSM, the precise torque and speed control of IPMSM becomes a complex issue due to nonlinear coupling among its winding currents and the rotor speed as well as the nonlinearity present in the electromagnetic developed torque due to magnetic saturation of the rotor core particularly at high speeds [22]. The hysteresis band PWM strategy is the most popular and common method to control the voltage source inverter (VSI) for IPMSM drive due to easy implementation, fast transient response, direct limiting of device peak current and practical insensitivity of dc link voltage ripple that permits a lower filter capacitor. But the PWM strategy suffers a few drawbacks as the PWM frequency is not constant and varies within fixed upper and lower band limits. As a result, non-optimum harmonic ripple is generated in the machine current and consequently it generates ripple in developed torque. An adaptive hysteresis

band can alleviate this problem [8]. The intelligent algorithms would be a better choice to adapt the bandwidth of the hysteresis controllers because of their simplicity, less intensive mathematical design requirements, and their adaptability to deal with nonlinearities and uncertainties of electric motors. Among the various intelligent controllers, fuzzy logic controller (FLC) is the simplest and better in terms of response time, insensitivity to parameter and load variation etc. [38-40, 82]. So the objective of the first FLC proposed in this chapter is to adapt the upper and lower limits of hysteresis band online on the basis of i_q response such that the developed torque ripple is minimized.

Fixed gain controllers for speed control have been used in industry for a long time because of simplicity, satisfactory steady state performance and easier real-time implementation. However, conventional controllers such as PI, PID are not suitable for HPVSD because of their sensitivity to plant parameter variations, load disturbance and any other kinds of disturbances like temperature change, command speed change, etc. [13-18]. So the controller gains have to be adjusted online such that it gives optimum performance with dynamic conditions. Thus, the objective of the FLC based tuned PI proposed in this chapter is to combine the advantages of both PI and FLC controllers where the PI controller gains are tuned online by an FLC. This second FLC is a Sugeno type and it has been chosen in order to reduce the computational burden as much as possible. The tuned PI controller acts as a speed controller for the closed loop vector control system and generates the command value of the torque component of stator current, i_q.

Another advantage of IPMSM is its ability of flux weakening, enabling operation

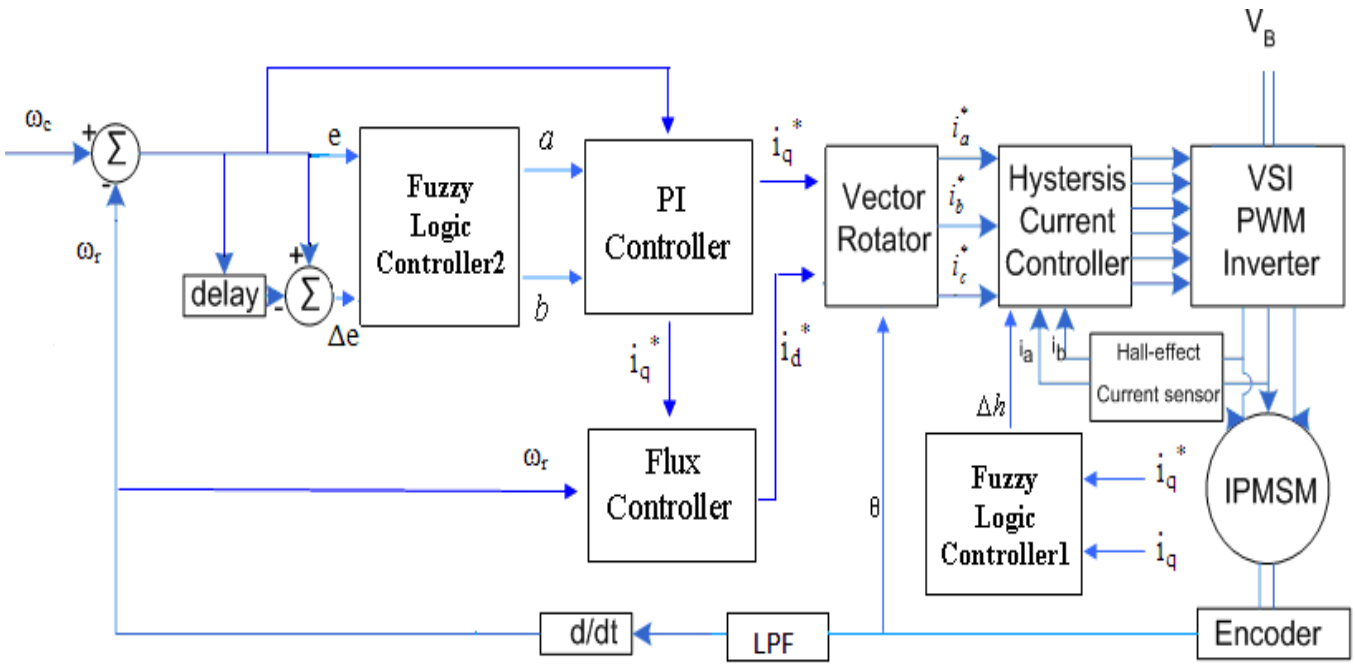

Figure 3.1: Block diagram of the proposed IPMSM Drive system.

above nominal speed at constant voltage and thereby also helps to reduce the harmonic losses in the motor [19, 22-25]. So without controlling the flux component, the main advantages of IPMSM over other PM motors cannot be achieved. But most of the reported works on controller design of IPMSM drive took an assumption of d-axis stator current (i_d) equal to zero in order to simplify the development of the controller. However, with this assumption it is not possible to utilize the reluctance torque of IPMSM and this assumption leads to an erroneous result for motor at all operating conditions. So in this work a flux controller is also incorporated which generates the appropriate d-axis current i_d above rated speed. The i_d is controlled to reduce the air gap flux by its demagnetizing effect.

The basic block diagram of the proposed IPMSM drive system incorporating FLC based tuned hysteresis and PI controllers with flux controller is shown in Fig. 3.1. In

the next sections, design and development of the proposed controllers are explained [83] with overview of relevant fuzzy logic theory and analysis of operating regions including flux weakening theory. Then simulation results of dynamic performance of the proposed IPMSM drive are presented and compared with those of a conventional PI based IPMSM drive.

3.2 Fuzzy Logic Controller: An Overview

Fuzzy logic controllers are based on fuzzy set and fuzzy logic theory which emerged as a consequence of the proposal of fuzzy set theory by Lotfi Zadeh [84]. A fuzzy control system is based on fuzzy logic which is a mathematical system that analyzes analog input values in terms of logical variables taking on continuous values between 0 and 1, in contrast to classical or digital logic which takes discrete values of either 0 or 1 (*true* or *false*). The fuzzy set (subset) A on the universe (set) X is defined by a membership function μ_A from X to the real interval [0, 1], which associates a number $\mu_A(x) \in [0,1]$ to each element x of universe X. The membership function $\mu_A(x)$ actually represents the grade of the membership function of x to A. For example, the equation $\mu_A(x) = 0.4$ means x has A-ness of about 40%. In fuzzy set theory, the boundaries of the fuzzy sets can be vague and ambiguous so as to make it useful for approximating real world imprecise systems. Fuzzy sets are represented graphically by means of their membership functions like triangular, Gaussian function, trapezoidal, singleton type etc. The particular choice of fuzzy logic membership functions depends on the designer's preference, experience and design/system requirements.

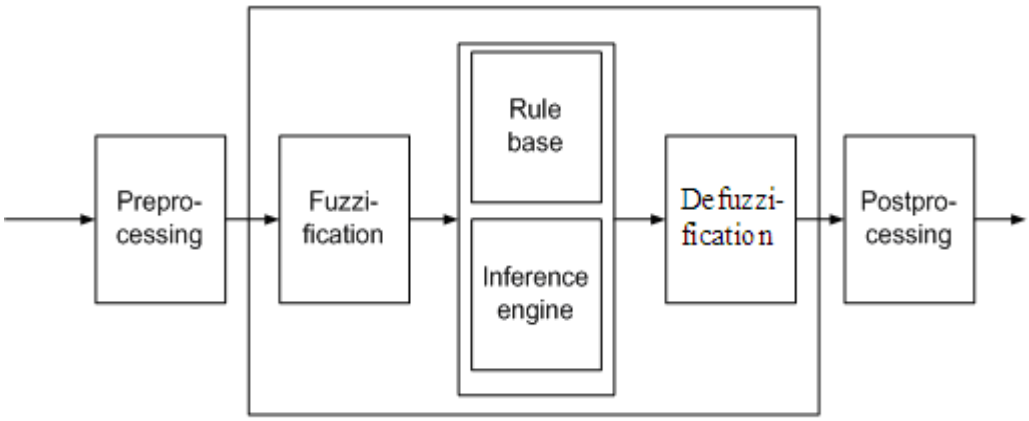

Figure 3.2: Simple block diagram of a fuzzy logic controller.

The basic block diagram of an FLC is shown in Fig. 3.2. The complete process of mapping from a given input to an output using fuzzy logic is known as fuzzy inference. There are two types of fuzzy inference methods namely Mamdani type and Sugeno type. The difference between the two methods is only the way their outputs are defined. In Mamdani type FLC, output is defined by the centroid of a two-dimensional function. But in Sugeno type FLC, the output membership functions are only linear or constant singleton spikes. In Sugeno type inference, implication and aggregation methods are fixed and cannot be edited. The implication method is simply multiplication and the aggregation operator just includes all of the singletons. Regardless of the type, a fuzzy inference is based on five steps which are: (a) pre-processing, (b) fuzzification, (c) fuzzy inference engine (rule base), (d) defuzzification and (e) post-processing.

3.2.1 Pre-processing

The inputs are usually crisp values from some measuring equipments rather than linguistic. A pre-processor processes or modifies the measurements before they enter the

controller. Some examples of pre-processing are scaling, filtering, quantization, differentiation, integration etc.

3.2.2 Fuzzification

The first step of a fuzzy inference system is to take inputs and find out the degree to which they belong to each of the appropriate fuzzy sets via membership functions. The process of converting a numerical variable, which is a real or crisp value, into a linguistic variable (fuzzy value) is called fuzzification. In an FLC, the input is a numerical value limited to the universe of input variable and the output is fuzzy degree of membership in the qualifying linguistic set which is inclusively between 0 and 1.

3.2.3 Fuzzy Inference Engine (Rule Base)

In an FLC, the fuzzy inference engine is composed of a set of control rules which are "if-then" like conditional statements, where both antecedent (if…) and consequent (then…) parts are in linguistic form. The fuzzy inference engine actually computes the output fuzzy value using a composition of two fuzzy inputs through a fuzzy rule base matrix. The rule evaluation is accomplished with two processes: (a) application of fuzzy operator (AND or OR) in the antecedent, and (b) implication from the antecedent to the consequent. A typical fuzzy rule can be set as follows,

$$\text{Rule } R_k : \text{If } \Delta\omega \text{ is } A_k \text{ and } \Delta e \text{ is } B_k, \text{ then } i \text{ is } C_k \tag{3.1}$$

where speed error ($\Delta\omega$) and change of speed error (Δe) are the input linguistic variables, current (i) is the output linguistic variable; and A_k, B_k, and C_k are the labels of linguistic

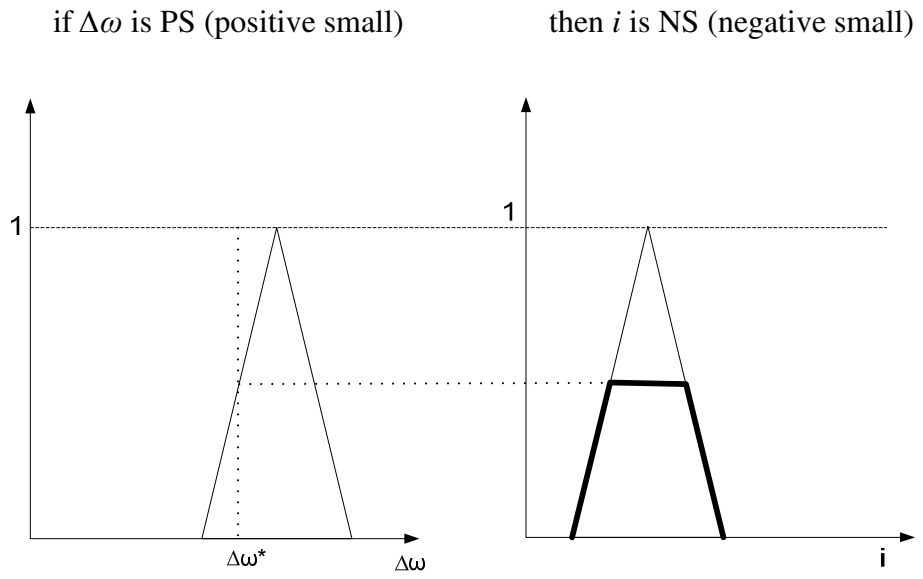

Figure 3.3: Graphical representation of the firing of a rule using Mamdani implication method.

variables $\Delta\omega$, Δe and i, respectively. If the antecedent is true to some degree of membership, the consequent will also be true to that same degree. The fuzzy operators used for fuzzy rules are AND ($\cap$), OR (U) and NOT ($^-$) which are defined as follows:

a) AND means classical intersection:

$$\mu_{A\cap B} = \min\{\mu_A(x), \mu_B(x)\} \tag{3.2}$$

b) OR means classical union:

$$\mu_{A\cup B} = \max\{\mu_A(x), \mu_B(x)\} \tag{3.3}$$

c) NOT means classical complement:

$$\bar{\mu}_A = 1-\mu_A(x) \tag{3.4}$$

According to rule R_k, $\mu_{ck}(x) = min(\mu_{Ak}(x), \mu_{Ak}(x))$. The fuzzy rules can be derived by using specific experience, from human operator behaviour or from a learning process.

The graphical representation of firing of a rule using Mamdani implication is

shown in Fig. 3.3. The rule shown here is: "if $\Delta\omega$ is *PS* (positive small), then *i* is *NS* (negative small)." Here, $\Delta\omega^*$ is the crisp input and the deep solid lines in the output membership function $\mu_{NS}(i)$ indicates the clipped membership function $\mu_{CNS}(i)$. Thus according to Mamdani implication method,

$$\mu_{CNS}(i) = min(\mu_{PS}(\Delta\omega^*), \mu_{NS}(i)) \tag{3.5}$$

The inference engine or rule firing can be of two basic types: (a) composition based and (b) rule based inferences. In case of composition based inference, the fuzzy relations representing the meaning of each rule are aggregated into one fuzzy relation describing the meaning of the overall set of rules. Then, firing with this fuzzy relation is performed via the operation composition between the fuzzified crisp input and the fuzzy relation representing the meaning of the overall set of rules. But in individual rule based inference, first each single rule is fired. This firing can be described as computing the degree of match between the crisp input and the fuzzy sets describing the meaning of the rule antecedent, and clipping the fuzzy set describing the meaning of the rule consequent to which the rule-antecedent has been matched by the crisp input. Finally, the clipped values for the control output of each rule are aggregated which gives the value of the overall control output.

In this thesis, the individual rule based inference is used as it is computationally efficient and saves a lot of memory. In case of individual rule based inference, the overall control output can be mathematically expressed as [85],

$$\mu_I(i) = max(\mu_{CLI(1)}(i),\ldots\ldots\ldots,\mu_{CLI(n)}(i)) \tag{3.6}$$

where $\mu_{CLI(k)}(i)$ $(k=1,2,...,n)$ is the clipped value of the control output *i*. In the case of individual *k-th* rule based inference,

$$\mu_{CLI(k)}(i) = min(min(\mu_{A(k)}(\Delta\omega^*),\mu_{B(k)}(\Delta e^*)),\mu_{C(k)}(i)) \quad (3.7)$$

where $\mu_{A(k)}(\Delta\omega^*)$ is the degree of membership of the crisp input $\Delta\omega^*$ in fuzzy set $\mu_{A(k)}$, $\mu_{B(k)}(\Delta e^*)$ is the degree of membership of the crisp input Δe^* in fuzzy set $\mu_{B(k)}$, and $\mu_{C(k)}(i)$ is the degree of membership of the output i in fuzzy set $\mu_{C(k)}$.

3.2.4 Defuzzification

Defuzzification is the final step of fuzzy inference to obtain the control output. The input for the defuzzification process is a fuzzy set, which is the combined output of each rule, and the output is a single number which is a non-fuzzy crisp value. There are several defuzzification methods like center of gravity/area, center of sums, center of largest area, first of maxima, middle of maxima etc. The center of gravity/area defuzzification method is the most popular among all the methods and it is used in this work. In this method, the crisp output value x is the abscissa under the centre of gravity of the fuzzy set,

$$u = \frac{\sum_i \mu(x_i)\, x_i}{\sum_i \mu(x_i)} \quad (3.8)$$

where, x_i is a operating point in a discrete universe and $\mu(x_i)$ is its membership value in the membership function. This expression can be interpreted as the weighted average of the elements in the support set.

3.2.5 Post-processing

The fuzzy output must be scaled to appropriate unit from a standard universe so that it can be meaningfully used with real world systems. An example is the scaling from

the standard universe [-1, 1] to the physical units [-15, 15] Amperes. Usually the post processing block contains an output gain that can be tuned, and sometimes an integrator.

3.3 FLC Based Online Hysteresis Current Controller Band Adaptation

The hysteresis current controller is used to control the current in such a way that it can follow the command current within a hysteresis band. It is widely used in power electronics and motor drives research area integrated with three-phase inverter and ac motors. It is very popular because of its simplicity and excellent dynamic response. A typical three-phase bridge inverter is shown in Fig. 3.4 and corresponding fixed hysteresis band PWM current controller is shown in Fig. 3.5. Actually three such hysteresis controllers will generate the appropriate switching signals for the six inverter switches Q_1, Q_2, Q_3, Q_4, Q_5, Q_6 in Fig. 3.4. Let's consider that N1, N2, N3, N4, N5, N6 are the logic signals for corresponding switches $Q_1 \ldots Q_6$ respectively. When the logic signal N1 is 1 then the IGBT switch Q_1 is ON, and when N1 is 0 then Q_1 is OFF. The same logic is valid for other five switches. The control logic of the hysteresis controller is as follows,

(i) For $i_a^* > 0$: N4=0 if $i_a > i_{up}$, then N1=0, else if $i_a < i_{lo}$ then N1=1.

(ii) For $i_a^* < 0$: N1=0 if $i_a > i_{up}$, then N4=1, else if $i_a < i_{lo}$ then N4=0.

where i_a^*, i_a are command and actual phase-a currents respectively, $i_{up} = i_a^* + HB$ is the upper band, $i_{lo} = i_a^* - HB$ is the lower band, and HB is the hysteresis band. The current waveforms and corresponding PWM voltage wave are shown in Fig. 3.6.

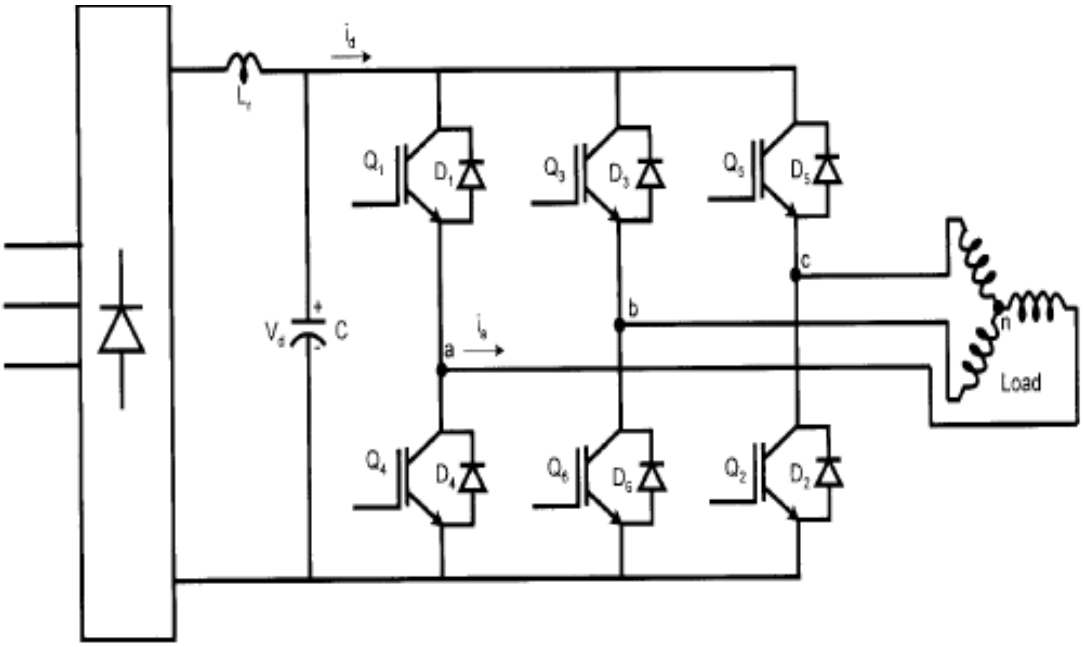

Figure 3.4: Three-phase bridge inverter used in IPMSM drive [8]

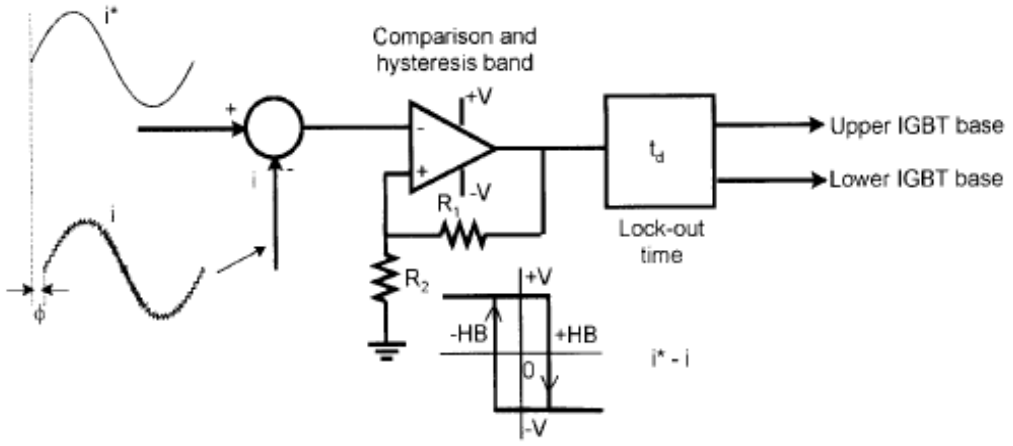

Upper switches ON: (i* - i) > +HB
Lower switches ON: (i* - i) < - HB

Figure 3.5: Control block diagram for Hysteresis Band PWM [8]

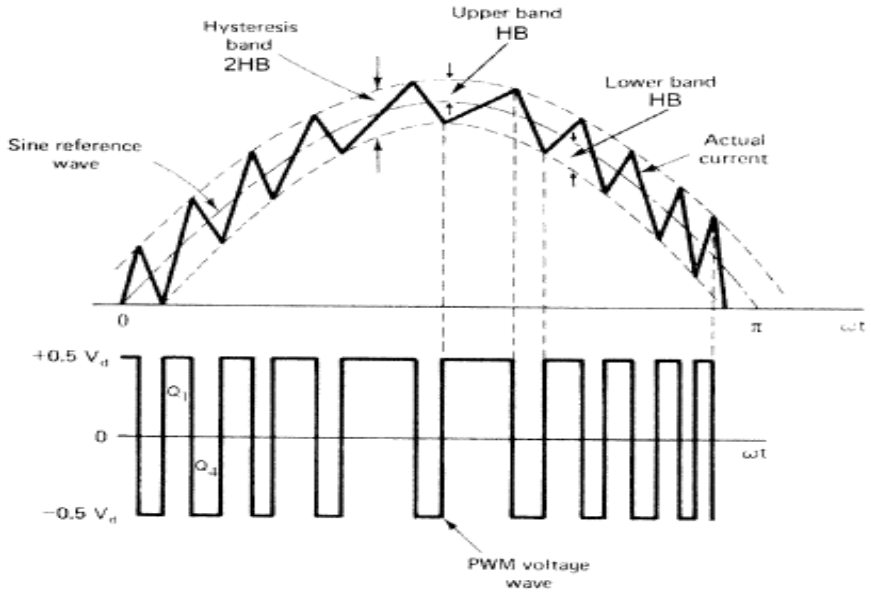

Figure 3.6: Principle of hysteresis band current control [8]

The major drawback of this fixed band hysteresis PWM controller is that it generates harmonic ripples in machine current and developed torque as the PWM frequency varies within band limits.

The solution method proposed in this thesis is that an FLC is developed to reduce the ripple in the developed torque by modifying the upper and lower limits of hysteresis band online. The input variable is the difference between the command and actual q-axis currents ($d_{iq} = |i_q - i_q^*|$) as the q-axis current has direct linear relationship with developed torque (ignoring i_d). The initial fixed upper and lower hysteresis band limits (H_u and H_l) are taken as 0.05 and -0.05. The output of the FLC is a fractional band limit (Δh) which will be added with or subtracted from those fixed limits as,

$$\tilde{H}_u = H_u + \Delta h \tag{3.9}$$

$$\tilde{H}_l = H_l - \Delta h \tag{3.10}$$

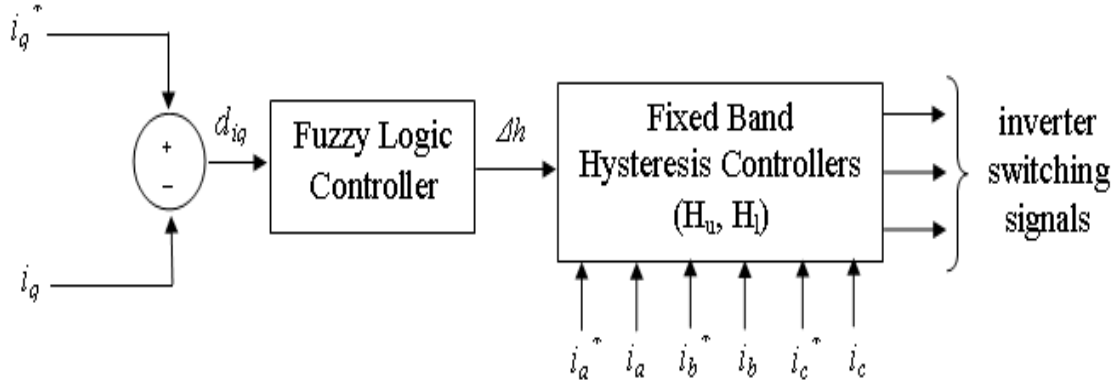

$$\tilde{H}_u = H_u + \Delta h \quad \text{and,} \quad \tilde{H}_l = H_l - \Delta h$$

Figure 3.7: Proposed Hysteresis Band Adaptation strategy

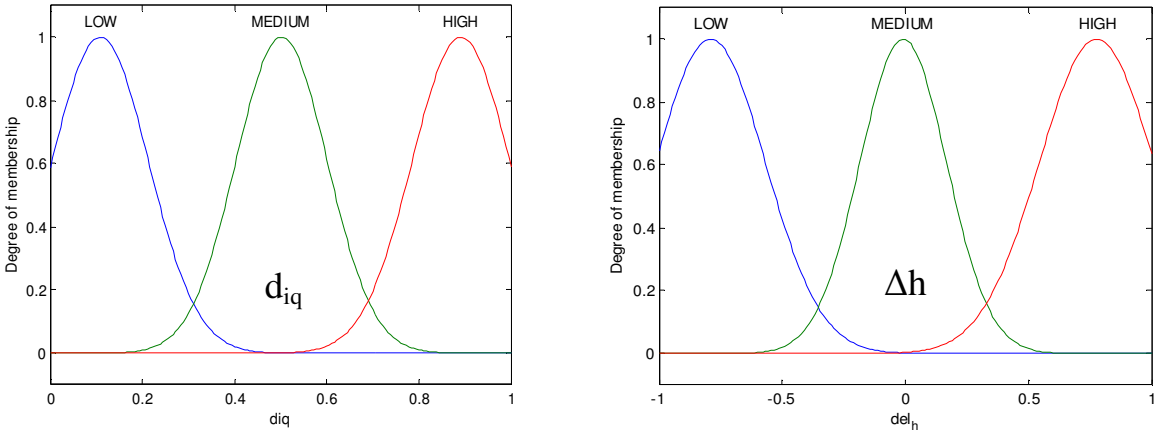

Figure 3.8: Membership functions of Hysteresis Band Adaptation FLC

The proposed hysteresis band adaptation strategy is described in the block diagram of Fig. 3.7. The membership functions of the input and output variables are shown in Fig. 3.8. The peak-to-peak current ripple and switching frequency are related to the width of the hysteresis band. For example, a smaller band will increase inverter switching frequency and lower the ripple whereas a wider band will reduce the switching

frequency but will result in higher ripple. An optimum band that maintains a balance between the harmonic ripple and inverter switching loss is desirable [8]. On the basis of this observation, the fuzzy rules are developed as,

1. If d_{iq} is LOW, then Δh is HIGH.
2. If d_{iq} is MEDIUM, then Δh is MEDIUM.
3. If d_{iq} is HIGH, then Δh is LOW.

3.4 FLC Based Tuned PI Controller

The second FLC is developed in such a way that it can tune the K_p, K_i gains of the PI controller online in order to accommodate the uncertainties. In this case, a Sugeno type FLC is chosen over commonly used Mamdani type FLC in order to reduce the undesired computational burden. For the proposed FLC, the input variables are actual speed, speed error (e) and change of speed error (Δe) and the output variables are constant factors *'a'* and *'b'*, which are multiplying factors for K_p, and K_i, respectively. In this regard, the defuzzification process and output of Sugeno type FLC is discussed in next paragraph.

Sugeno fuzzy inference system is similar to the Mamdani method in many respects. In fact the first two parts of the fuzzy inference process, fuzzifying the inputs and applying the fuzzy operator, are exactly the same. The main difference between Mamdani-type of fuzzy inference and Sugeno-type is that the output membership functions are only linear or constant for Sugeno-type fuzzy inference. Zero-order Sugeno type FLC has been used in this work. A typical fuzzy rule in a zero-order Sugeno fuzzy model has the form,

$$\text{if } x \text{ is } A \text{ and } y \text{ is } B, \text{ then } z = k$$

where *A* and *B* are fuzzy sets in the antecedent, while *k* is a crisply defined constant in the consequent. When the output of each rule is a constant like this, the similarity with Mamdani's method is striking. The only distinctions are the fact that all output membership functions are singleton spikes, and the implication and aggregation methods are fixed and can not be edited. The implication method is simply multiplication, and the aggregation operator just includes all of the singletons [86].

The proposed FLC based PI controller tuning strategy [83] is described in the block diagram of Fig. 3.9. The membership functions of the input variables are shown in Fig. 3.10. In order to achieve high performance with simplicity and less computations minimum number of membership functions is used for input variables. But in this case, one additional membership function can be employed for Δe variable to make the fuzzy inference more flexible. This one is considered as a future extension of work. As it is a Sugeno type FLC, the output membership functions are chosen as the congregation of three bars on the points 0.5 (LOW), 1 (MEDIUM) and 1.5 (HIGH). The present samples of $K_p[n]$ and $K_i[n]$ are updated as follows:

$$K_p[n] = a*K_P[n-1] \quad and \quad K_i[n] = b*K_i[n-1] \tag{3.11}$$

where *'a'* and *'b'* are some constant factors which are the outputs of the FLC, and [n-1] indicates the previous sample values. The initial K_p and K_i gains of the PI controller are chosen as 5 N-m/rad/s and 10 N-m/rad, respectively.

The rules are developed on the basis of observation of responses of a tested PI controller of the IPMSM. It was observed that for a conventional PI controller, if K_i is increased, then overshoot in speed response increases but the settling time decreases. Similarly, an increase in K_p results in corresponding decrease in overshoot and settling

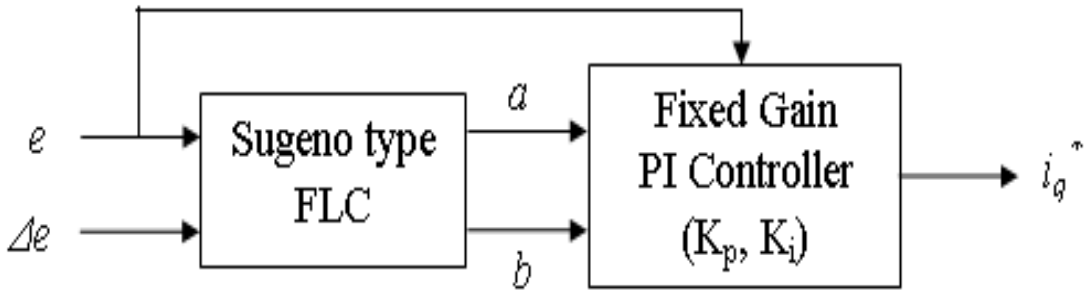

Figure 3.9: Proposed FLC based PI controller tuning strategy

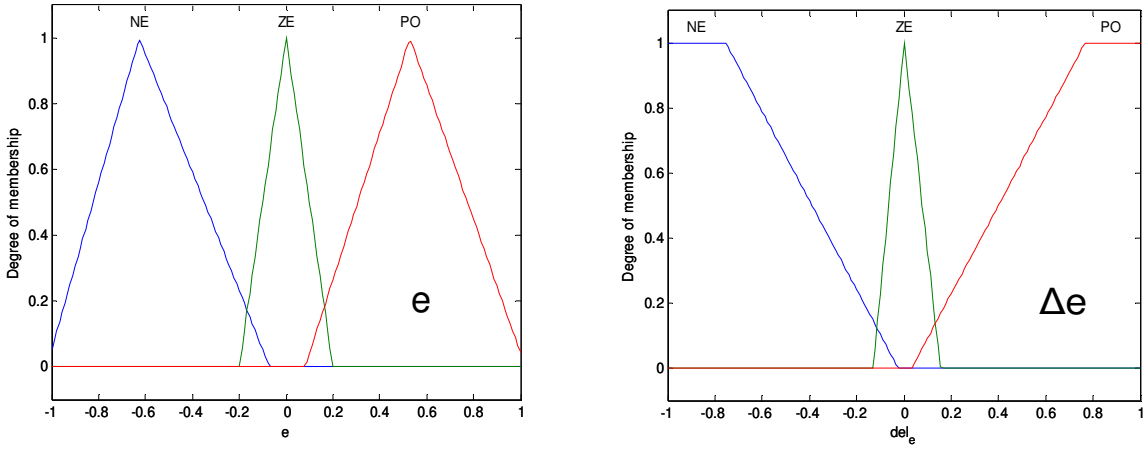

Figure 3.10: Membership functions of PI Controller tuning FLC

time. Furthermore, it was observed that the speed response became unstable when both gains are reduced simultaneously towards the same value. Based on these observations, fuzzy rules decision was made, which are given below,

1. If *e* is NE (negative), then *'b'* is LOW and *'a'* is HIGH.
2. If *e* is PO (positive), *'b'* is LOW and *'a'* is HIGH.
3. If *e* is ZE (zero) and *Δe* is ZE (zero), then *'b'* is LOW and *'a'* is LOW.
4. If *e* is PO and *Δe* is PO, then *'b'* is MEDIUM and *'a'* is LOW.
5. If *e* is NE and *Δe* is PO, then *'b'* is LOW and *'a'* is MEDIUM.
6. If *e* is NE and *Δe* is NE, then *'b'* is HIGH.
7. If *e* is PO and *Δe* is NE, then *'b'* is HIGH.

3.5 Flux Controller

Very often command current i_d is set to zero in order to simplify the development of the controller of IPMSM which consequently leads to erroneous or non-optimal results for motor at all operating conditions [15-18]. With $i_d=0$, the resultant air gap flux remains constant as the direct control of flux is not possible for IPMSM. In order to operate the motor above the rated speed within the voltage and current constraints, the flux has to be decreased which can be done by controlling i_d. Previously researchers worked on flux weakening operation of IPMSM [19, 22-25]. To enable that operation, in this work a flux controller is integrated with the proposed FLC based tuned PI controller so that the IPMSM drive can be operated over the whole wide speed range, namely, constant torque and constant power (field weakening) regions. In the following subsection, both regions are discussed and relevant mathematical formulae are derived to design the flux controller [82].

3.5.1 Constant Torque Region

There exists an inverter output voltage limit, output current limit and power capacity limit for a practical inverter-fed motor drive. Let's assume that the maximum available phase voltage amplitude and the maximum line current amplitude are V_a and I_a, respectively. Then the feasible operation range can be explained by these inequalities,

$$(v_q^r)^2 + (v_d^r)^2 \le V_a^2 \tag{3.12}$$

$$(i_q^r)^2 + (i_d^r)^2 \le I_a^2 \tag{3.13}$$

Maximum torque per ampere (MTPA) control technique is very attractive to achieve fast transient response and low loss in constant torque region. The basic principle of MTPA technique is that for a given torque demand, the line current amplitude is minimized to achieve the maximum torque. It can be achieved by proper controlling of flux utilizing the armature reaction effect of i_d^r. Below the rated speed, with the assumption of keeping the absolute value of stator current constant at its maximum value (I_a), i_d^r can be calculated in terms of i_q^r for MTPA control. This can be obtained by differentiating torque equation (2.24) with respect to i_q^r and setting it to zero as [82],

$$i_{dM}^r = \frac{\psi}{2(L_q - L_d)} - \sqrt{\frac{\psi^2}{4(L_q - L_d)^2} + i_q^{r\,2}} \tag{3.14}$$

where i_{dM}^r is the value of i_d^r corresponding to MTPA. So the corresponding maximum available torque is as follows,

$$T_{eM} = \frac{3P}{2}\{\psi i_{qM}^r + (L_d - L_q) i_{qM}^r i_{dM}^r\} \tag{3.15}$$

where,
$$i_{qM}^r = \sqrt{I_a^2 - (i_{dM}^r)^2} \tag{3.16}$$

The trajectory of the MTPA curve, the current limit curve, voltage limit curves and constant torque curves are shown in Fig. 3.11. The constant torque curves are drawn for constant amount of torque T_1, T_2, $T_{eM,}$ where $T_{eM} > T_2 > T_1$. So the maximum torque available (keeping $i_d^r = 0$ and maintaining current constraint) is T_2, which can be obtained with MTPA technique at lower amount of current. The distance between any points of the constant torque curve and the origin point 'O', indicates the stator current requirement to achieve the desired torque. The point at which the constant torque curve intersects with the MTPA curve is the lowest distance of that constant torque curve from the origin. Thus

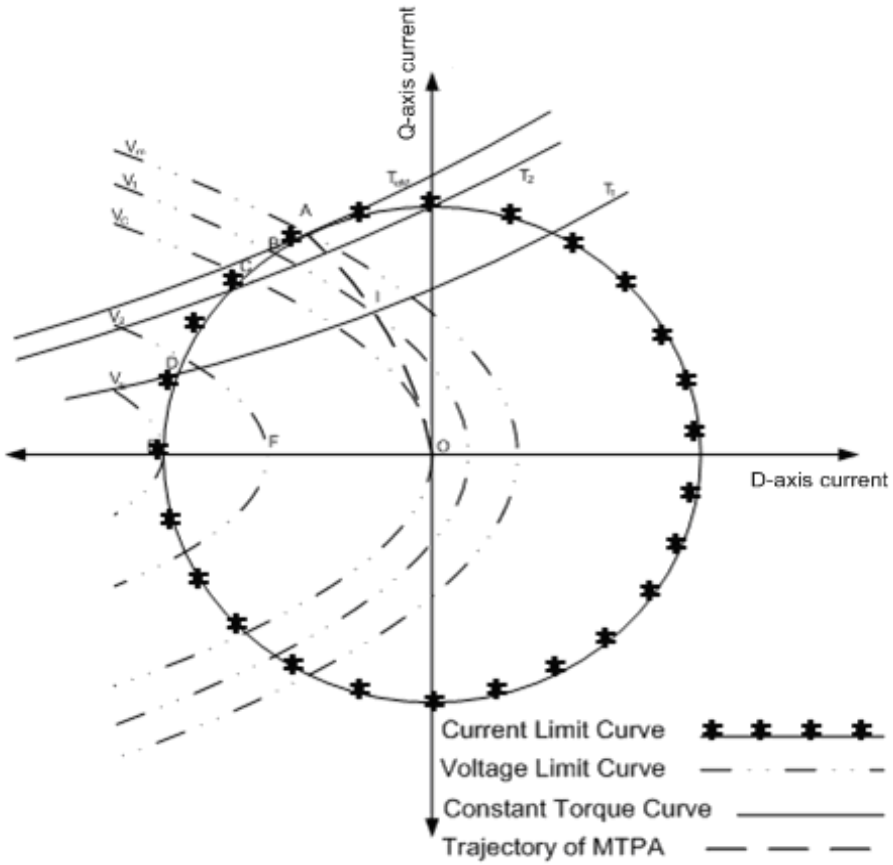

Figure 3.11: MTPA trajectory, current limit curve, voltage limit curves and constant torque curves of IPMSM in d-q axes plane neglecting stator resistance.

the MTPA technique ensures the lowest current requirement to achieve the desired torque. Eqn. (3.14) is used to design the flux controller below rated speed.

3.5.2 Constant Power Region

Above rated speed, the traditional control strategy is to reduce the magnetic flux intensity by applying negative d-axis current resulting in field weakening control. But the flux component of current i_d still can be controlled by MTPA technique if the torque requirement is low enough to satisfy voltage constraint. Constant power region or field weakening (FW) region can be sub-divided into partial FW region and full FW region.

(a) Partial Field Weakening Region:

It can be observed from Fig. 3.11 that MTPA can be even applied above rated speed, but the generated torque decreases to maintain the current and voltage constraint because of insufficient demagnetization. But as long as the generated torque is sufficient, it is a good choice to use MTPA. Otherwise field weakening control can be applied. Substituting (2.20) and (2.21) in (3.12), the voltage constraint can be redefined as,

$$(r_s i_d^r - P\omega_r L_d i_q^r + L_d \frac{di_d^r}{dt})^2 + (r_s i_q^r + P\omega_r L_d i_d^r + L_q \frac{di_q^r}{dt} + P\omega_r \psi)^2 \le V_a^2 \qquad (3.17)$$

At steady state condition,

$$(r_s i_d^r - P\omega_r L_d i_q^r)^2 + (r_s i_q^r + P\omega_r L_d i_d^r + P\omega_r \psi)^2 \le V_a^2 \qquad (3.18)$$

Here the rotor angular frequency is less than the critical frequency ω_{rc} which can be obtained from (3.18) by setting both i_d and i_q to zero as,

$$\omega_{rc} = V_a / P\psi \qquad (3.19)$$

From (3.18), neglecting armature resistance,

$$(P\omega_r L_d i_q^r)^2 + (P\omega_r L_d i_d^r + P\omega_r \psi)^2 \le V_a^2 \qquad (3.20)$$

However, depending on the load requirement, (3.20) may not be satisfied even if the speed is below ω_{rc}. When the motor follows MTPA trajectory it takes minimum amount of stator current, and consequently copper loss is reduced and the drive efficiency is increased. If the current controller is saturated due to voltage constraint, a flux weakening technique will be used as shown by the arrow sign in Fig. 3.12. The flux weakening technique is explained in the next subsection.

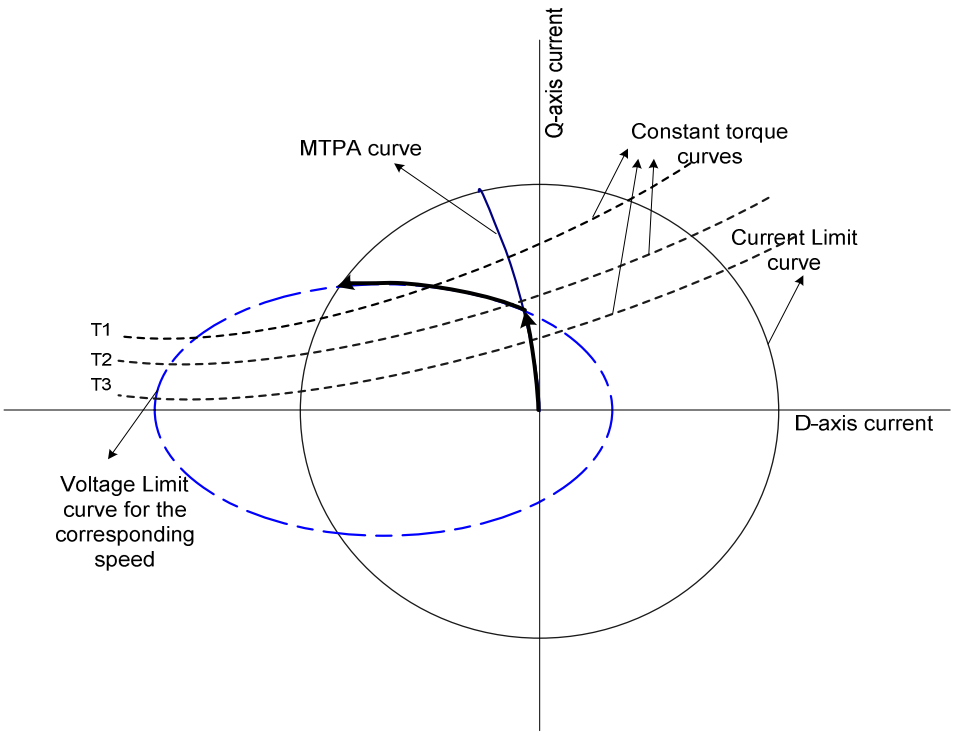

Figure 3.12: Control in partial field weakening region

(b) Full Field Weakening Region:

When the speed is above critical speed ω_{rc}, it is called full field weakening region. To control the motor above ω_{rc} considering current and voltage constraints, the operating region is limited by the d-axis current line, current limit curve and voltage limit curve. It can be easily understood from Fig. 3.13 that the intersecting point of voltage limit curve with constant torque curve gives the minimum current point to generate the required torque. So it is the best choice for low copper loss. The relation between d and q axes command currents for field weakening while maintaining current and voltage constraints can be obtained as [82],

$$i_d^r = -\frac{\psi}{L_d} + \frac{1}{L_d}\sqrt{\frac{(V_a')^2}{P^2\omega_r^2} - L_q^2 i_q^2} \tag{3.21}$$

where V_a' is the maximum stator phase voltage neglecting the stator resistance voltage

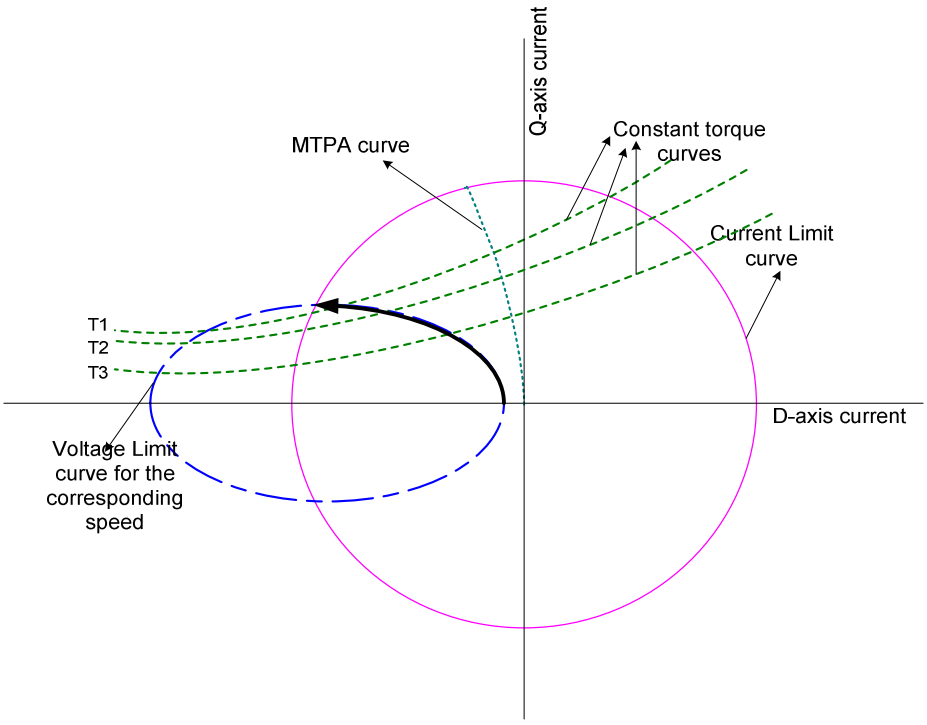

Figure 3.13: Control in full field weakening region

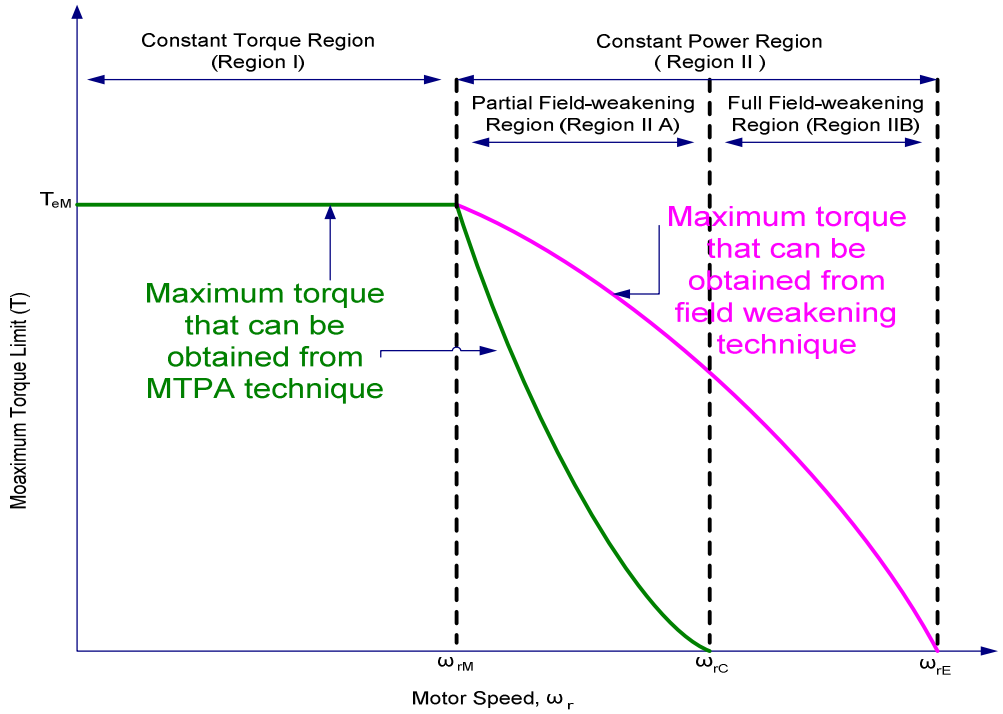

Figure 3.14: Maximum torque limit curve at different operating regions.

drop. Eqn. (3.21) is also used to design the flux controller above rated speed. From (3.21), one can calculate the maximum speed, called the extreme angular frequency ω_{rE} that a motor can achieve, as,

$$\omega_{rE} = \frac{\sqrt{V_a^2 - (r_s I_a)^2}}{P(L_d I_a + \psi)} \tag{3.22}$$

The maximum torque limit curve for different operating regions discussed above is presented in Fig. 3.14.

3.6 Simulation Results and Discussion

The performance of the proposed FLC based tuned PI with hysteresis band adaptation based drive has been investigated extensively at different dynamic operating conditions. A comparison of the proposed drive with a conventional PI based IPMSM drive is also provided. Simulations are performed on the basis of parameters of the laboratory 5 HP IPMSM which is also used later for real-time experimentation. This motor's parameters are provided in Appendix-A. Simulation model for the complete IPMSM drive is developed using Matlab/Simulink which is shown in Fig. 3.15. The internal subsystem blocks are provided in Appendix-B.

Simulation results are presented below from Fig. 3.16 to Fig. 3.27, which demonstrate the comparison of performances of the proposed IPMSM drive with conventional PI based drive. The proportional and integral gains of the conventional fixed gain PI controller are taken as 0.5 N-m/rad/s and 4 N-m/rad, respectively which exhibit good performance in steady state for the lab IPMSM. A better PI controller can be found by changing the gains with trial-and-error. But it has not been done here as it is a

random and time consuming process. Rather the PI gains have been tuned by the proposed FLC. Fig. 3.16 shows the initial speed responses of the IPMSM drives at rated speed (183 rad/s) with 50% rated load (9.55 N-m). Here it is easily observed in Fig. 3.16(a) that the proposed FLC based tuned IPMSM drive enables the motor to reach command speed with minimum settling time and without any overshoot, whereas the conventional PI based drive reaches the command speed with higher settling time and large overshoot as shown in Fig. 3.16(b). Figs. 3.17(a), 3.17(b) show the starting torque responses at rated speed and 50% rated load, which clearly demonstrates the minimized ripple in developed torque of the proposed drive. Fig. 3.17(b) also emphasizes the effectiveness of the hysteresis band adaptation FLC as it shows that the adaptation of hysteresis band limits further reduces the developed torque ripple from the instant t=0.5s when that FLC was actually activated. The corresponding online variations of hysteresis band limit values are shown in Fig. 3.17(c). Fig. 3.18 shows the corresponding phase current responses of the drives at rated speed and 50% rated load condition, which clearly shows that the conventional PI based drive draws noisier and higher current than the proposed drive. This noise content in the current also results in higher harmonic loss for the conventional PI based drive. Corresponding d-q axes current responses at rated speed and 50% rated load condition are presented in Fig. 3.19 which demonstrates that PI based drive suffers higher ripple than the proposed drive.

The performance of the proposed drive is also tested in very high and very low speeds and the results are presented in Figs. 3.20 and 3.21. The high speed response of the proposed drive at 300 rad/s command speed with corresponding d-q axes currents at 50% rated load condition are plotted in Fig. 3.20. It shows that the proposed drive

smoothly follows the high speed command by applying flux weakening operation with a more negative d-axis current. Here it is worth mentioning that the d-q axes currents are scaled five times in this figure for the better visibility of the reader. Fig. 3.21 shows the low speed response of the proposed drive at 25 rad/s command speed with corresponding torque response at 50% rated load condition. Again the proposed drive successfully follows the low speed command.

Next, the drive performance is tested in dynamic speed condition. Fig. 3.22 shows superior dynamic performance of the proposed drive for a step change of command speed from 150 rad/s to 220 rad/s with 50% rated load at t=0.5s, where the proposed drive does not suffer any overshoot and reaches the command speed with minimum settling time as it does in rated speed condition. But the PI based drive takes higher settling time and suffers speed overshoot twice. Fig. 3.23 shows the corresponding q-axis and d-axis current responses during this speed change. The negative d-axis current of the proposed drive in Fig. 3.23(a) points out that the flux weakening operation is triggered at t=0.5s as the command speed is changed to above rated speed and thus ensures the desired utilization of reluctance torque.

Good performance in dynamic load condition, as well as dynamic speed response, is also desired, and it has been considered in this work too. Fig. 3.24 shows the speed responses of the drives with corresponding torque responses when the load torque is abruptly increased from 50% (9.55 N-m) to 75% (14.325 N-m) rated load at t=1s. Fig. 3.24(a) demonstrates that the proposed drive is almost insensitive to load disturbance, whereas the conventional drive suffers speed undershoot during load transition as shown in Fig. 3.24(b). Fig. 3.25 presents the corresponding phase current responses during this

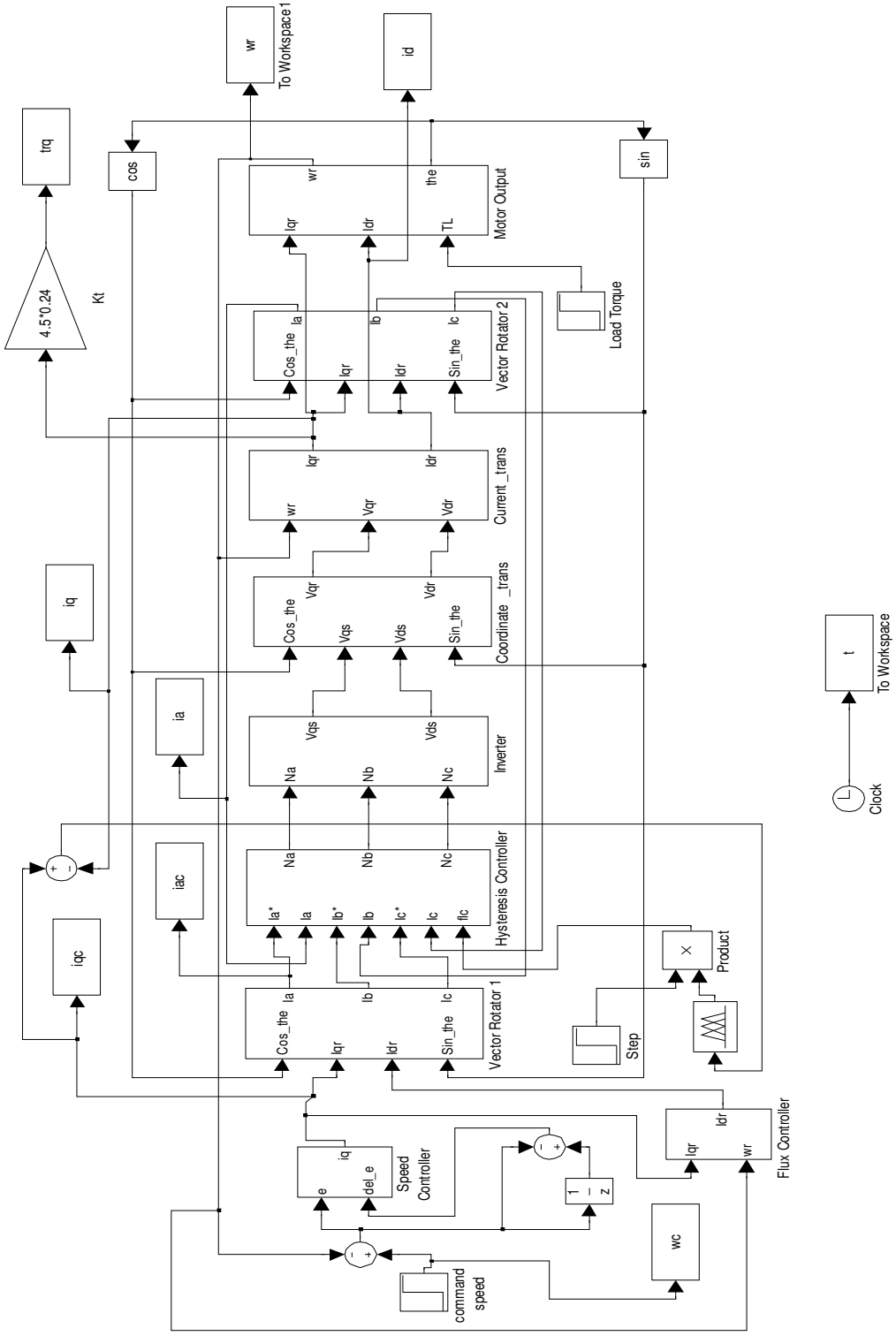

Figure 3.15: Complete Simulink schematic of the proposed IPMSM drive system.

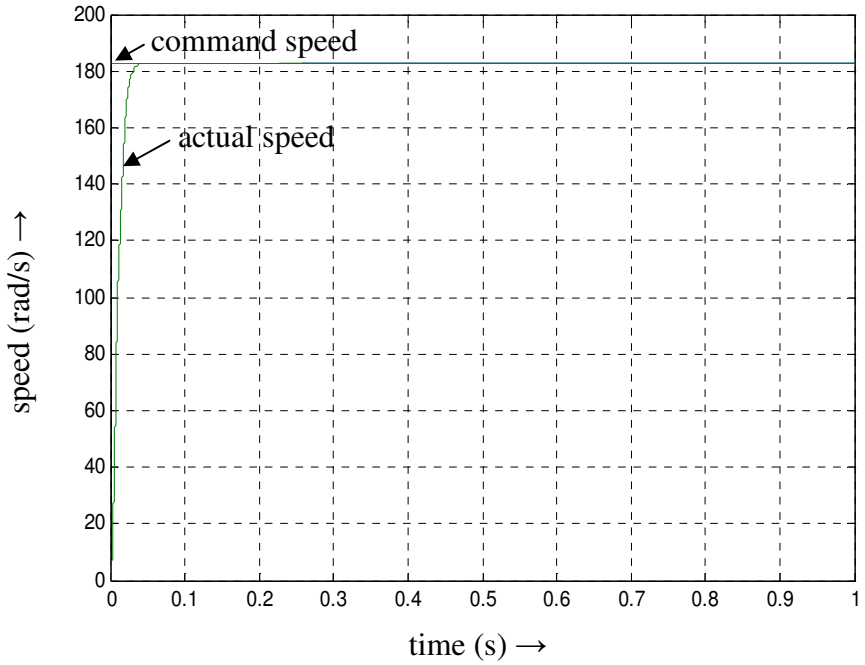

(a)

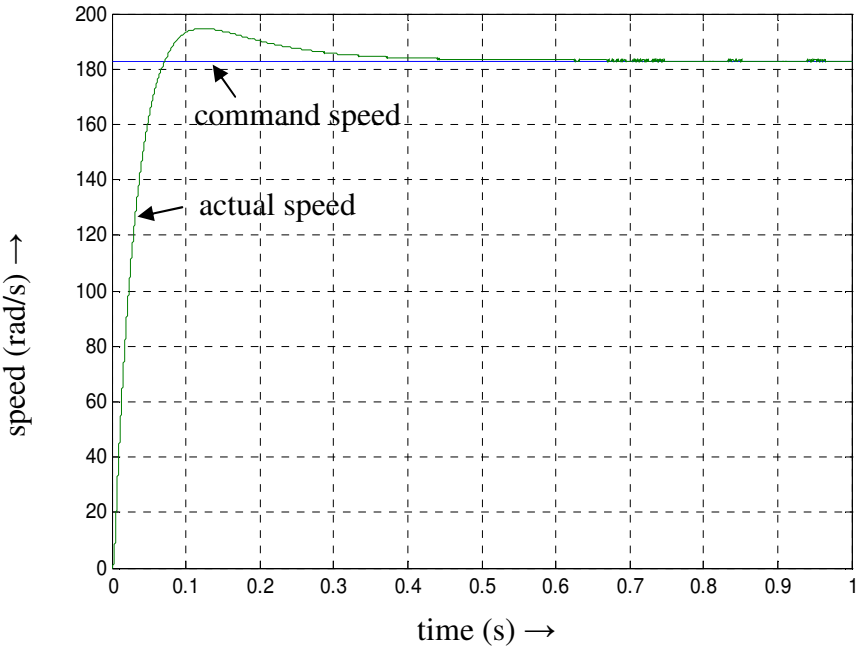

(b)

Figure 3.16: Initial rated speed (183 rad/s) responses of IPMSM drives at 50% rated load (9.55 N-m), a) FLC based tuned PI with hysteresis band adaptation, b) conventional PI.

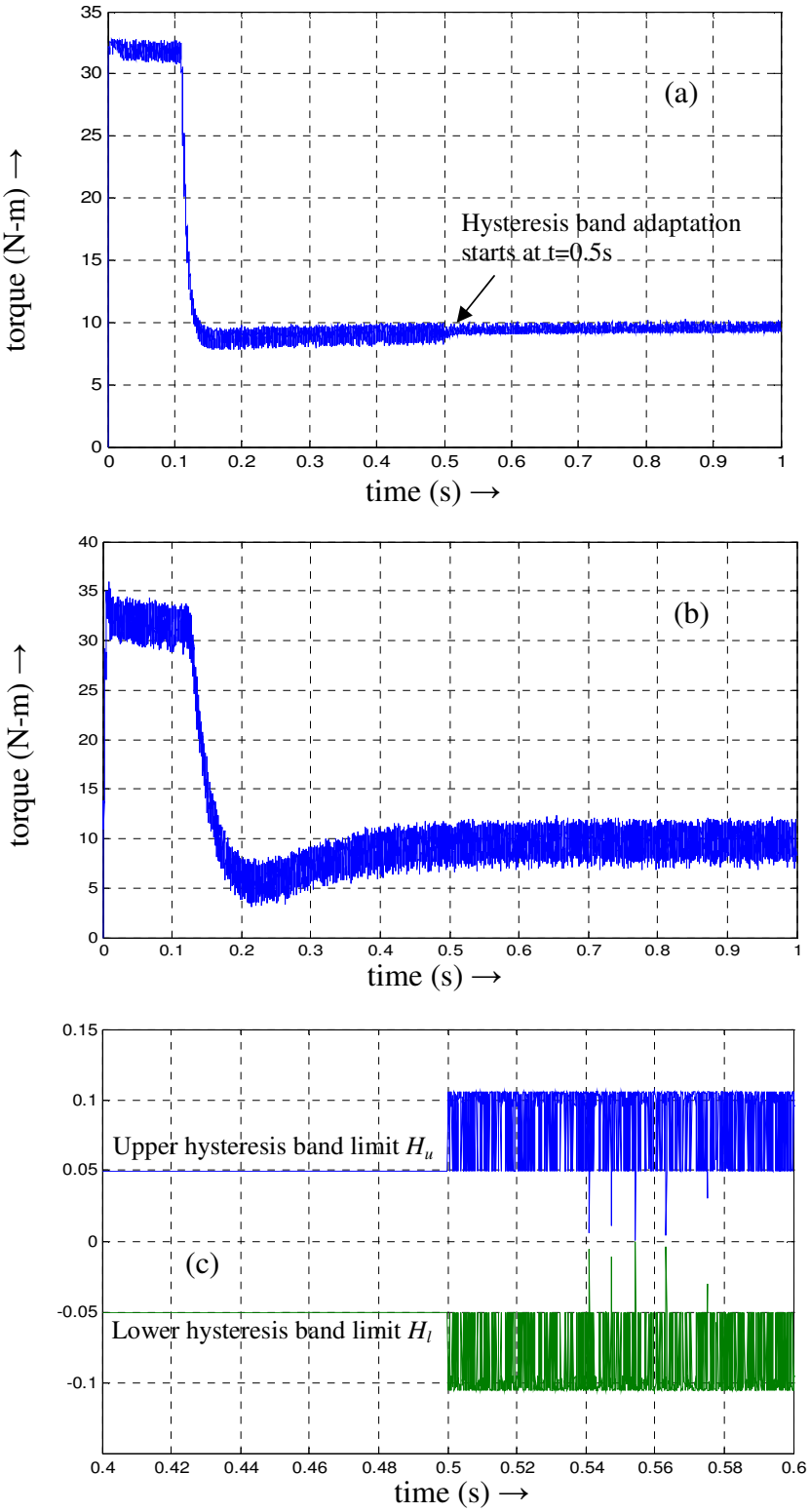

Figure 3.17: Developed torque responses of IPMSM drives at rated speed (183 rad/s) and 50% rated load (9.55 N-m), a) proposed FLC based tuned PI (with and without hysteresis band adaptation), b) conventional PI, c) corresponding online variations of hysteresis band limits of the proposed drive.

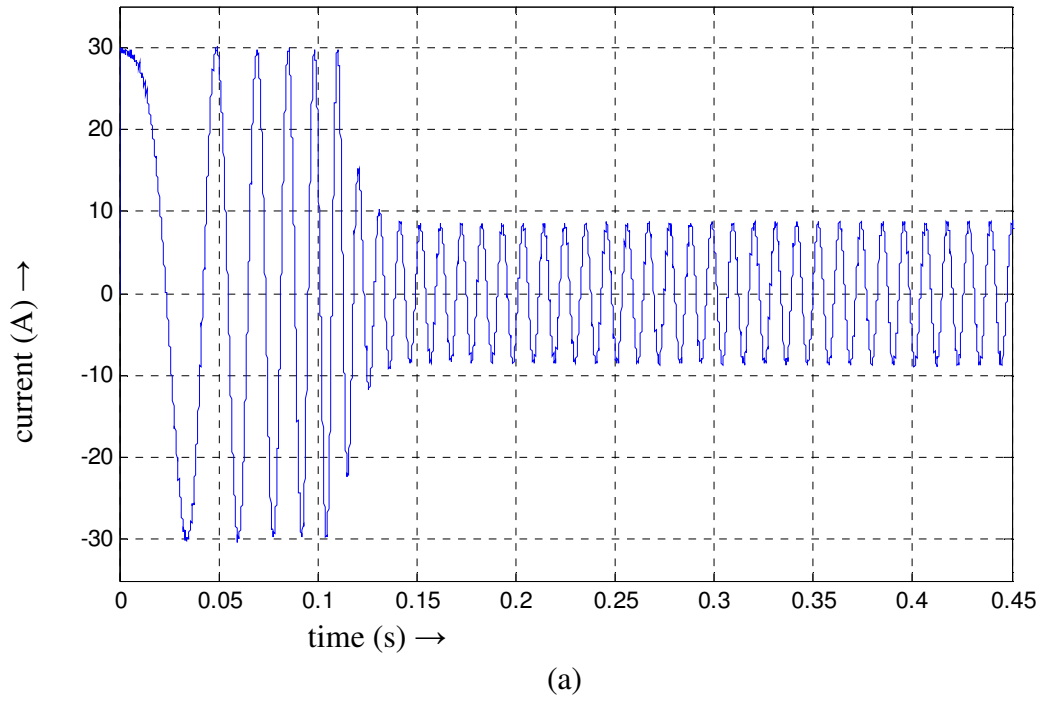

(a)

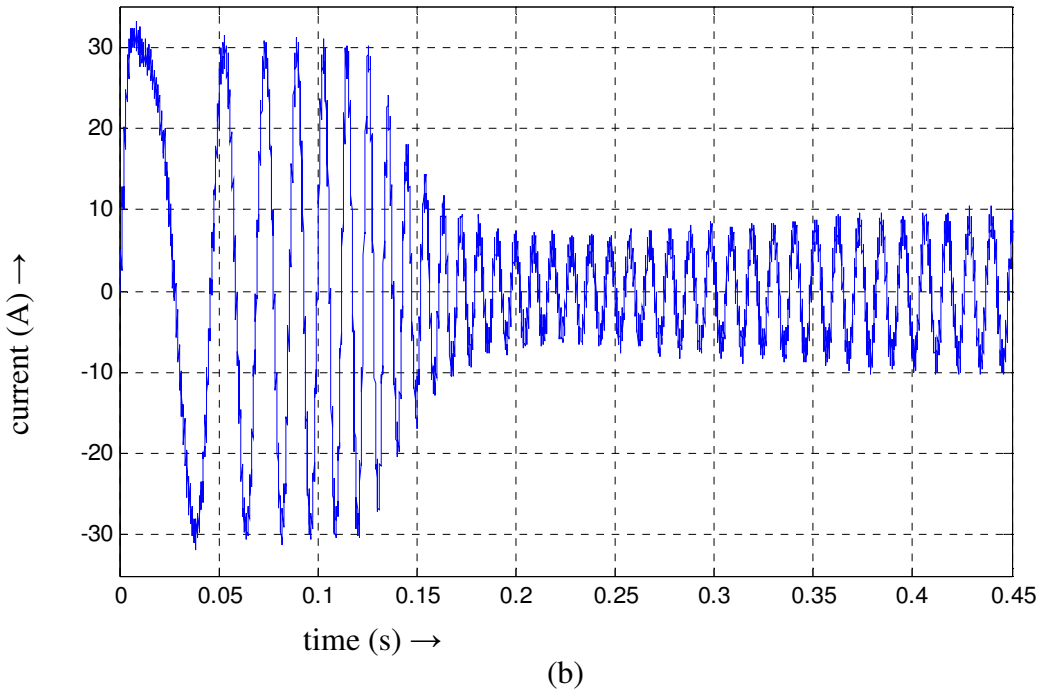

(b)

Figure 3.18: Phase current responses of IPMSM drives at rated speed (183 rad/s) and 50% rated load (9.55 N-m), a) FLC based tuned PI with hysteresis band adaptation, b) conventional PI.

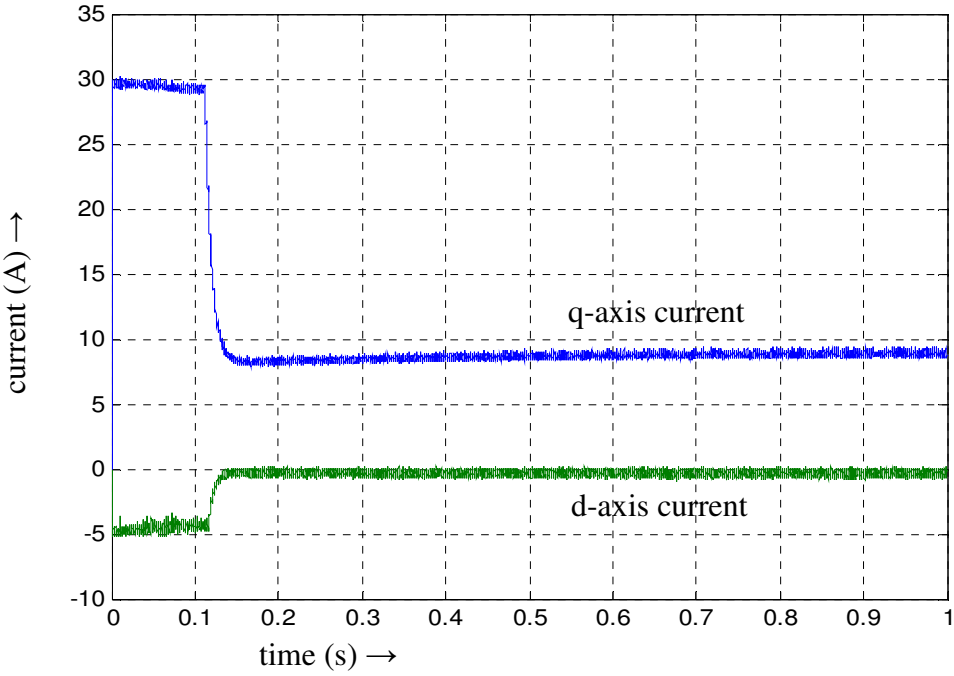

(a)

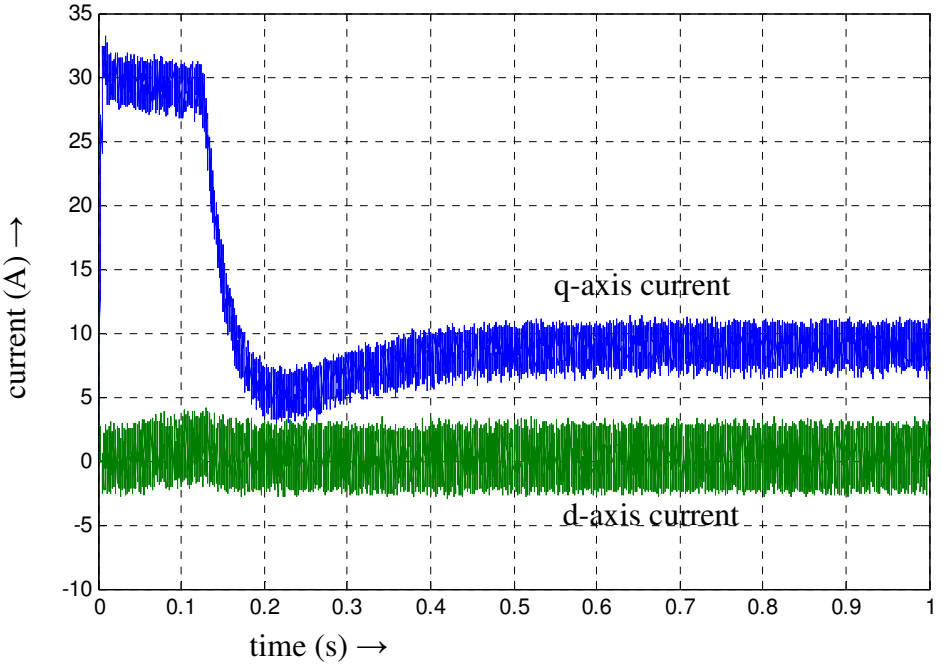

(b)

Figure 3.19: d-q axes current responses of IPMSM drives at rated speed (183 rad/s) and 50% rated load (9.55 N-m), a) FLC based tuned PI with hysteresis band adaptation, b) conventional PI.

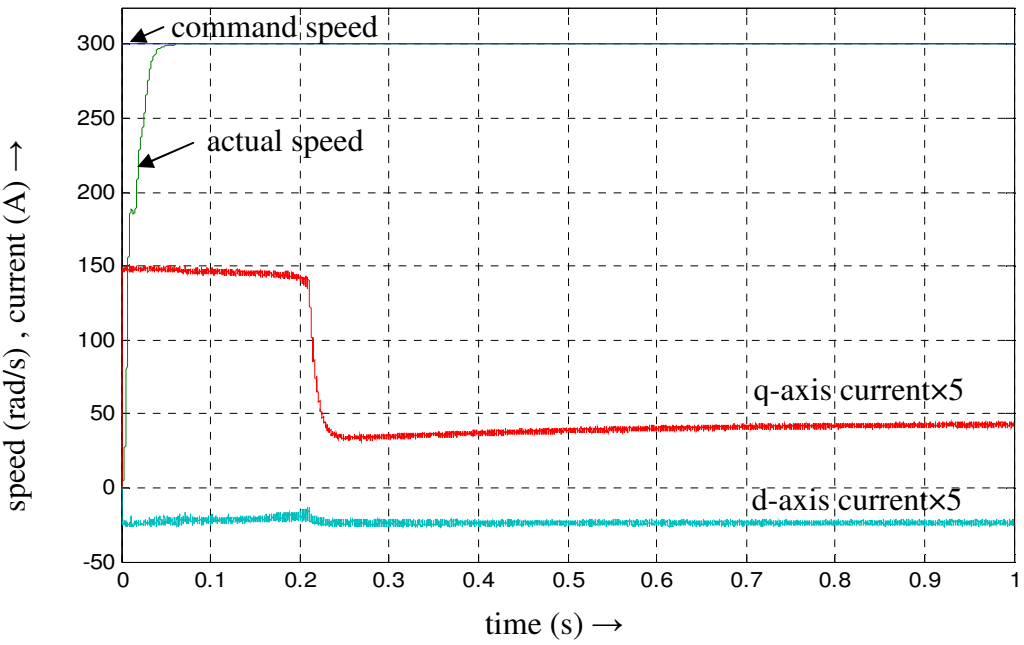

Figure 3.20: Initial high speed (300 rad/s) response and corresponding d-q axes current responses of the proposed IPMSM drive at 50% rated load (9.55 N-m).

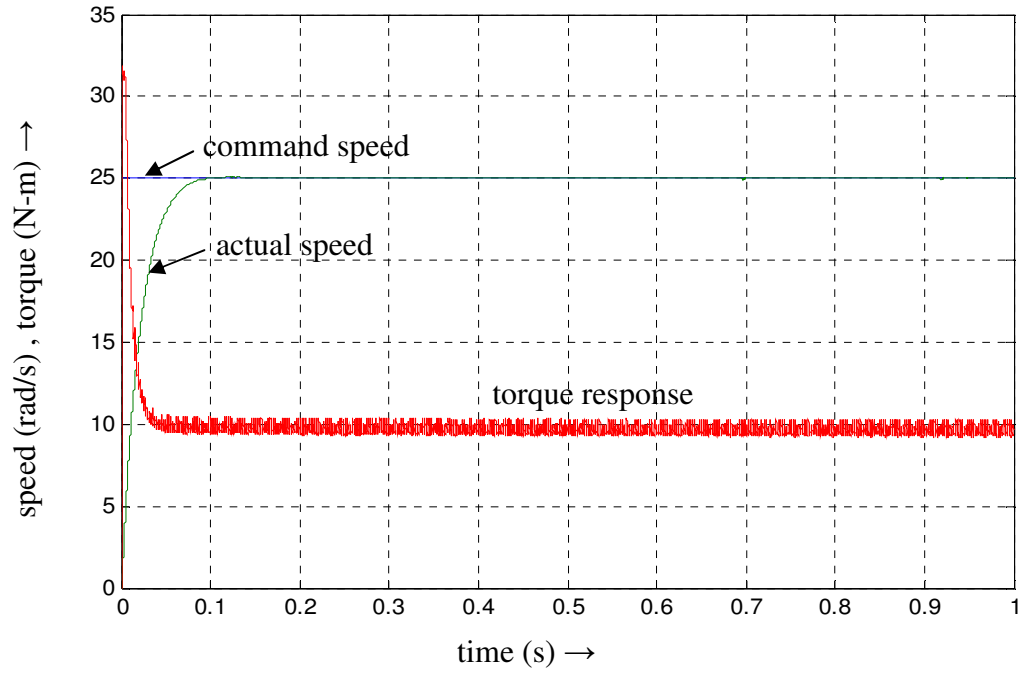

Figure 3.21: Initial low speed (25 rad/s) response and corresponding torque response of the proposed IPMSM drive at 50% rated load (9.55 N-m).

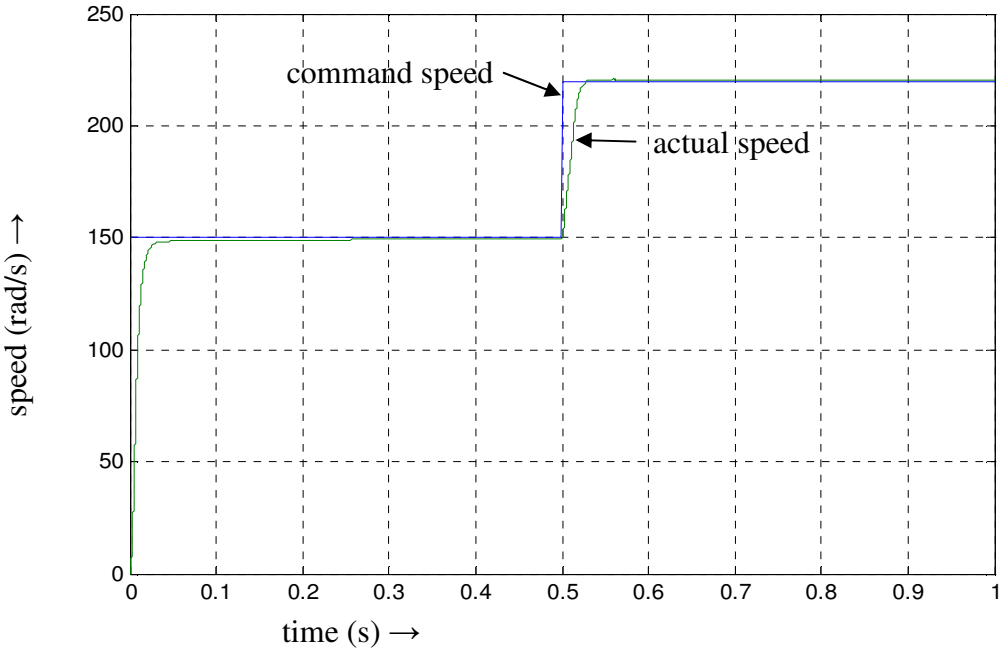

(a)

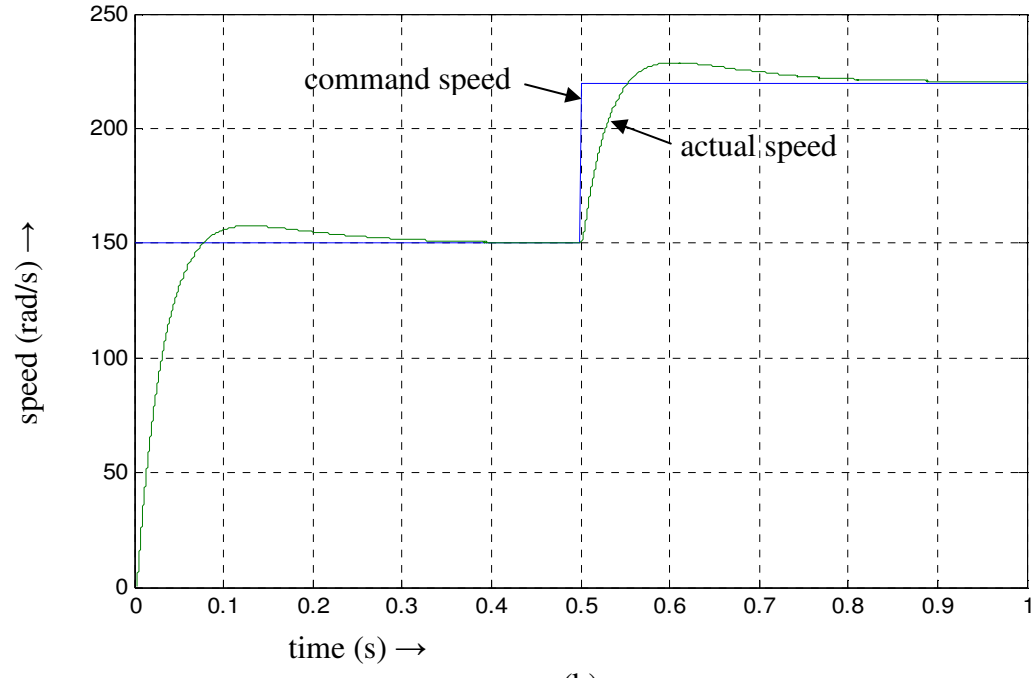

(b)

Figure 3.22: Speed responses of IPMSM drives at 50% rated load (9.55 N-m) with abrupt speed change from 150 rad/s to 220 rad/s at t=0.5s, a) FLC based tuned PI with hysteresis band adaptation, b) conventional PI.

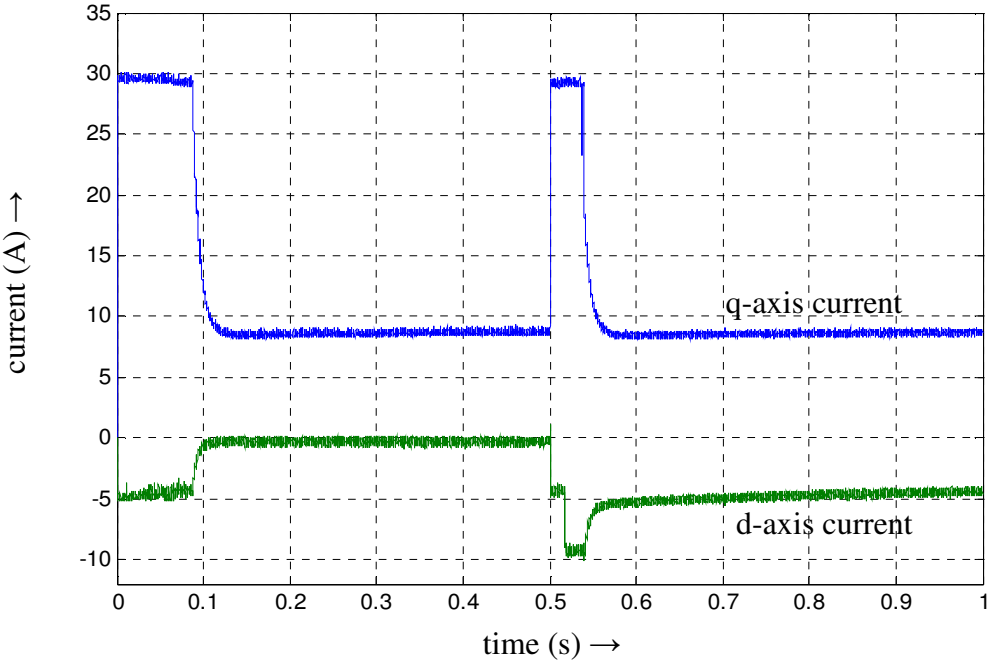

(a)

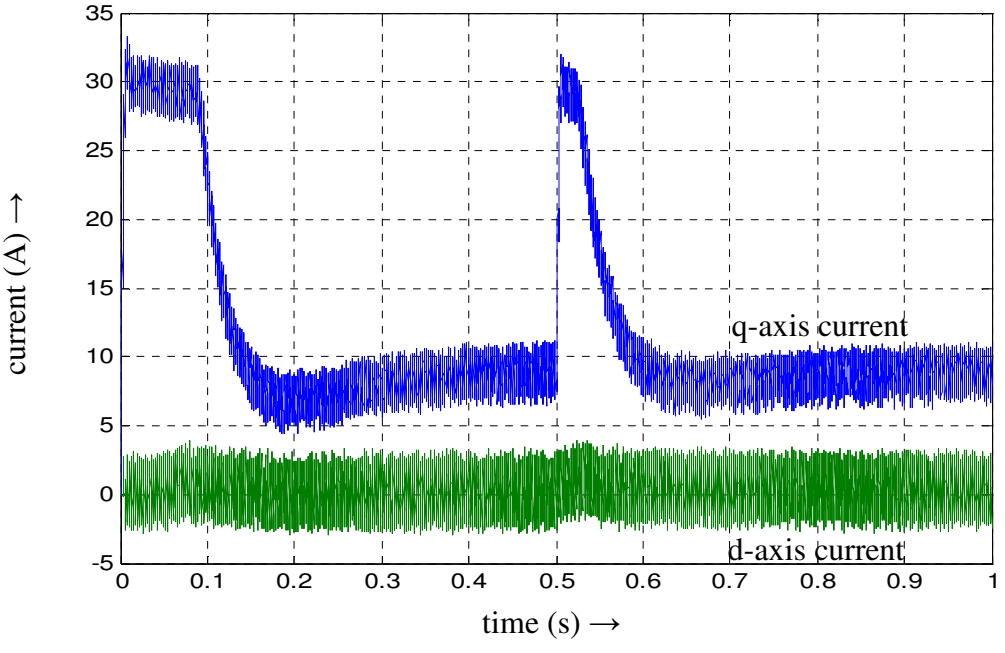

(b)

Figure 3.23: d-q axes current responses of IPMSM drives at 50% rated load (9.55 N-m) with abrupt speed change from 150 rad/s to 220 rad/s at t=0.5s, a) FLC based tuned PI with hysteresis band adaptation, b) conventional PI.

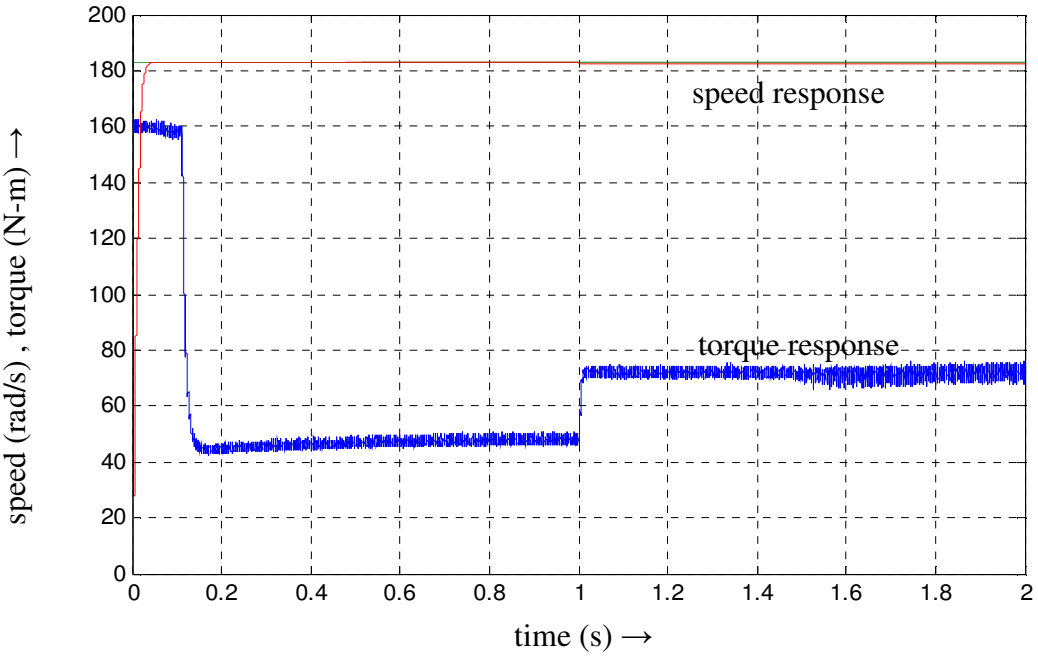

(a)

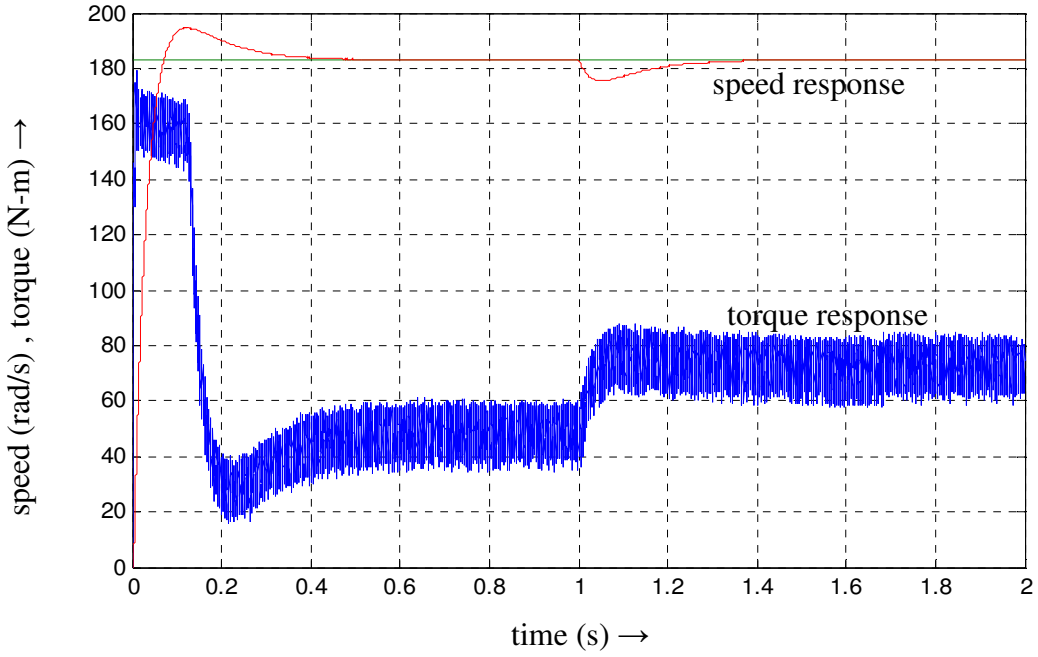

(b)

Figure 3.24: Speed and torque (5 times scaled) responses of IPMSM drives at rated speed (183 rad/s) with abrupt load change from 50% (9.55 N-m) to 75% (14.325 N-m) rated load at t=1s, a) FLC based tuned PI with hysteresis band adaptation, b) conventional PI.

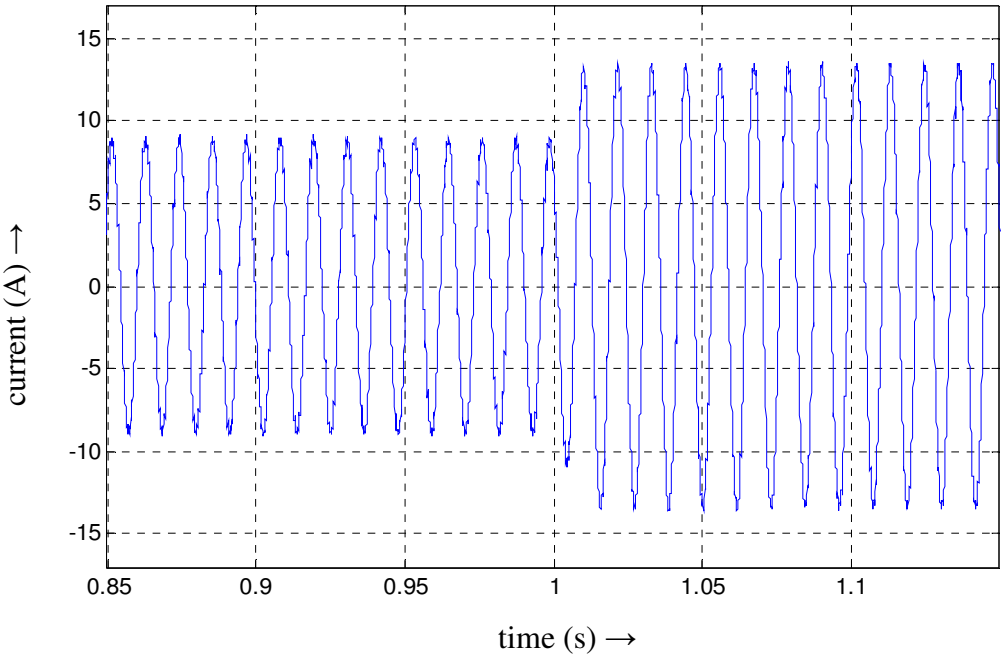

(a)

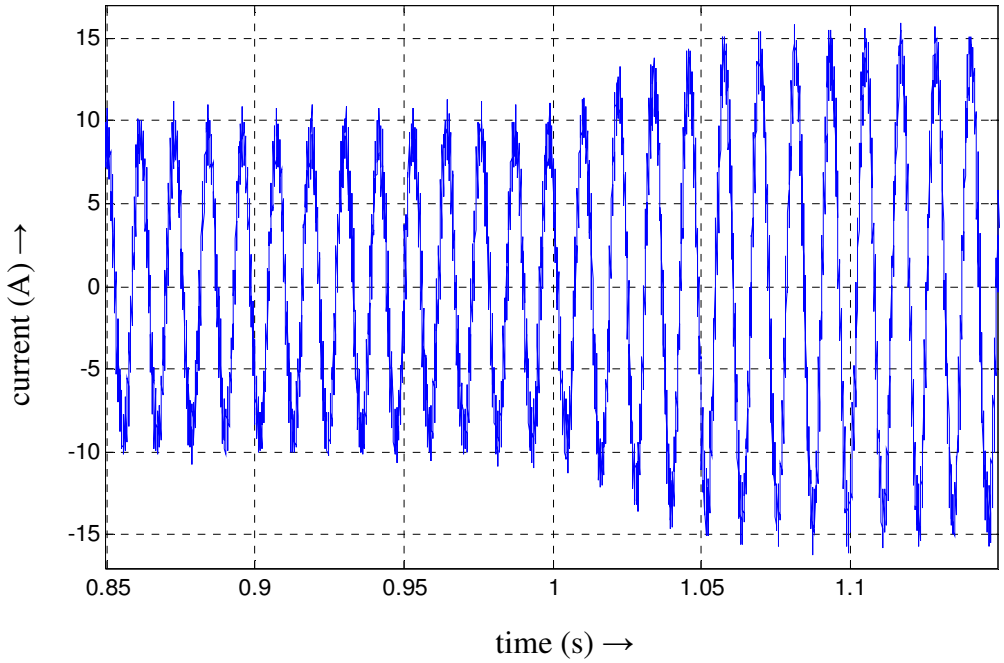

(b)

Figure 3.25: Phase current responses of IPMSM drives at rated speed (183 rad/s) with abrupt load change from 50% (9.55 N-m) to 75% (14.325 N-m) rated load at t=1s, a) FLC based tuned PI with hysteresis band adaptation, b) conventional PI.

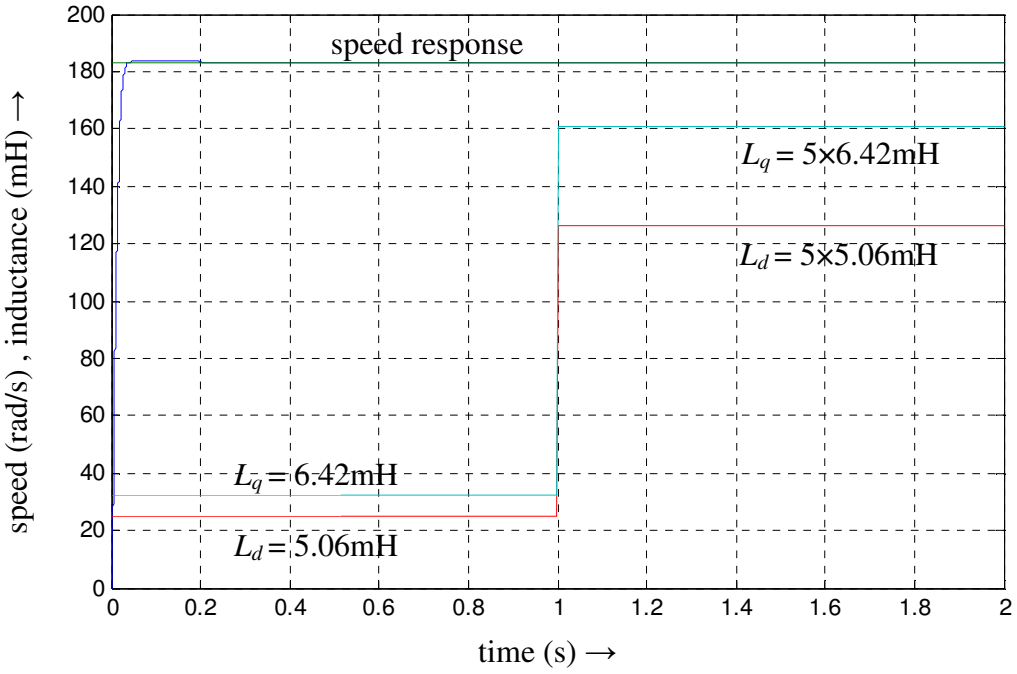

(a)

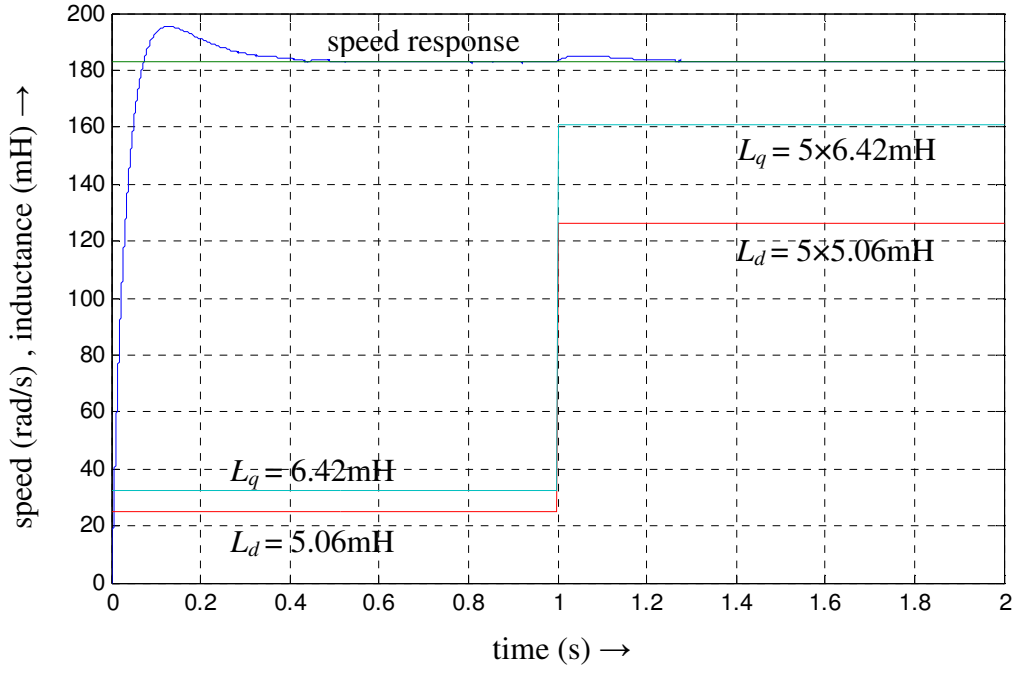

(b)

Figure 3.26: Speed responses of IPMSM drives at rated speed (183 rad/s) and 50% rated load (9.55 N-m) with abrupt change of L_d and L_q (5 times increase) at t=1s, a) FLC based tuned PI with hysteresis band adaptation, b) conventional PI.

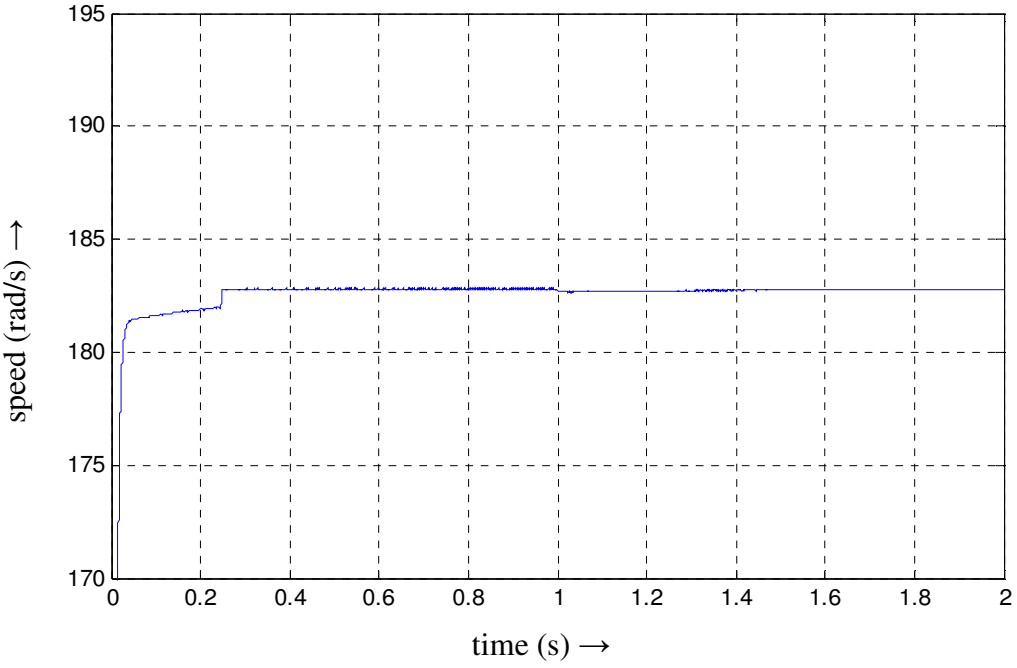

(a)

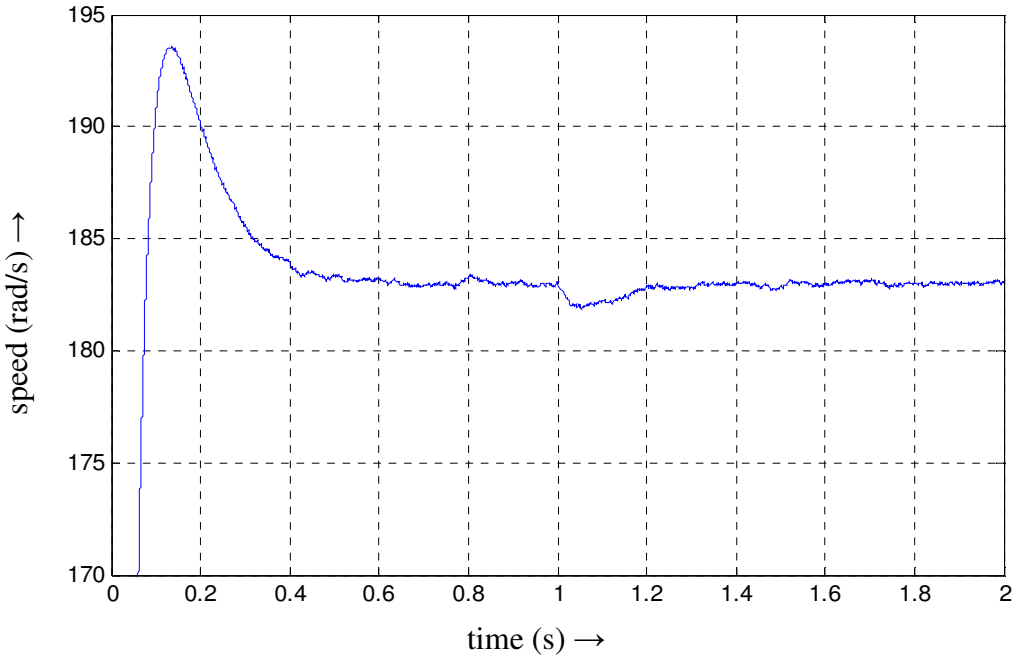

(b)

Figure 3.27: Speed responses of IPMSM drives at rated speed (183 rad/s) and 50% rated load (9.55 N-m) with abrupt change of B_m and r_s (5 times increase) at t=1s, a) FLC based tuned PI with hysteresis band adaptation, b) conventional PI.

load change. It shows that the proposed drive takes lower amplitude and less noisy current than PI based drive, and it also smoothly shifts the amplitude level during load transition.

The adaptability of the drives to parameter variations is also tested and the investigation results are presented in Figs. 3.26 and 3.27. Speed responses of the drives with abrupt five-fold increase of both d-q axes inductances at t=1s are shown in Fig. 3.26. This figure implies that the PI based drive responds with a significant speed overshoot during inductance change but the proposed drive remains insensitive to the same change. In case of Fig. 3.27, the stator resistance R_s and friction damping constant B_m are increased five times abruptly at t=1s. Again in this case, the proposed drive absorbed the change comfortably whereas the PI based drive suffers a dip in speed.

3.7 Concluding Remarks

In this chapter, a novel IPMSM drive scheme incorporating an FLC based tuned PI speed controller and another FLC based adaptive hysteresis current controller, and a flux controller has been proposed. The proposed system design and development has been explained step by step with discussion of relevant fuzzy logic theory and flux weakening theory. Simulation model of the proposed drive has been developed using Matlab/Simulink. Finally, simulation results have been presented to investigate and compare the performance of the proposed drive with conventional PI controller based drive. Simulation results demonstrate that the proposed drive yields better performance than the conventional PI controller based drive at different dynamic conditions like speed, load and parameter variations.

Chapter 4

Real-time Implementation

4.1 Introduction

In this chapter, the experimental implementation procedure for the proposed interior permanent magnet synchronous motor (IPMSM) drive incorporating FLC based tuned PI with hysteresis band adaptation is provided. The proposed drive is implemented in real-time using DSP controller board DS1104 for a laboratory 5 HP IPMSM. First the experimental setup and both hardware and software implementation of the drive are described in detail. Then the obtained experimental results are presented and discussed to verify the effectiveness of the proposed scheme in real-time.

4.2 Experimental Setup

The block diagram of hardware schematic for experimental setup of the drive is shown in Fig. 4.1. It shows the closed loop connection of the IPMSM with DSP controller board DS1104 inside a computer, three-phase rectifier-inverter and other peripheral devices. The IPMSM is fed by the inverter driven by the six PWM gating signals generated by the DS1104 board via an interface base drive circuit. The DSP board also takes speed signal and current inputs from an encoder mounted on the rotor and from Hall-effect currents sensors respectively which are also shown in Fig. 4.1. The board also

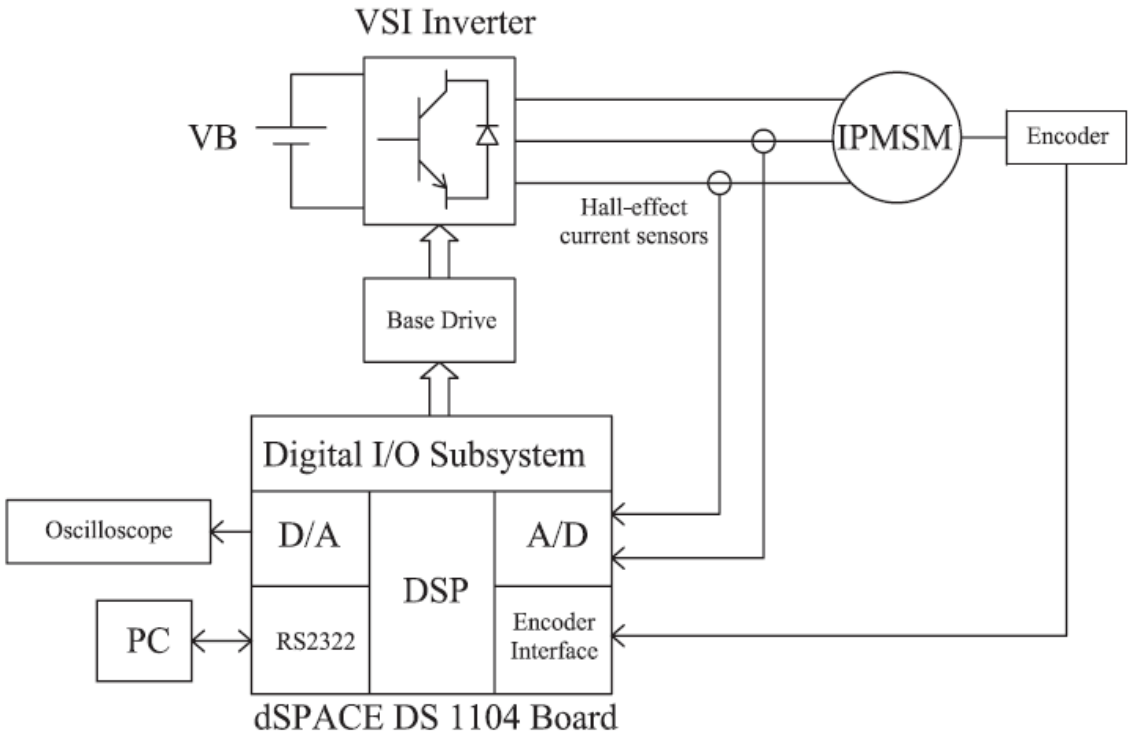

Figure 4.1: Block diagram of the experimental setup.

gives the provision to display waveforms in oscilloscope from its D/A ports. The DSP board, encoder and current sensors will be further discussed in the next section.

The snapshots of the experimental setup are presented in Figs. 4.2 and 4.3 with symbols for the different parts and devices associated. In Fig. 4.2, the test IPMSM is labelled as ‘M’. The optical incremental encoder ‘E’ is directly connected to the rotor shaft of the IPMSM to measure the rotor position. The motor is coupled with a DC generator (L) which works as a loading machine to the motor. The actual motor currents are measured by the two Hall-effect current transducers (CS). These current sensors have a linear response over a wide range of frequencies up to 250 kHz. The DSP controller board DS1104 is actually installed inside the desktop computer (PC) and the oscilloscope (OSC) is placed beside it. The power circuit consists of a three-phase variable ac

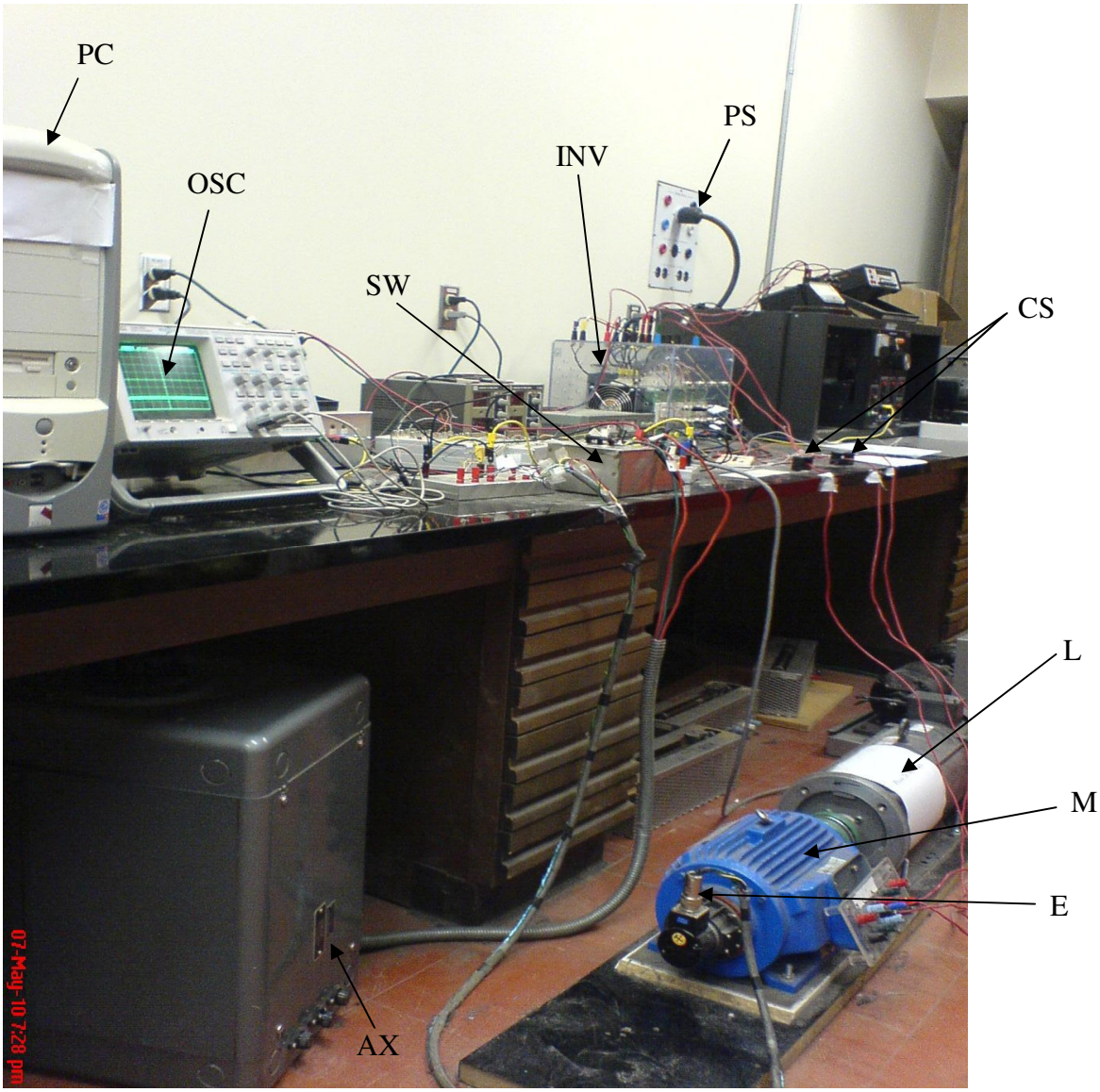

Figure 4.2: Snapshot of the experimental setup of the proposed IPMSM drive.

autotransformer (AX), power supply (PS) and a three-phase IGBT rectifier-inverter (INV). The variable three-phase input ac power of the rectifier is supplied by the autotransformer (AX) through a single pole single throw (SPST) switch (SW). The DC bus voltage of the voltage source inverter (VSI) is obtained by rectifying three-phase ac voltage and then it is filtered by a large capacitor of approximately 1000μF. This inverter

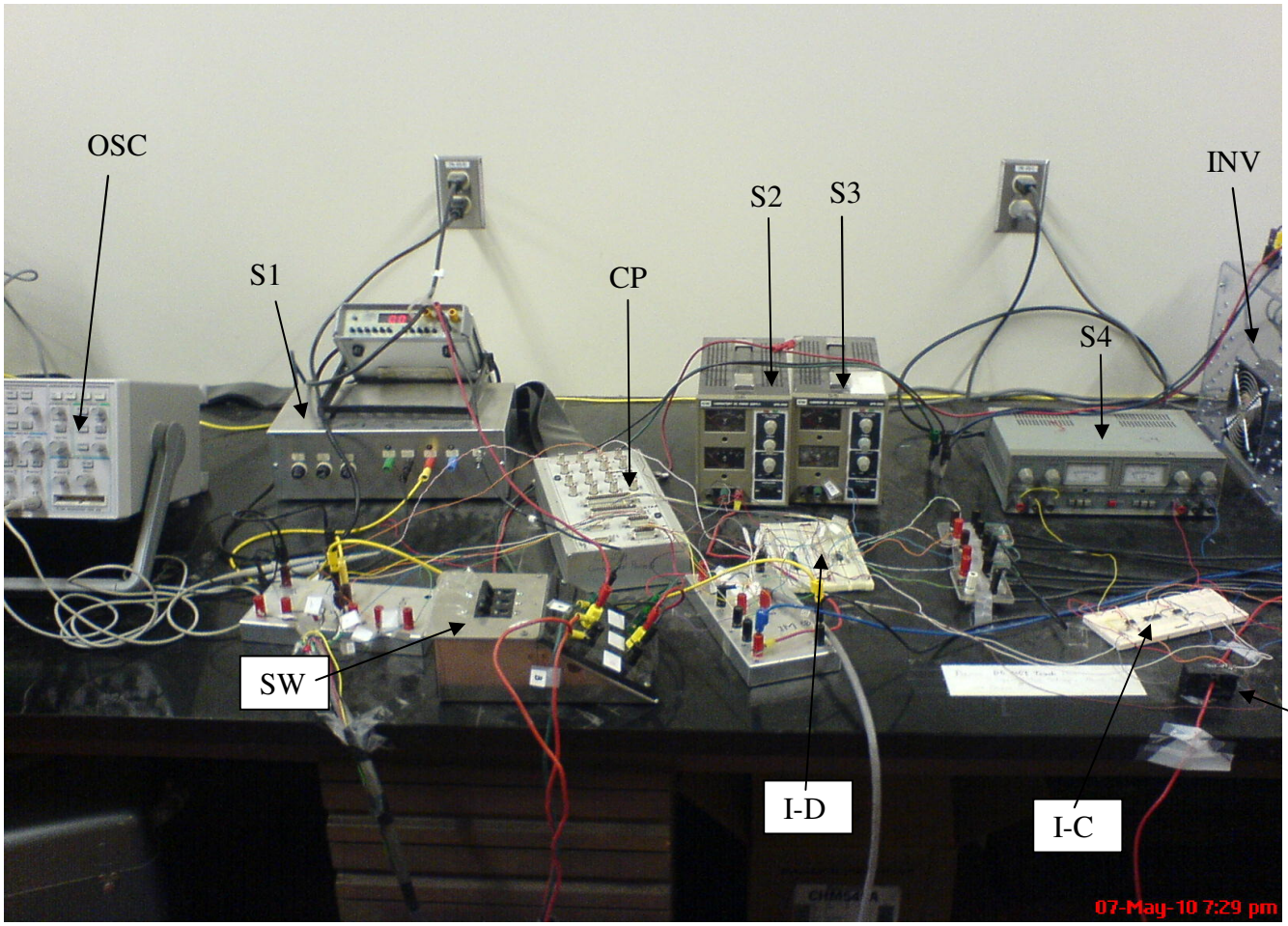

Figure 4.3: Snapshot of the experimental setup (close-up view).

has active security features against short circuit, under voltage of power supply as well as built-in thermal protection which prohibits destructive heat sink temperatures within the device. The interface drive circuits, the voltage sources and the connector panel are visible in Fig. 4.3. The current interface circuit (I-C) is placed in a breadboard between the Hall-effect current sensors (CS) and the A/D channel of the DSP board. The gate drive circuit is built-in with the inverter. The inverter gate drive interface circuit (I-D) on another breadboard is used to increase the voltage and power level of the firing pulses so that they are sufficient enough to drive the IGBT switches of the inverter. The voltage

source S1 is used to power up the encoder and voltage sources S2, S3, S4 are used to bias the interface circuit's chips. The connector panel CP1104 of the DSP board is labelled as 'CP' in Fig. 4.3 which will be further discussed in the next section.

4.3 DSP Based Hardware Implementation

The DSP controller board DS1104 board is specifically designed for the development of high-speed multivariable digital controllers and real-time simulations in various fields. The board is plugged into a PCI slot inside an Intel desktop computer with uninterrupted communication capability through dual port memory. The block diagram of the hardware schematic of the DS1104 board is shown in Fig. 4.4. The DS1104 board is mainly based on a 64-bit PowerPC type PPC603e processor. This processor operates at the clock frequency of 250 MHz with 32 kB cache memory. This board has a 32 MB of SDRAM global memory and 8 MB of flash memory. The DSP is also supplemented by a set of on-board peripherals used in digital control systems including analog to digital (A/D) converter, digital to analog (D/A) converter and digital incremental encoder interfaces. This board is also equipped with a Texas Instruments TMS320F240 16-bit DSP microcontroller that acts as a slave processor and provides necessary digital I/O ports configuration, and powerful timer functions such as input capture, output capture and PWM signal generation [87]. In this work, the slave processor is used only for digital I/O subsystem configuration. The PC-based controller generates and sends the numerical switching signals to the DSP board, whereas the outputs of the DSP board are sent to the interface gate drive circuit (I-D) to drive the VSI inverter (INV) IGBT switches.

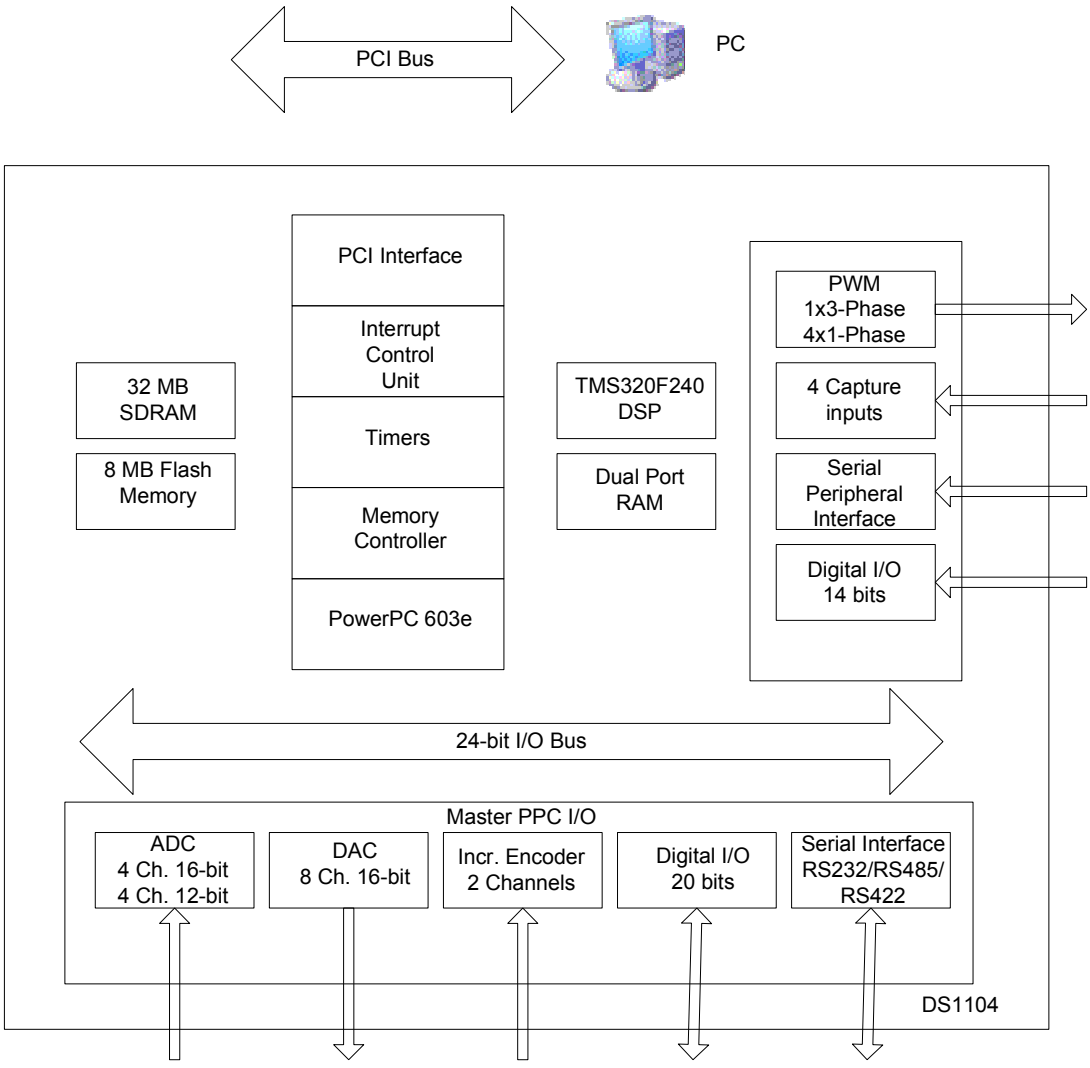

Figure 4.4: Block diagram of the hardware schematic of DS1104 board.

A connector panel (CP) is used to ensure high-density connection between the DS1104 board and the external devices, and easy access to all the input and output signals. The connector panel is connected with the DS1104 board via an adapter cable. It actually provides easy-to-use connections between the DS1104 controller board and the devices to be connected to it. Devices can be individually connected, disconnected or interchanged without soldering via BNC connectors and Sub-D connectors. This

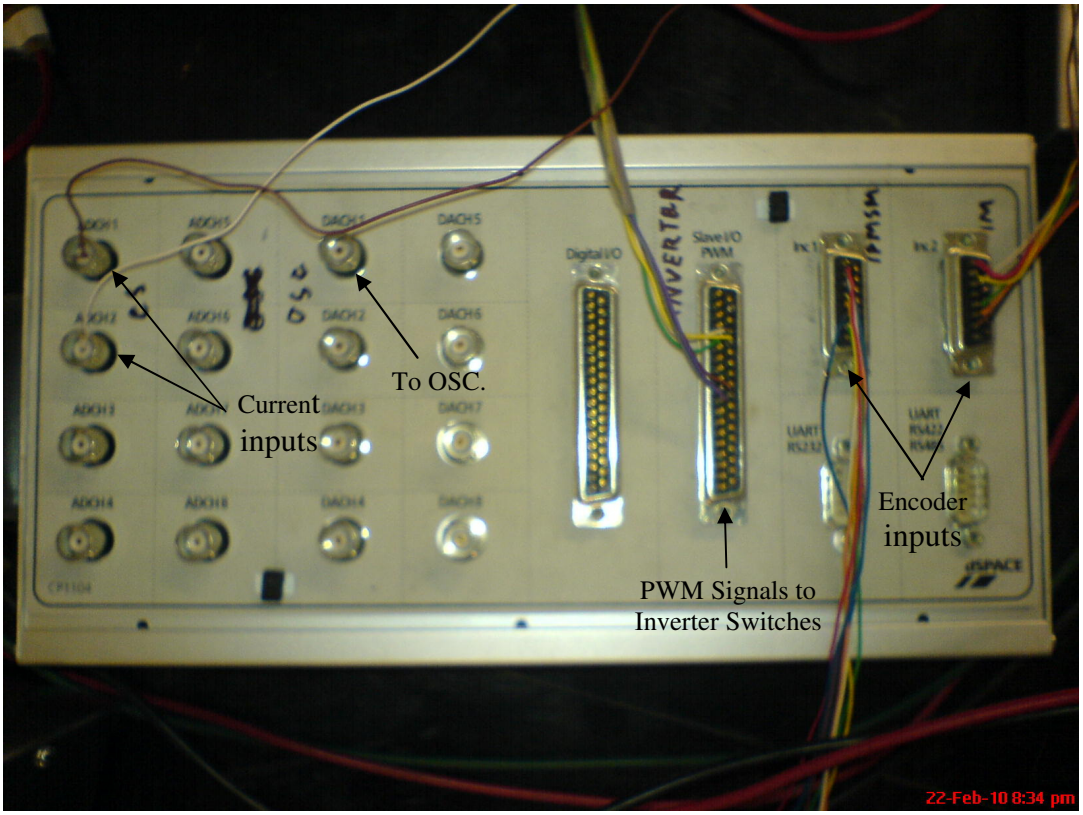

Figure 4.5: Snapshot of the connector panel CP1104.

simplifies system construction, testing and troubleshooting [87]. The snapshot of the connector panel is shown in Fig. 4.5.

The rotor position is measured by an optical incremental encoder mounted at the rotor shaft of IPMSM and is fed back to the DS1104 board via the connector panel (CP). The optical encoder used in this experiment generates 1024 pulses per revolution. In order to get a better resolution, the output of the encoder is increased to 4×1024 pulses per revolution by using a built-in 4-fold pulse multiplication. Thus the effective resolution of the encoder is 0.087890625° or 5.2734375′. These pulses are fed to the one of two digital incremental encoder interface channels on the connector panel. A 24-bit position counter is used to count the encoder pulses and is read by a calling function in

the software program. The counter is reset in each revolution by the index pulse generated from the encoder.

The actual motor currents are sensed by the Hall-effect sensors (model CS100A-P), which have current range of 0 ~ ±200A and a frequency range of 0-250 kHz. Its nominal current is ±100A and turns ratio is 2000/1. So the nominal output current is 50mA. The output current signal of these sensors is converted to a voltage signal across the resistor connected between the output terminal of the sensor and ground. The output voltage can be scaled by selecting the value of the resistors which can be within the range of 0-100Ω. As the output voltages from these current sensors are very low, a current interface circuit (I-C) is required to amplify the output of the sensor and also to reduce the noise. The interface circuit consists of two non-inverting amplifiers for phase-a and phase-b forming by operational amplifier LM741CN. Then these amplified signals are fed back to DSP board through A/D channels. As the motor neutral is not grounded, only phase-a and phase-b currents are measured in this experiment and phase-c current is calculated using Kirchhoff's Current Law in the developed Simulink model. The resistors used (R1, R2, R3) for both current sensors and operational amplifiers have been mentioned in Appendix-C and respective gains have been calculated there.

The command phase currents are generated from the proposed controller in the Simulink model and compared with the actual sensed currents. This generates the six logic signals which act as the gating pulses for the six IGBT switches of the three-phase inverter. These six logic signals are the output of the DS1104 Board. But these outputs of the digital I/O subsystem have magnitudes of only +5V which are not sufficient enough to drive the IGBTs requiring +15V voltage levels. Therefore, these voltage signals are

first fed to the base drive circuit (I-D) to shift the voltage level from +5V to +15V. Then the drive circuit provides the appropriate +15V gating signals for the IGBT switches. In this work, DM7407N is used as the driver chip. Both current interface circuit (I-C) and gate drive interface circuit (I-D) are provided in Appendix-C.

4.4 Real-time Software Development

In order to implement the proposed IPMSM drive, a real-time Simulink model is developed as shown in Appendix-D. Now the DS1104 board is a self-reliant system and not an embedded system. So the host PC does not perform any processing for a system implemented on this board. Therefore, the DS1104 board requires that real-time model to be created and downloaded to it for the system to function. The real-time model is built and downloaded to the DS1104 board using the dSPACE ControlDesk software [87]. The ControlDesk software is also used to start and stop the function of the board as well as create a layout for interfacing with global variables in dSPACE programs. The sampling frequency used in this experiment is found to be 5kHz. If higher sampling frequency is chosen, the 'overrun error' occurs, which indicates too much computational burden for the DS1104 processor. So the values of the currents and rotor position angle are read at every 200μs.

The motor currents obtained in the dSPACE program through analog to digital converter (ADC) channels l and 2 do not match the actual currents in terms of amplitude. So, before comparing with corresponding command currents, they must be multiplied by appropriate gains in order to obtain the actual current values in software. These gain values depend on the Hall-effect sensors' specifications, the resistors used at the output

node of these sensors and the resistors used in the interface circuit. Another problem is that those current waves are also vertically shifted downwards. So vertical balance offsets or compensation values have to be calculated and applied to ensure that the current waves oscillate around time axis and have zero average value. To calculate appropriate gains and offsets, a separate open loop test was performed. In this test, single-phase ac supply is applied across a 45Ω load. The current across the load was measured by an ammeter (rms value) and that same current signal passing through current sensor was observed in ControlDesk software. The rms value obtained in the ControlDesk program was compared with the ammeter value to calculate the required gain. Also the positive and negative peaks of the sinusoidal current waveform were noted down and required offset balance was obtained by simple calculation. This test is performed with seven observations each for both the current sensors. The test data for phase-a and phase-b current sensors are provided in Table 4.1 and Table 4.2. Finally the gains for phase-a and phase-b were found to be nearly 47 and 55.3 respectively, whereas the balance offsets were calculated to be 0.0035 and 0.003 respectively. The load current using phase-a current sensor and with appropriate gain and offset is shown in Fig. 4.6 which implies that the waveform has zero average value.

The rotor position angle is sensed by the optical incremental encoder. As discussed in the last section, the index pulse is generated by the encoder to reset the counter to zero after each revolution completed which means that the maximum rotor angle equals to 2π. So the rotor position angle can be calculated in radian by the formula 2π/1024. Then the rotor speed is calculated from the measured rotor position angles using numerical backward differentiation. The speed error between actual and command speed

Table 4.1: Required Offset and Gain calculation for Phase-A Current Sensor

Obs.	I_{rms} (ammeter)	I_{rms} (dSpace)	Gain Required	Positive peak (dSpace)	Negative peak (dSpace)	Vertical Offset balance
1	0.5A	0.011136932A	44.89566865	0.0125A	-0.019A	0.00325
2	0.7A	0.014495689A	48.2902192	0.017A	-0.024A	0.0035
3	1A	0.021213203A	47.14045208	0.026A	-0.034A	0.004
4	1.2A	0.025279067A	47.47010559	0.0325A	-0.039A	0.00325
5	1.5A	0.031819805A	47.14045208	0.042A	-0.048A	0.003
6	1.7A	0.036062446A	47.14045208	0.048A	-0.054A	0.003
7	2A	0.04277996A	46.75086157	0.056A	-0.065A	0.0045
Average:			46.97545875			0.0035

Table 4.2: Required Offset and Gain calculation for Phase-B Current Sensor

Obs.	I_{rms} (ammeter)	I_{rms} (dSpace)	Gain Required	Positive peak (dSpace)	Negative peak (dSpace)	Vertical Offset balance
1	0.5A	0.01A	50	0.011A	-0.017A	0.003
2	0.7A	0.01A	70	0.017A	-0.023A	0.003
3	1A	0.02A	50	0.024A	-0.03A	0.003
4	1.2A	0.02A	60	0.029A	-0.035A	0.003
5	1.5A	0.03A	50	0.037A	-0.043A	0.003
6	1.7A	0.03A	56.67	0.042A	-0.048A	0.003
7	2A	0.04A	50	0.051A	-0.056A	0.0025
Average:			55.24			0.002928571

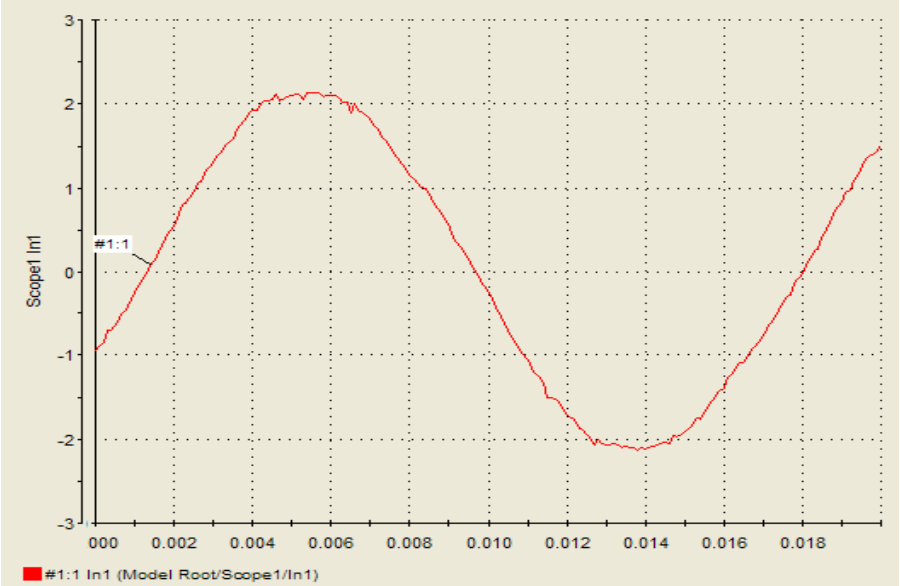

Figure 4.6: Load current waveform at dSPACE ControlDesk software after using calculated gain and vertical offset balance from Table 4.1 (using phase-a current sensor).

is then calculated. Using the speed error the reference d-q axes currents are calculated according to the proposed controllers explained in Chapter 3. Then the reference phase currents are obtained using Park's transformation equations. Finally those reference phase currents are compared with sensed and modified actual currents (as explained in the previous paragraph) to generate the PWM gating signals for the inverter. All off-to-on transitions of the PWM pulses are delayed by the dead time of 0.5ms in order to prevent the shorting of the dc bus voltage to ground. These pulses are sent to the inverter gates through digital I/O subsystem of the board and the base drive circuit.

4.5 Experimental Results and Discussion

Several experimental tests have been performed to verify the feasibility and effectiveness of the proposed FLC based tuned PI with hysteresis band adaptation based

IPMSM drive. Its performance is also compared with a conventional fixed gain PI controller based drive. The proportional and integral gains of the conventional PI controller are taken as 0.5 and 4 respectively as it was in the case of simulation tests in Chapter 3.

Experimental results are shown in Figs. 4.7 to 4.14. The initial real-time speed response of the proposed drive for a step change of command speed from zero to 120 rad/s at no load is compared with that of the conventional PI controller based drive, which is shown in Fig. 4.7. Here the PI based drive actually takes almost thrice the settling time of the proposed drive to reach the steady-state speed, 120 rad/s. Fig. 4.8 shows the speed responses for an online change of command speed abruptly from 100 rad/s to 140 rad/s for both the drives. In this case, it is clearly observed that the PI based drive takes nearly twice the settling time of the proposed drive to adjust to the new speed level. Dynamic phase current response of the proposed drive for a step change of command speed from 50 rad/s to 150 rad/s is shown in Fig. 4.9. This figure implies that the phase current smoothly adjusts to a higher frequency with the step change to higher speed without going through any distortion.

The flux weakening capability of the proposed drive is tested by running the motor above rated speed. Fig. 4.10 shows the starting speed response of the proposed drive for a step input of command speed of 220 rad/s. It is seen from this figure that the motor can follow the high command speed smoothly without any steady-state error.

The effect of hysteresis band adaptation on developed torque response of the proposed drive is demonstrated in Fig. 4.11 where it is observed that the developed torque ripple reduces considerably when the hysteresis band adaptation FLC was activated.

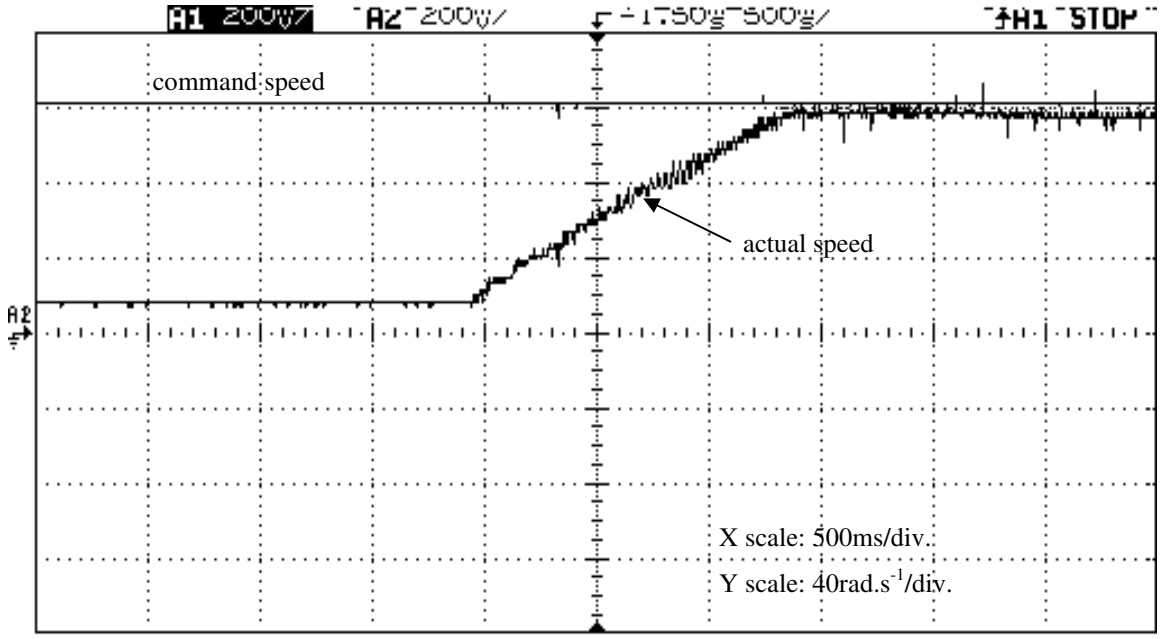

(a)

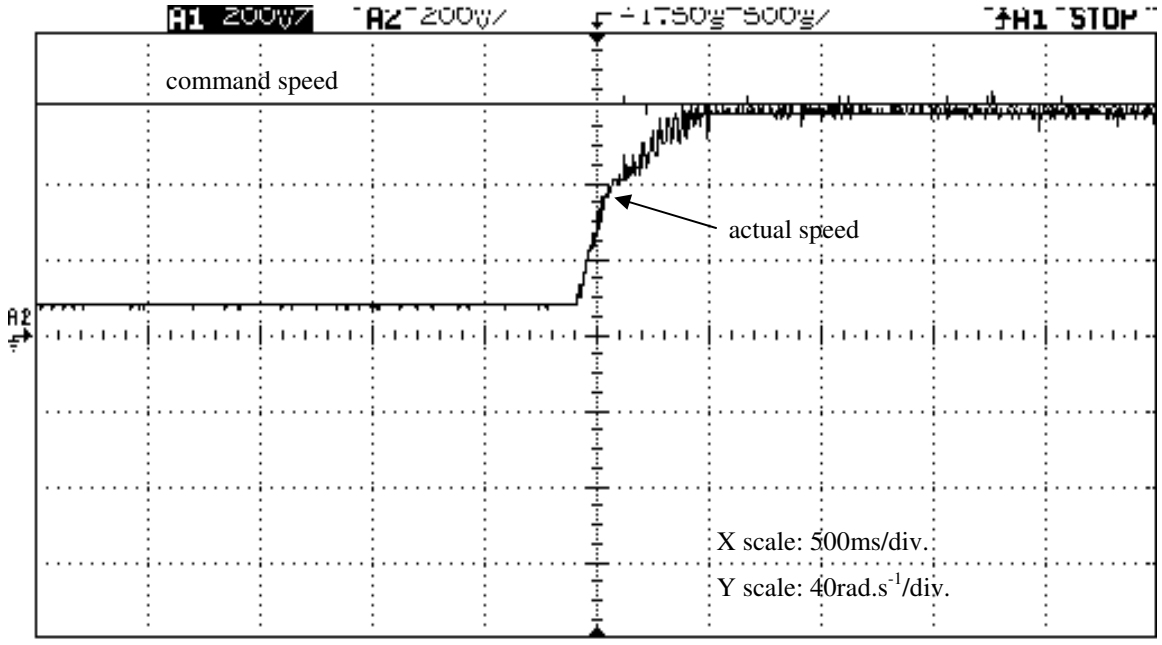

(b)

Figure 4.7: Initial speed responses with abrupt change of speed from zero to 120 rad/s at no-load condition, a) conventional PI controller based drive, b) proposed IPMSM drive.

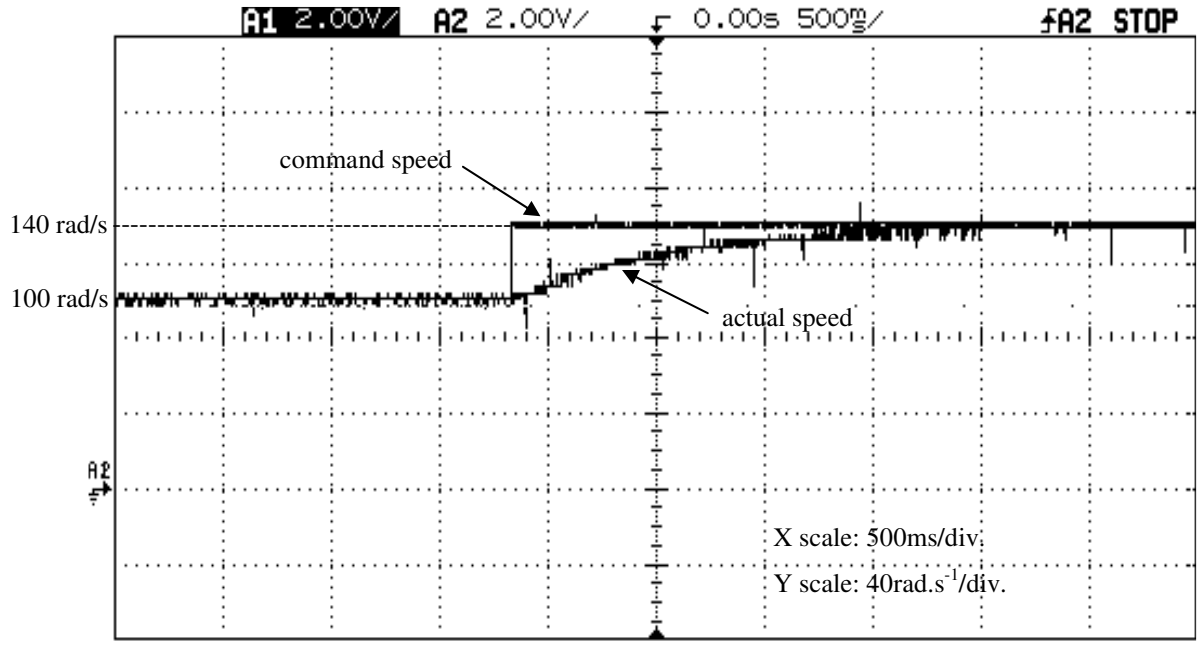

(a)

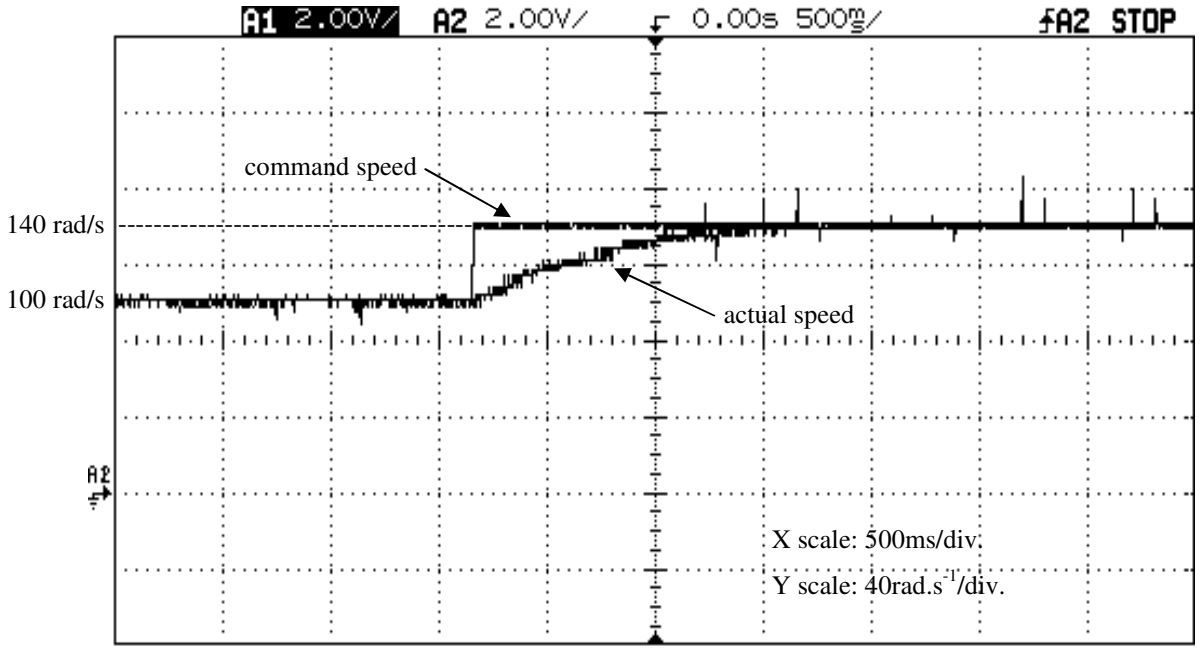

(b)

Figure 4.8: Dynamic speed responses with abrupt online change of speed from 100 rad/s to 140 rad/s at no-load condition, a) conventional PI controller based drive, b) proposed IPMSM drive.

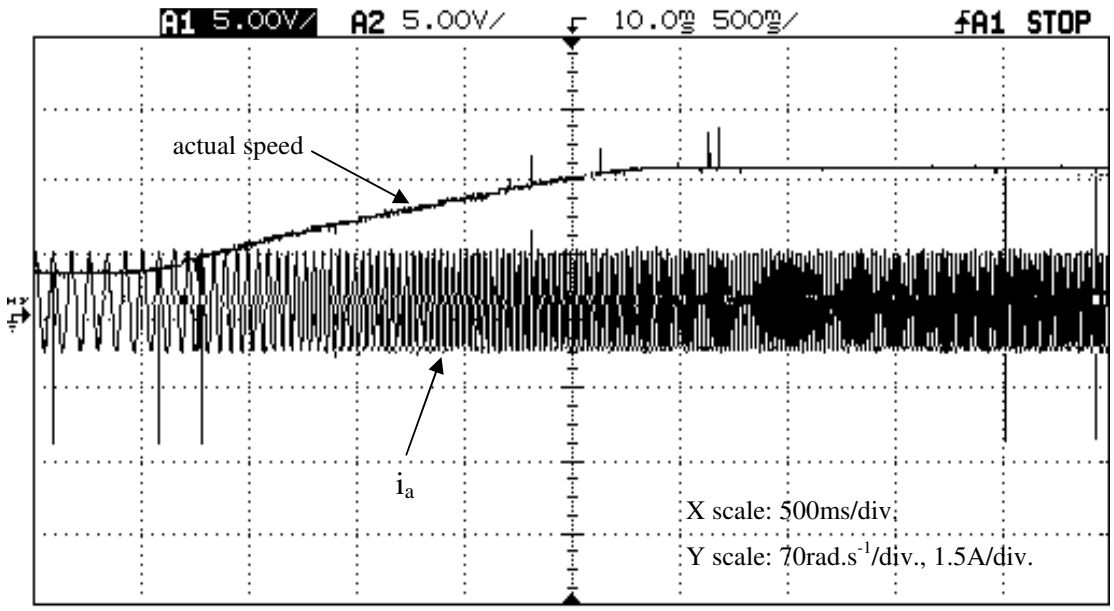

Figure 4.9: Dynamic speed response with corresponding phase-a current response of the proposed IPMSM drive with abrupt online change of speed from 50 rad/s to 150 rad/s at no-load condition.

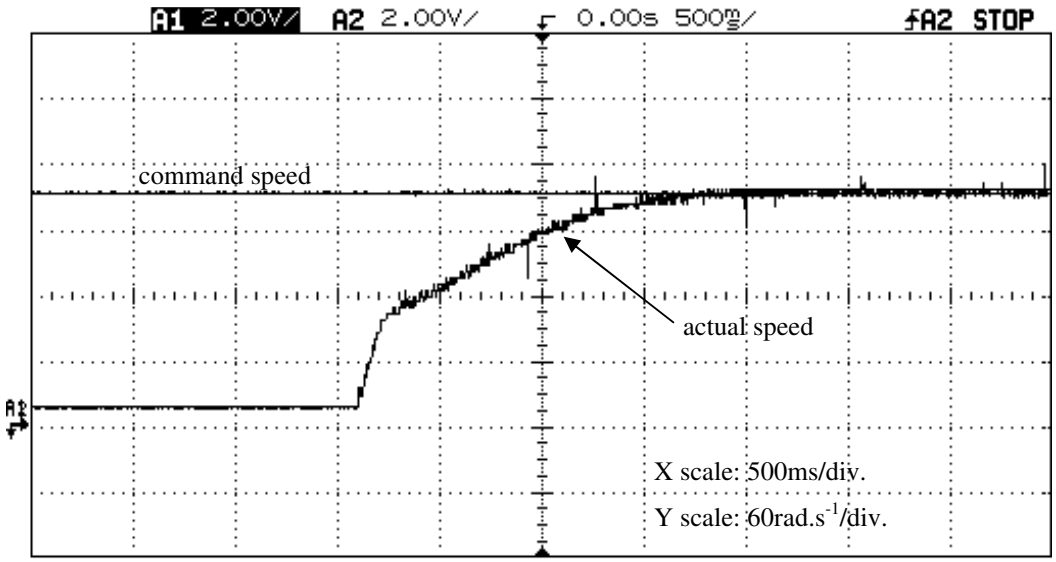

Figure 4.10: Initial high speed response of the proposed IPMSM drive with abrupt change of speed from zero to 220 rad/s at no-load condition.

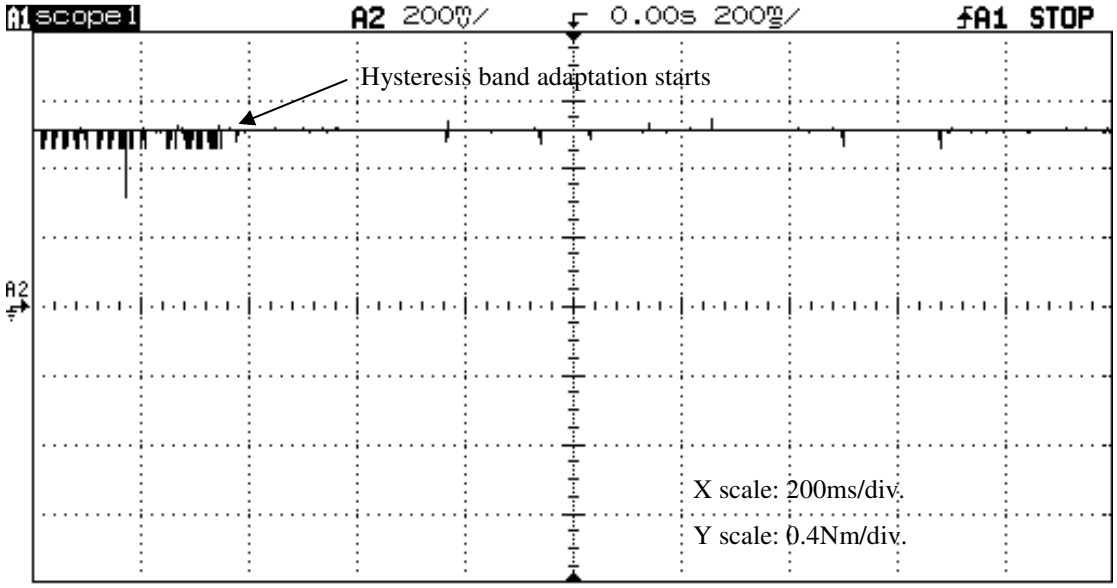

Figure 4.11: Steady state torque response of the proposed IPMSM drive at 140 rad/s speed before and after hysteresis band adaptation.

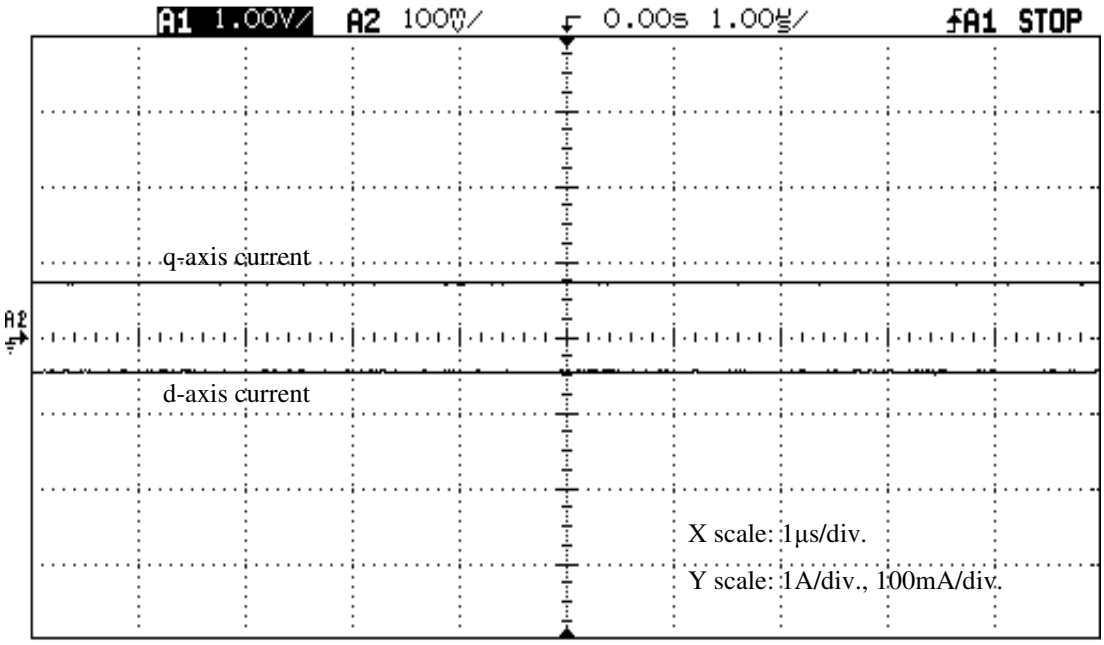

Figure 4.12: Steady state *d* and *q*-axis current responses of the proposed IPMSM drive at 140 rad/s speed at no-load condition.

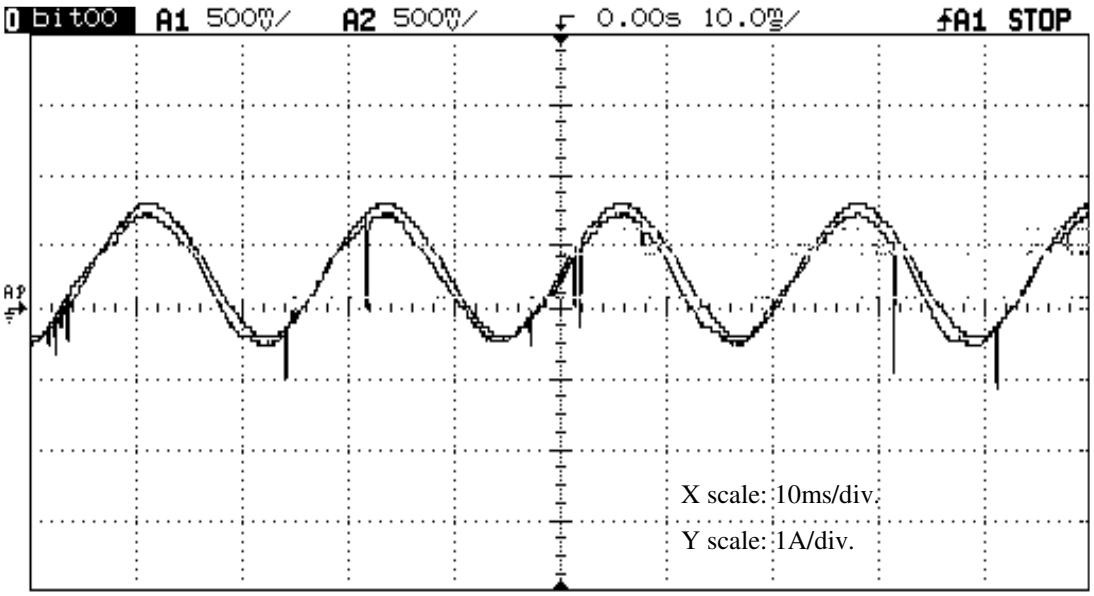

Figure 4.13: Steady state reference and actual phase-a current waveforms of the proposed IPMSM drive at 100 rad/s speed and no-load condition.

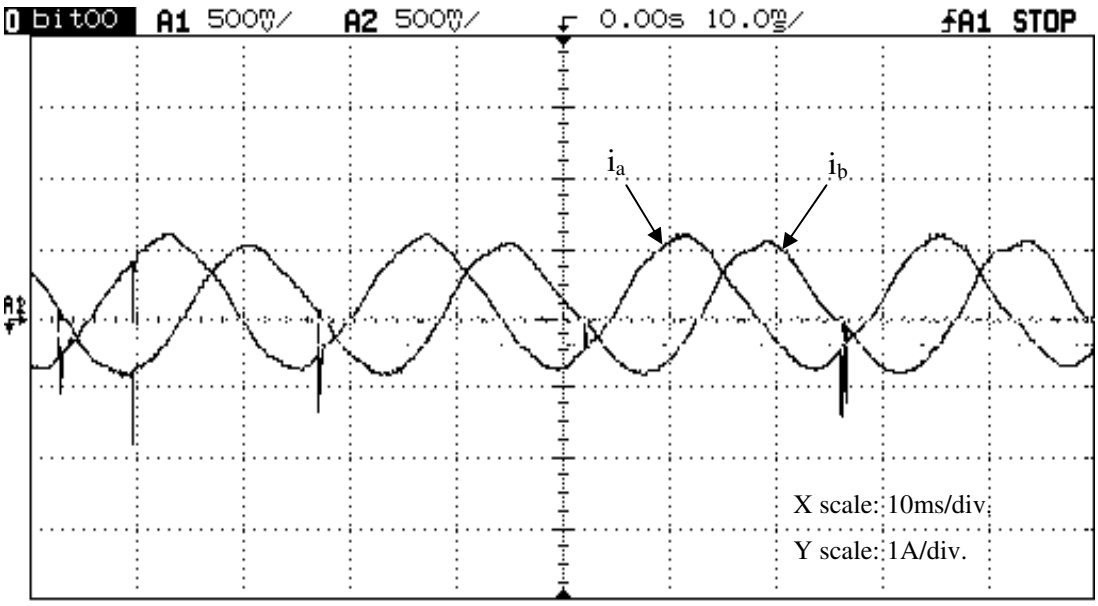

Figure 4.14: Steady state actual phase-a and phase-b current waveforms of the proposed IPMSM drive at 100 rad/s speed and no-load condition.

Steady state d-q axes current responses of the proposed drive at 140 rad/s speed and no load are shown in Fig. 4.12. Here the d-axis current is nonzero which indicates that the motor is developing some reluctance torque. Fig. 4.13 shows the steady state reference and actual phase-current waveforms of the proposed IPMSM drive at 100 rad/s speed and no load condition. It is seen from this figure that the actual phase current very closely follows the command current. Steady state actual phase-a and phase-b current waveforms at the same speed and load condition are shown in Fig. 4.14 where phase-a current leads phase-b current by 120°.

Chapter 5

Conclusion

The interior permanent magnet synchronous motor (IPMSM) is arguably the best choice for high performance variable speed drives (HPVSD). But its precise speed and torque control appear to be a complex task for researchers due to nonlinear coupling among its winding currents and the rotor speed, as well as the nonlinearity present in the electromagnetic developed torque because of magnetic saturation of the rotor core. The most tangible option for researchers is to employ simple fixed gain PI, PID controllers which provide good steady state performance but suffer from poor dynamic performance, sensitivity to parameter variations and occasional instability. Meanwhile, the conventional adaptive controllers require complex circuitry for real-time implementation. Artificial intelligent controllers like fuzzy, neural network, neuro-fuzzy controllers are good options in this case because they are capable of handling nonlinear systems without much knowledge of the system model and also they yield better transient speed response. But most often, researchers overlook the possibility of simultaneous torque ripple control while achieving better dynamic speed response. So in this thesis, a new IPMSM drive has been proposed with a combined approach of optimizing torque ripple and achieving better dynamic speed performance over a wide speed range.

The review of different types of electric motors with various control techniques has been provided in the first chapter. Relevant previous works have been studied and discussed thoroughly to identify the drawbacks of the existing methods. Then the

research motivation is described and the choice of the research topic is explained. In the second chapter, the mathematical model of IPMSM is developed using Park's transformation equations which has been followed in the rest of the work. Then based on the motor model, the closed loop vector control strategy of IPMSM is also discussed.

The detailed step by step design and development of the proposed closed loop vector control scheme has been provided in the third chapter. Two fuzzy logic controllers have been employed in the proposed scheme. At the beginning of the chapter, a brief review on fuzzy logic theory has also been provided. Then the conventional fixed band hysteresis PWM current controller working principle has been described. In order to improve the performance of the conventional hysteresis controller, an FLC based hysteresis band adaptation scheme has been developed and explained. Then a new fuzzy tuned PI controller has been developed for achieving better dynamic speed performance. A flux controller has also been incorporated in this scheme for wide speed range operation and its mathematical formulae have been explained with discussion of different IPMSM operating regions including flux weakening operation. Finally a simulation model for the proposed drive has been developed using Matlab/Simulink. The performance of the proposed drive has been thoroughly investigated at different dynamic speed, load and parameter change conditions. The simulation results have also been compared with those of a fixed gain PI controller based drive. The comparison results prove the superiority of the proposed drive over conventional PI based drive.

The fourth chapter provides the details of real-time implementation of the proposed drive described in the third chapter. The proposed drive has been implemented in real-time using DSP controller board DS1104 for a laboratory 5 HP IPMSM. The lab

experimental setup has been described and both hardware implementation and software development have been discussed. Then the real-time Simulink model of the proposed drive has been developed and real-time experiments have been performed. Experimental results for the proposed drive have been provided and compared with conventional fixed gain PI based drive in order to verify the feasibility and effectiveness of the proposed drive.

5.1 Major Contributions of this Thesis

The major contributions of this thesis can be discussed as follows:

- A Mamdani type fuzzy logic controller (FLC) has been designed to minimize developed torque ripple of the IPMSM by varying online the hysteresis band limits of the PWM current controller on the basis of q-axis current error.
- A Sugeno type FLC has been developed to tune the parameters of a PI controller online which consequently serves as the speed controller. Thus an attempt has been made to combine the advantages of both fixed gain and artificial intelligent controllers. The proposed hybrid speed controller exhibits very good dynamic and steady state speed performance.
- The two proposed controllers mentioned above have been combined in the same IPMSM drive to achieve better torque and speed responses simultaneously.
- A flux controller has also been incorporated successfully in the proposed scheme to widen the drive's operating speed range.

5.2 Future Work

In this work, the PI speed controller parameters have been tuned by a Sugeno type FLC. In future instead of tuning by FLC, an improved neuro-fuzzy controller (NFC) can be employed as the speed controller to achieve even better dynamic speed performance. Attempt can be also made to implement and operate that NFC based drive with sampling frequency higher than 5kHz which is the frequency used in this work. Moreover, some speed ripple has been visible in real-time results though it has not been encountered in simulation results. To eliminate that speed ripple by hardware control or by using any improved algorithm can be a significant extension of this work.

In case of the first hysteresis band adaptation FLC, change of current error (Δd_{iq}) can be employed as an additional input variable to make the FLC more effective and meaningful.

Minimum number of membership functions has been used for input variables of the PI tuning FLC in order to avoid computational burden. But may be it is advisable to add one more membership function for Δe variable to make the fuzzy inference more flexible.

Though both torque and speed performances are considered in this work, loss minimization or efficiency optimization of the IPMSM drive is not discussed here. This work may also be extended to verify its loss minimization capability or additional algorithm or controller may be added in the scheme to improve the drive's efficiency as well as retaining better torque and speed performance.

References

[1] Ervan G. Garrison, *A History of Engineering and Technology*, CRC Press, 1998.

[2] Petar Miljanic, "Tesla's Polyphase System and Induction Motor," *Record of 6th International Symposium Nikola Tesla*, Oct. 18-20, 2006, Belgrade, Serbia.

[3] S. J. Chapman, *Electric Machinery Fundamentals*, New York, NY: McGraw-Hill, 1999.

[4] B. L. Theraja and A. K. Theraja, *A Textbook of Electrical Technology in S.I. Units Volume II: AC & DC Machines*, New Delhi: S. Chand & Co. Ltd., 2001.

[5] A. F. Puchstein, T. C. Lloyd and A. G. Conrad, *Alternating Current Machines*, John Wiley & Sons, 3rd Edition, 1949.

[6] J. F. Gieras and M. Wang, *Permanent Magnet Motor Technology*, New York, NY: Marcel Dekker Inc., 2002.

[7] R. S. Colby, "Classification of Inverter Driven Permanent Magnet Synchronous Motor**s,"** *Conference Record of IEEE Industry Applications Society Annual Meeting,* Oct. 2-7, 1988, vol. 1, pp 1-6.

[8] Bimal K. Bose, *Modern Power Electronics and AC Drives*, Upper Saddle River, NJ: Prentice Hall, 2002.

[9] *Super Energy Saving Variable Speed Drives Manual*, Literature No. KAE-S686-15D, Yaskawa Electric Inc.

[10] R. H. Park, "Two Reaction Theory of Synchronous Machines: Generalized Method of Analysis Part I**,"** *AIEE Transactions,* vol. 52, June 1993, pp 352-355.

[11] Muhammad H. Rashid, *Power Electronics: Circuits, Devices and Applications*, Prentice Hall, 1988.

[12] T. H. Liu, C. M. Young and C. H. Liu, "Microprocessor Based Controller Design and Simulation of Permanent Magnet Synchronous Motor Drive," *IEEE Trans. on Industrial Electronics,* vol. 35, no. 4, Nov. 1988, pp 516-523.

[13] B.K. Bose, P.M. Szczesny, "A Microcomputer-Based Control And Simulation of an Advanced IPM Synchronous Machine Drive System for Electric Vehicle Propulsion," *IEEE Trans. on Industrial Electronics*, vol. 35, no. 4, Nov. 1988, pp 547–559.

[14] B.K. Bose, "A High Performance Inverter Fed Drive System of an Interior Permanent Magnet Synchronous Machine." *IEEE Trans. on Industry Applications,* vol. IA-24, no. 6, 1988, pp 987–997.

[15] P. Pillay and R. Krishnan, "Modelling of Permanent Magnet Motor Drives," *IEEE Trans. on Industrial Electronics*, vol. 35, no. 4, Nov. 1988, pp 537–541.

[16] P. Pillay and R. Krishnan, "Modelling, Simulation and Analysis of Permanent Magnet Motor Drives, Part I: The Permanent Magnet Synchronous Motor Drive," *IEEE Trans. on Industry Applications*, vol. 25, no. 2, March/April 1989, pp 265–273.

[17] P. Pillay and R. Krishnan, " Modelling, Simulation and Analysis of a High Performance Vector Controlled Permanent Magnet Synchronous Motor Drive," *IEEE/IAS Annual Meeting Conference Record*, 1987, pp 253–261.

[18] P. Pillay and R. Krishnan, "Control Characteristics and Speed Controller Design for High Performance Permanent Magnet Synchronous Motor Drive," *IEEE Trans. on Power Electronics*, vol. 5, no. 2, April 1990, pp 151–159.

[19] T. M. Jahns, “Flux-Weakening Regime operation of an Interior Permanent Magnet Synchronous Motors Drive,” *IEEE Transactions on Industrial Applications,* vol. IA-23, no. 4, 1987, pp 681–689.

[20] S.R. Macminn, T.M. Jahns, "Control Techniques for Improved High-Speed Performance of Interior PM Synchronous Motor Drives," *IEEE Transactions on Industry Applications,* Vol. 27, No. 5, Sept.-Oct. 1991, pp. 997 – 1004.

[21] T. M. Jahns, G. B. Kliman and T. W. Neumann, “Interior Permanent Magnet Synchronous Motors for Adjustable Speed Drives,” *IEEE Transactions on Industry Applications*, Vol. IA-22, No. 4, July-Aug. 1986, pp. 738-747.

[22] S. Morimoto, M. Sanada And Y. Takeda, “Effects and Compensation of Magnetic Saturation in Flux-Weakening Controlled Permanent Magnet Synchronous Motor Drives,” *IEEE Transactions on Industry Applications*, Vol. 30, No. 6, Nov./Dec. 1994, pp. 1632-1637.

[23] R. Krishnan, "Control and Operation of PM Synchronous Motor Drives in the Field Weakening Region," *IEEE/IECON’93 Conference Record, Hawaii*, 1993, pp 745–750.

[24] R. Dhanuadi and N. Mohan, “Analysis of Current-Regulated Voltage Source Inverters for Permanent Magnet Synchronous Motor Drives in Normal and Extended Speed Range,” *IEEE Transactions on Energy Conversion*, Vol. 5, No. 1, March 1990, pp. 137-147.

[25] A. Kumamoto and Y. Hirame, "A Flux-Weakening Method for a Buried Permanent Magnet Motor with Consideration of Parameter Detuning on System Performance," *IPEC Conference Record, Tokyo, Japan*, 1990, pp 950–955.

[26] T. S. Radwan, M. A. Rahman, A. M. Osheiba and A. E. Lashine, "Performance of a Hybrid Current-Controlled VSI Permanent Magnet Synchronous Motor Drive," *IEEE/PESC Conference Record,* 1996, pp 951–957.

[27] M. Kadjoudj, M.E.H. Benbouzid, C. Ghennai, D. Diallo, "A Robust Hybrid Current Control for Permanent-Magnet Synchronous Motor Drive," *IEEE Transactions on Energy Conv.,* Vol. 19, No. 1, March 2004, pp.109 – 115.

[28] C. Mademlis, V.G. Agelidis, "A High-Performance Vector Controlled Interior PM Synchronous Motor Drive with Extended Speed Range Capability," *Annual Conference of IEEE Industrial Electronics Society,* 29 Nov.-2 Dec. 2001, Vol. 2, pp.1475 – 1482.

[29] Ting-Yu Chang, Ching-Tsai Pan, J.H. Liaw, S.M. Sue, "A Hall-Sensor-Based IPM Traction Motor Drive," *Proceedings of The IEEE International Symposium on* Industrial Electronics, 26-29 May, 2002, Vol. 3, pp.840 – 843.

[30] I. Choy, T. Yoon, K. Kim and M. Park, "Microprocessor based Permanent Magnet Synchronous Motor Drives using MRAC," *IPEC Conference Record, Tokyo, Japan*, 1990, pp. 481-488.

[31] Y. Sozer and D. A. Torrey, "Adaptive Flux Weakening Control of Permanent Magnet Synchronous Motors," *IEEE/IAS Annual Meeting Conference Record*, 1998, pp. 475-482.

[32] C. Namudri and P. C. Sen, "A Servo-Control System using a Self-Controlled Synchronous Motor (SCSM) with Sliding Mode Controller," *IEEE/IAS Annual Meeting Conference Record*, 1987, pp. 283-295.

[33] A. Consoli and Antonio, "A DSP Based Sliding Mode field oriented control of an interior permanent magnet synchronous motor drive," *IPEC Conference record, Tokyo, Japan*, 1990, pp. 263-303.

[34] R. B. Sepe and J. Lang, "Real-time Observer-based (Adaptive) Control of a Permanent Magnet Synchronous Motor without Mechanical Sensors," *IEEE Transactions on Industry Applications,* vol. 28, no. 6, pp. 1345-1352, Nov./Dec. 1992.

[35] F. J. Lin and Y. S. Lin, "A Robust PM Synchronous Motor Drive with Adaptive Uncertainty Observer," *IEEE Transactions on Energy Conversion*, 1999, vol. 14, no. 4, pp 989-995.

[36] S. Brock, J. Deskur, and K. Zawirski, "Robust Speed and Position Control of PMSM," *in Proc. IEEE International Symposium on Industrial Electronics*, vol. 2, 1999, pp. 667-672.

[37] B. Zhang and Y. Li, "A PMSM Sliding Mode Control System Based on Model Reference Adaptive Control," *in Proc. PIEMC Power Electronics and Motion Control Conference*, vol. 1, 2000, pp. 336-341.

[38] Y. Tang and L. Xu, "Fuzzy Logic Application for Intelligent Control of a Variable Speed Drive," *IEEE Transactions on Power Electron*., Vol.12, Nov. 1997, pp. 1028-1039.

[39] M N Uddin and M A Rahman, "Fuzzy Logic Based Speed Control of an IPM Synchronous Motor Drive," *Journal of Advanced Computational Intelligence*, Vol. 4, No. 3, 2000, pp. 212-219.

[40] C. Butt, M.A. Hoque, M.A. Rahman, "Simplified Fuzzy Logic Based MTPA Speed Control of IPMSM Drive," *IEEE Transactions on industry applications,* 2004, Vol. 40, No.6, pp. 1529– 1535.

[41] M. N. Uddin, M. A. Abido and M. A. Rahman, "Real-Time Performance Evaluation of a Genetic Algorithm Based Fuzzy Logic Controller for IPM Motor Drives," *IEEE Transactions on Industry Applications*, Vol. 41, No. 1, Jan./Feb. 2005, pp. 246-252.

[42] S Bolognani and M. Zigliono, "Fuzzy Logic Control of a Switched Reluctance Motor Drive,'' *IEEE Transactions on Industry Applications*, Vol. 32, No. 5, Sept./Oct. 1996, pp. 1063-1068.

[43] Yang Yi, D.M. Vilathgamuwa, M.A. Rahman, "Implementation of an Artificial-Neural-Network-Based Real-Time Adaptive Controller for an Interior Permanent-Magnet Motor Drive," *IEEE Transactions on Industry Application,* Vol. 39, No. 1, Jan.-Feb. 2003, pp. 96 – 104.

[44] M. A. Rahman and M.A. Hoque, "On-Line Adaptive Artificial Neural Network Based Vector Control of Permanent Magnet Synchronous Motors," *IEEE Transactions on Energy Conversion,* Vol. 13, No. 4, 1998, pp. 311-318.

[45] N. Urasaki, T. Senjyu, K. Uezato, "Neural Network Based High Efficiency Drive for Interior Permanent Magnet Synchronous Motors Compensating EMF Constant Variation," *Power Conversion Conference, Osaka, Japan,* April 2002, Vol. 3, pp. 1273 - 1278 .

[46] B.N. Mobarakeh, F. Meibody-Tabar, F.M. Sargos, "A Self Organizing Intelligent Controller for Speed and Torque Control of a PMSM," *IEEE Conference on Industry Applications,* 8-12 Oct., 2000, Vol. 2, pp. 1283 – 1290.

[47] M. N Uddin. M A Abido and M. A Rahman, “Development and Implementation of a Hybrid Intelligent Controller for Interior Permanent Magnet Synchronous Motor Drive,” *IEEE Transactions on Industry Applications*, Vol. 40, No. 1, Jan./Feb. 2004, pp. 68-76.

[48] C. T. Lin, “A neural fuzzy control system with structure and parameter learning,” *Fuzzy Sets Syst.*, vol. 70, 1995, pp. 183–212.

[49] Faa-Jeng Lin,Chih-Hong Lin, and Po-Hung Shen, "Self-Constructing Fuzzy Neural Network Speed Controller for Permanent-Magnet synchronous Motor Drive," *IEEE Transactions on Fuzzy Systems*, Vol. 9, No. 5, Oct. 2001, pp. 751 – 759.

[50] M. Chiaberge, G. Di Bene, S. Di Pascoli, B. Lazzerini, A. Maggiore, L.M. Reyneri, “An Integrated Hybrid Approach to the Design of High-Performance Intelligent Controllers,” *International IEEE/IAS Conference on Industrial Automation And Control: Emerging Technologies,* 22-27 May, 1995, pp.436 – 443.

[51] C. Vlachos, D. Williams and J. B. Gomm, “A genetic approach to decentralized PI controller tuning for multivariable processes,” *IEE Proc. Control Theory Appl.,* vol. 146, no.1, pp.58-64, 1999.

[52] A. Uchikata and Y. Ohnishi, “A Tuning method of Nonlinear PI controllers by using RBFN,” *in Proc. of 2009 IEEE International Conference on Networking, Sensing and Control,* Okayama, Japan, March 26-29, pp 735-739.

[53] X. Zhou, X. Dong, Y. Zhang, Y. Fang, “Automatic Tuning of PI Controller for Atomic Force Microscope Based on Relay with Hysteresis,” *in Proc. of 18th IEEE International Conference on Control Applications, Petersburg, Russia,* July 8-10, 2009, pp 1271-1275.

[54] K. Cheung and L. Wang, "Fuzzy System Tuned PI Controller for a Benchmark Drum-Boiler Model," *in Proc. of the 37th IEEE Conference on Decision & Control, Tampa, Florida, USA,* December 1998, pp 3171-3176.

[55] A. Routray, P. K. Dash, and S. K. Panda, "A Fuzzy Self-Tuning PI Controller for HVDC Links," *IEEE Transactions on Power Electronics*, Vol. 11, No. 5, Sep. 1996, pp. 669-679.

[56] A. Sreenath, Y. R. Atre, D. R. Patil, "Two Area Load Frequency Control with Fuzzy Gain Scheduling of PI Controller," *in Proc. of the 2008 First International Conference on Emerging Trends in Engineering and Technology*, pp 899-904.

[57] M. Abdolmaleki, P. Ansarimehr, A. M. Ranjbar, "A Robust Fuzzy Logic Adaptive PI Controller for Hydro Power Plants," *in Proc. of SICE Annual Conference, Kagawa University, Japan,* Sept. 17-20, 2007, pp 2592-2595.

[58] S. Lee, M. Jeong, B. Jang, C. Yoo, S. Kim, and Y. Park, "Fuzzy Precompensated PI Controller for A Variable Capacity Heat Pump," *in Proc. of IEEE International Conference on Control Applications,* Trieste, Italy, 1-4 September, 1998, pp 953-957.

[59] M. Tursini, F. Parasiliti, and D. Zhang, "Real-Time Gain Tuning of PI Controllers for High-Performance PMSM Drives," *IEEE Transactions on Industrial Applications*, Vol. 38, July/Aug. 2002, pp. 1018–1026.

[60] Seok-Beom Lee, "Closed-Loop Estimation of Permanent Magnet Synchronous Motor Parameters by PI Controller Gain Tuning," *IEEE Transactions on Energy Conversion,* Vol. 21, No. 4, Dec. 2006, pp 863-870.

[61] L. Song and J. Peng, "The Study of Fuzzy- PI Controller of Permanent Magnet Synchronous Motor," *in Proc. of IPEMC '09: IEEE 6th International Power Electronics and Motion Control Conference,* 2009, pp 1863-1866.

[62] S. Hsu, C. Liu, C. Liu, and N. Wang, "Fuzzy PI Controller Tuning for a Linear Permanent Magnet Synchronous Motor Drive," *in Proc. of IECON'01: The 27th Annual Conference of the IEEE Industrial Electronics Society*, 2001, pp 1661-1666.

[63] D. P. Iracleous, A. T. Alexandridis, "Fuzzy tuned PI controllers for series connected DC motor drives," *in Proceedings of the IEEE International Symposium on Industrial Electronics,* 1995, pp 495-499.

[64] A. Hazzab, M. Zerbo, I. K. Bousserhanel, P. Sicard, "Real Time Implementation of Adaptive P1 Controller by Fuzzy Inference for Induction Motor Speed Control," *in Proc. of 2006 IEEE International Symposium on Industrial Electronics,* pp 278-283.

[65] Oyas Wahyunggoro, Nordin Saad, "Evaluations of Fuzzy-Logic-Based Self Tuning PI Controller and Fuzzy-Scheduled PID Controller for DC Servomotor," *in Proc. of International Symposium on Information Technology*, 2008, vol. 4, pp 1-7.

[66] C. Lin, C. Hung, and C. Liu, "Fuzzy PI Controller for BLDC motors Considering Variable Sampling Effect," *in Proc. of the 33rd Annual Conference of the IEEE Indl. Electronics Society (IECON),* Nov. 5-8, 2007, Taipei, Taiwan, pp 1180-1185.

[67] Mukesh Kumar, Bhim Singh, and B. P. Singh, "Fuzzy Pre-compensated PI Controller for PMBLDC Motor Drive," *in Proc. of International Conference on Power Electronics, Drives and Energy Systems (PEDES),* 2006, pp 1-5.

[68] F. Syed, H. Ying, M. Kuang, S. Okubo, M. Smith, "Rule-Based Fuzzy Gain-Scheduling P1 Controller to Improve Engine Speed and Power Behavior in a

Power-split Hybrid Electric Vehicle," *in Proc. of Annual Meeting of the North American Fuzzy Information Processing Society*, 2006, pp 284-289.

[69] S.R.Bowes, S.GrewaI and D.Holliday, "Novel adaptive hysteresis band modulation strategy for three-phase inverters," *IEE Proceedings of Electric Power Applications,* Vol. 148, No. 1, 2001, pp 51-61.

[70] F. Liu and A. Maswood, "A Novel Variable Hysteresis Band Current Control of Three-Phase Three-Level Unity PF Rectifier with Constant Switching Frequency," *IEEE Transactions on Power Electronics*, Vol. 21, No. 6, Nov. 2006, pp. 1727-1734.

[71] Xunjiang Dai, Qin Chao, "The Research of Photovoltaic Grid-Connected Inverter Based on Adaptive Current Hysteresis Band Control Scheme," *in Proc. of International Conference on Sustainable Power Generation and Supply*, 2009, pp.1-8.

[72] M. Kale, E. Ozdemir, "A Novel Adaptive Hysteresis Band Current Controller for Shunt Active Power Filter," *in Proc. of 2003 IEEE Conference on Control Applications*, vol. 2, pp 1118-1123.

[73] Y. Dongmei, G. Qingding, H. Qing, L. chunfang, "A Novel DSP Based Current Controller with Fuzzy Variable-Band hysteresis for Active Power Filters*," in Proc. of Transmission and Distribution Conference and Exhibition: Asia and Pacific, 2005 IEEE/PES, Dalian, China*, pp 1-5.

[74] C. Cecati, S. Corradi, N. Rotondale, "Digital Adaptive Hysteresis Current Control Based on the Fuzzy Logic," *in Proceedings of the IEEE International Symposium on* Industrial Electronics, 1997, vol. 3, pp 1232-1237.

[75] S. K. Sahoo, S. K. Panda, J. X. Xu, "Iterative Learning-based High-performance Current Controller for Switched Reluctance Motors," IEEE Transactions on Energy Conversion, Vol. 19, No. 3, Sept. 2004, pp 491-498.

[76] M.R.Benhadria, K.Kendouci, B.Mazari, "Torque Ripple Minimization of Switched Reluctance Motor Using Hysteresis Current Control," *2006 IEEE International Symposium on Industrial Electronics, Montreal, Canada*, Vol. 3, pp 2158-2162.

[77] S. Kaboli, M. R. Zolgbadri, A. Emadi, "Hysteresis Band Determination of Direct Torque Controlled Induction Motor Drives with Torque Ripple and Motor-Inverter Loss Considerations," *in Proc. of IEEE 34th Annual Power Electronics Specialist Conference*, 2003, vol. 3, pp 1107-1111.

[78] H. I. Okumus, M. Aktas, "Direct Torque Control of Induction Machine Drives Using Adaptive Hysteresis Band for Constant Switching Frequency," *in Proc. of IEEE International Electric Machines & Drives Conference,* 2007, vol. 2, pp 1762-1767.

[79] C. B. Jabeur-Seddik, F. Fnaiech, "Hysteresis and Fuzzy Based Nonlinear Controllers for a Direct Torque Control of an Induction Machine," *in Proc. of IEEE International Conference on Industrial Technology,* 2004, vol. 1, pp 38-43.

[80] P. Zhou, M. A. Rahman, M. A. Jabbar, "Field circuit analysis of permanent magnet synchronous motors," *IEEE Transactions on Magnetics,* Vol. 30, No. 4, Part 2, Jul. 1994, pp. 1350 – 1359.

[81] P. C. Krause, *Analysis of Electric Machinery*, McGraw-Hill Inc., 1986.

[82] M. N. Uddin and M. A. Rahman, "High Speed Control of IPMSM Drives Using Improved Fuzzy Logic Algorithms," *IEEE Transactions on Industry Applications*, Vol. 54, No. 1, Feb. 2007, pp. 190-199.

[83] M. Nasir Uddin and Ronald S. Rebeiro, "Performance of FLC Based Online Adaptation of Both Hysteresis and PI Controllers for IPMSM Drive," *IEEE/IAS Annual Meeting Conference Record*, Houston, TX, USA, October 3-7, 2010.

[84] L. A. Zadeh, "Outline of a new approach to the analysis of complex system and decision processes,", *IEEE Transactions on System, Man and Cyber*, vol. SMC-3, 1973, pp.28-44.

[85] T. Takagi and M. Sugeno, "Fuzzy Identification of Systems and its Applications to Modeling and Control,", *IEEE Transactions on System, Man and Cyber*, vol. 15(1), 1985, pp.116-132.

[86] *Matlab, Simulink User Guide*, The Math Works Inc., 2004.

[87] *dSPACE*, "*Digital Signal Processing and Control Engineering,*" Implementation Guide, Paderborn, Germany, 2003.

Appendix A

Lab IPMSM Parameters:

(for both simulation and real-time experiment)

Number of phases = 3

Number of poles = 6

Rated Frequency = 87.5 Hz

Rated power = 5 HP

Rated Speed = 1750 rpm (183 rad/s)

Rated input line-to-line voltage = 183 V

Rated current = 14.2 A

Rated Torque = 19.1 N-m

q-axis inductance, L_q = 6.42 mH

d-axis inductance, L_d = 5.06 mH

Stator resistance per phase, r_s = 0.242 Ω

*Rotor inertia constant, J = 0.0133 kg-m^2

*Friction damping constant, B_m = 0.001 N-m/rad/s

Permanent magnet flux linkage, ψ_m = 0.24 Wb

(*Rotor inertia constant and Friction damping constant values mentioned here are only for the IPMSM. They do not include the effect of DC generator load coupled with IPMSM.)

Appendix B

Simulink internal subsystem blocks for the proposed IPMSM drive model

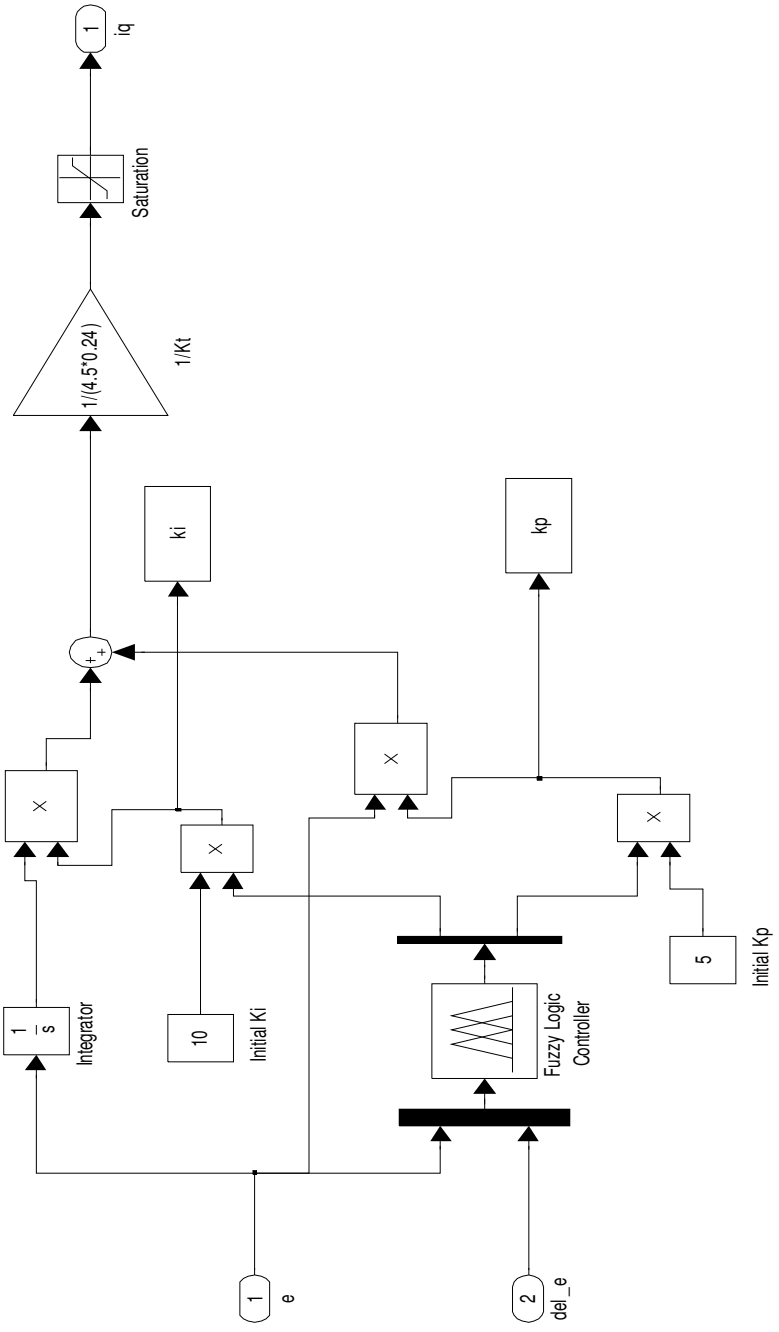

Figure B.1: Speed Controller subsystem (Fuzzy-tuned PI Controller).

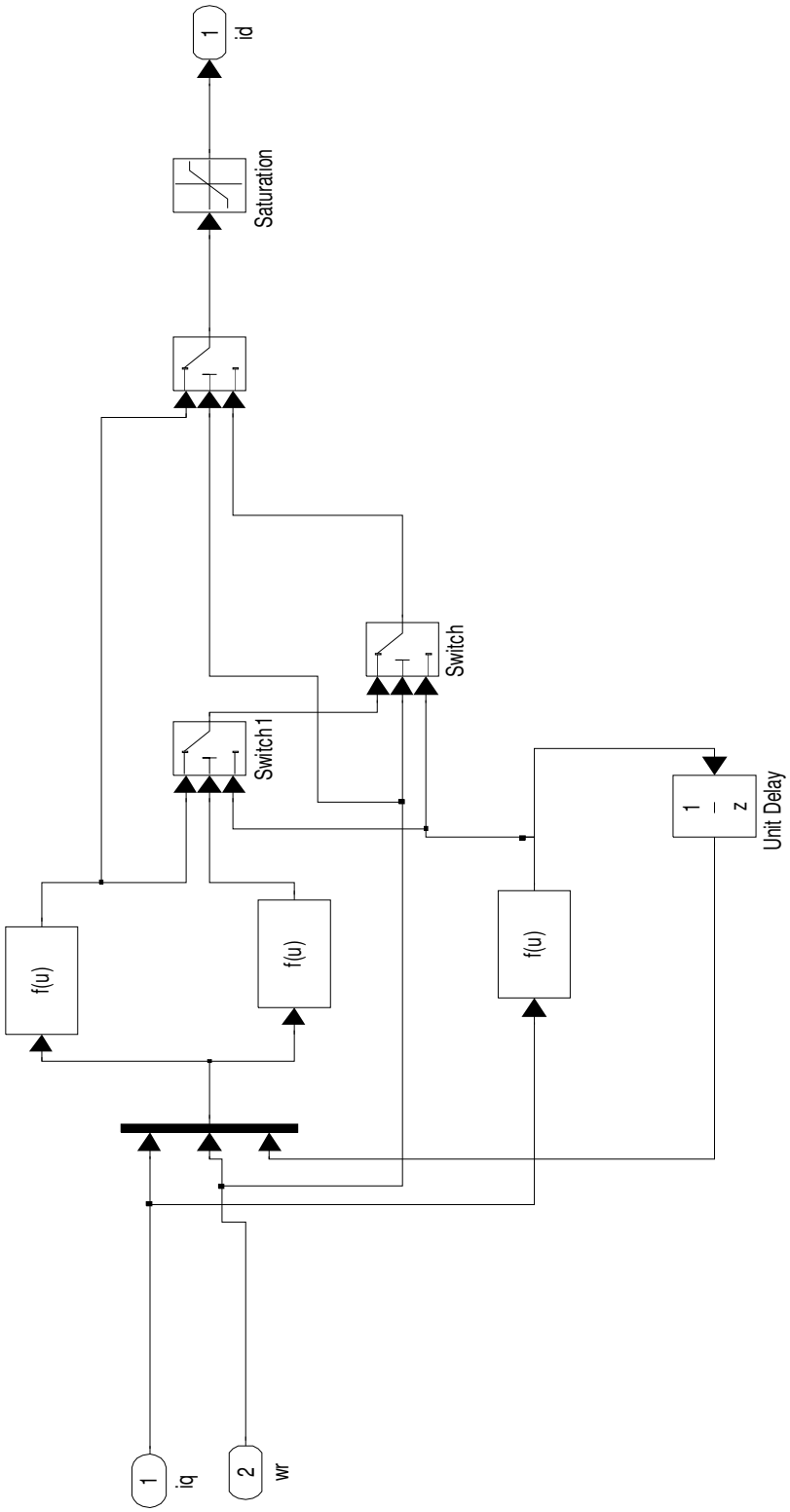

Figure B.2: Flux Controller subsystem.

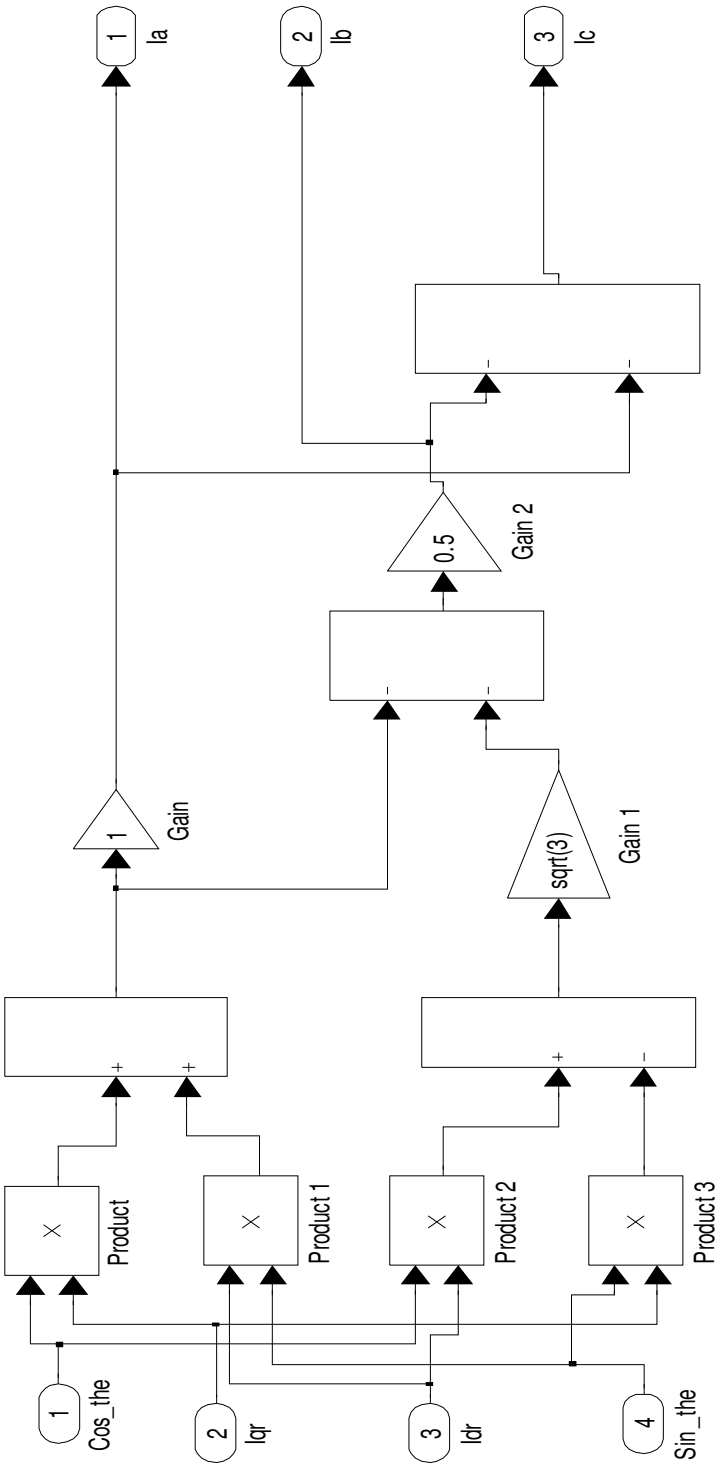

Figure B.3: Vector Rotator subsystem.

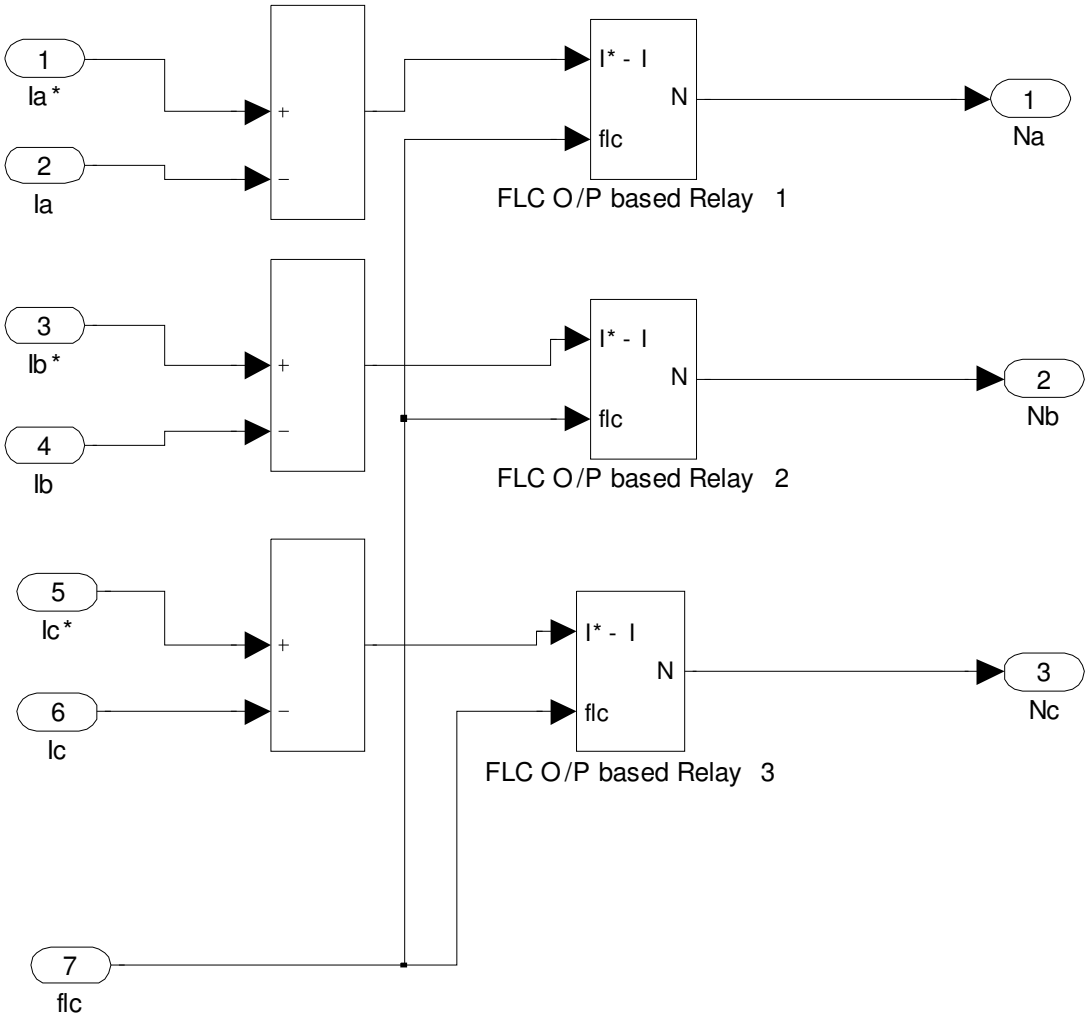

Figure B.4: Hysteresis Current Controller subsystem.

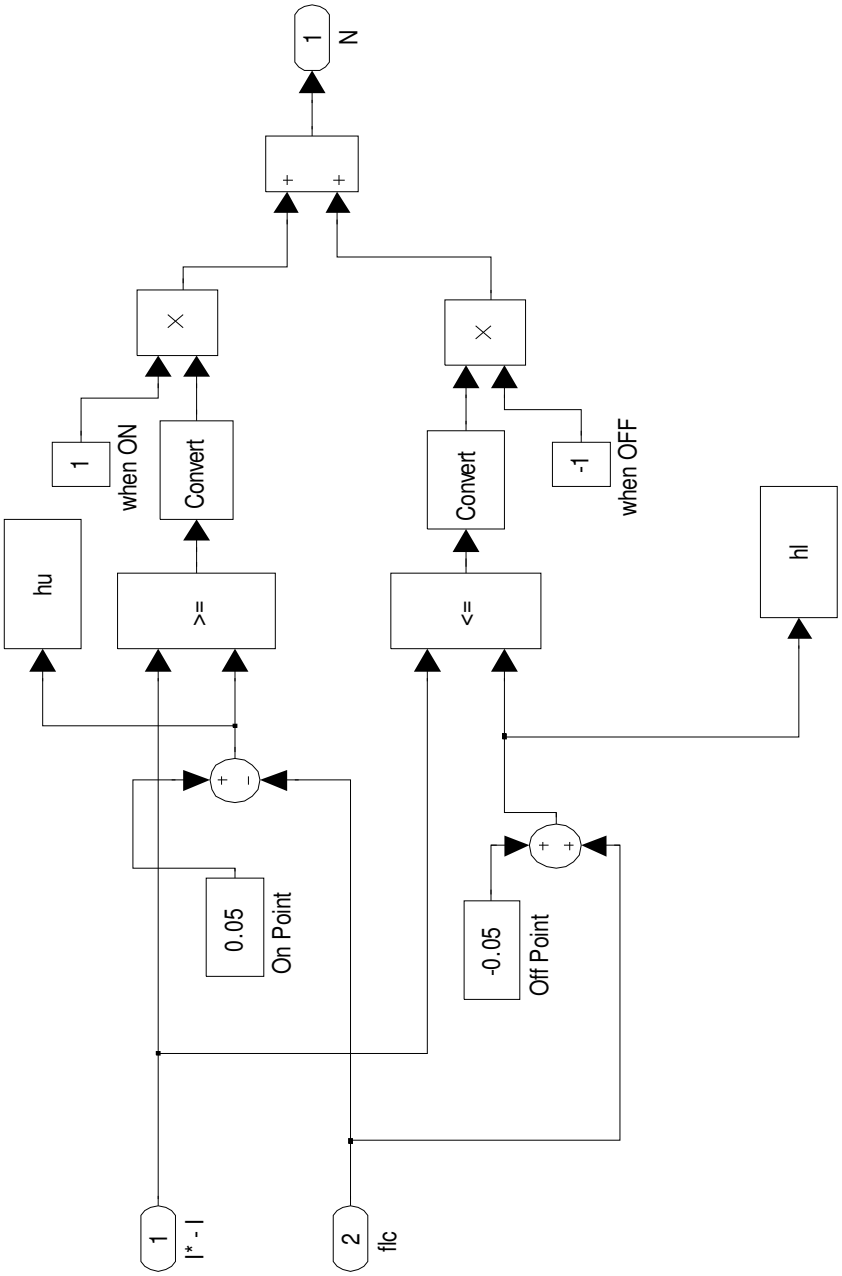

Figure B.5: FLC O/P based Relay subsystem.

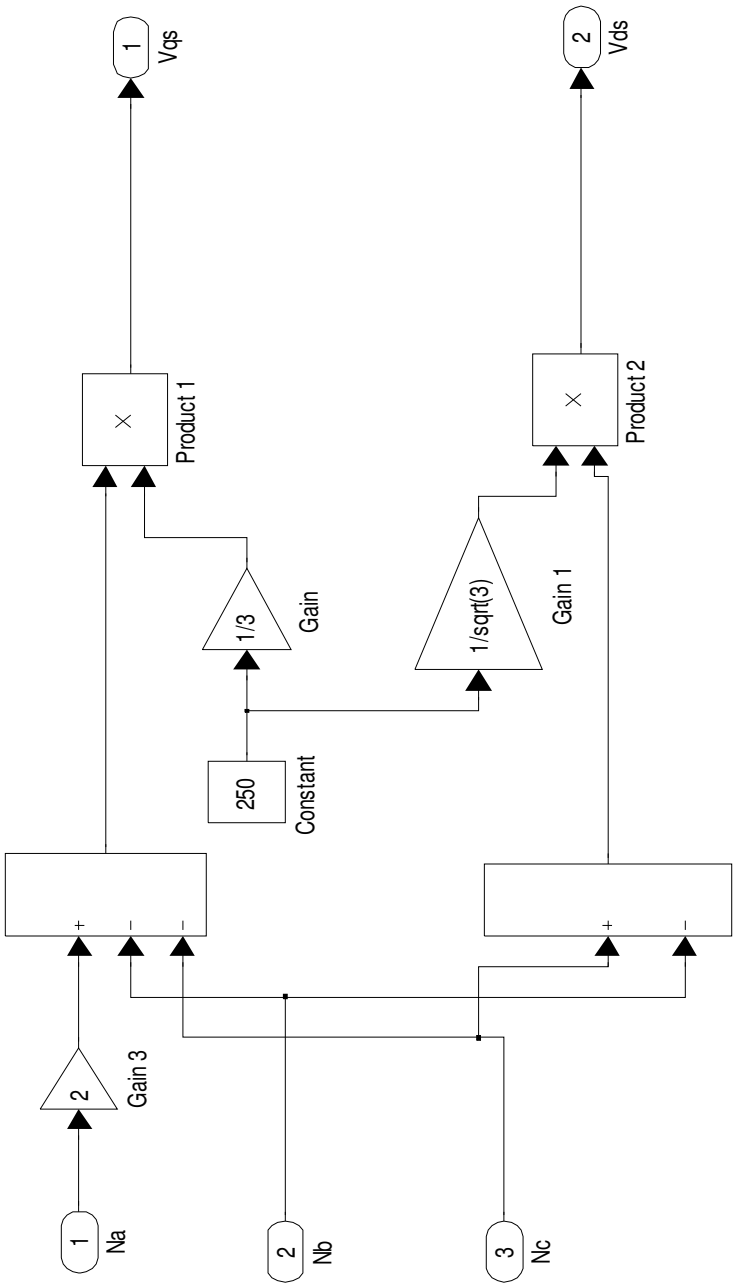

Figure B.6: Inverter subsystem.

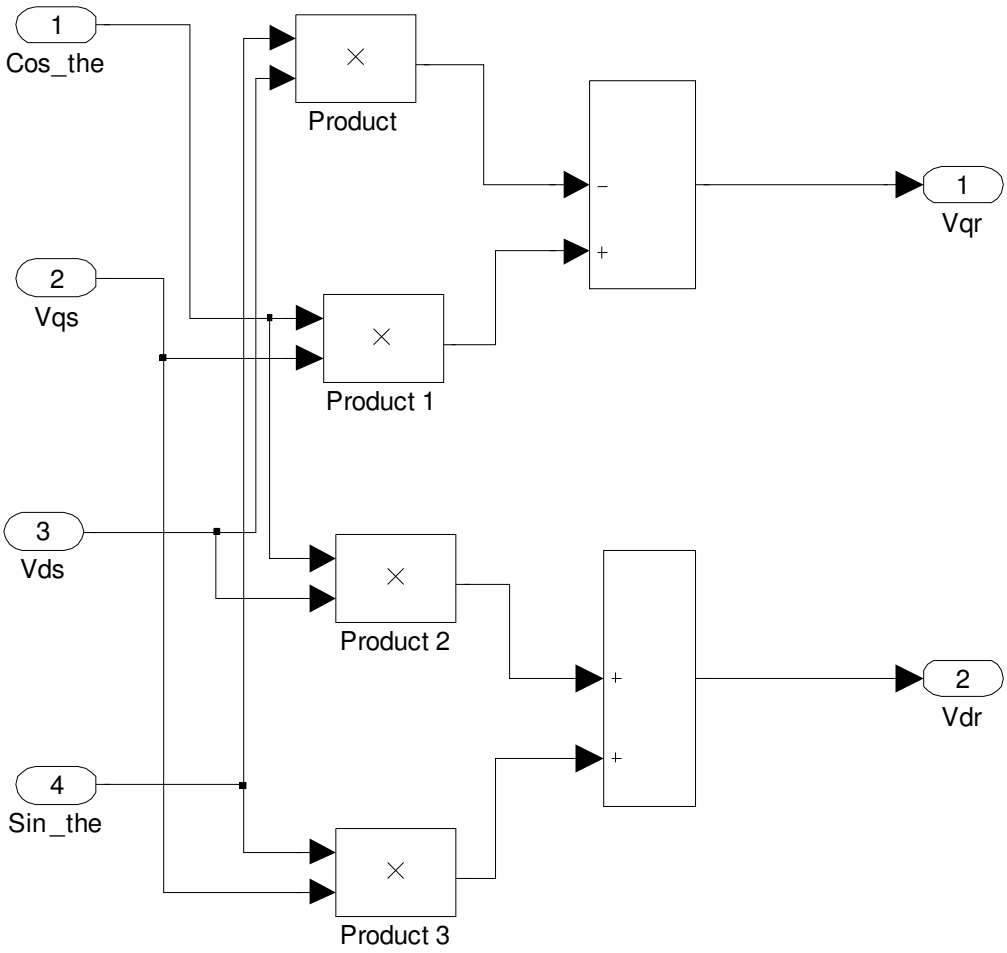

Figure B.7: Coordinate Transformation subsystem.

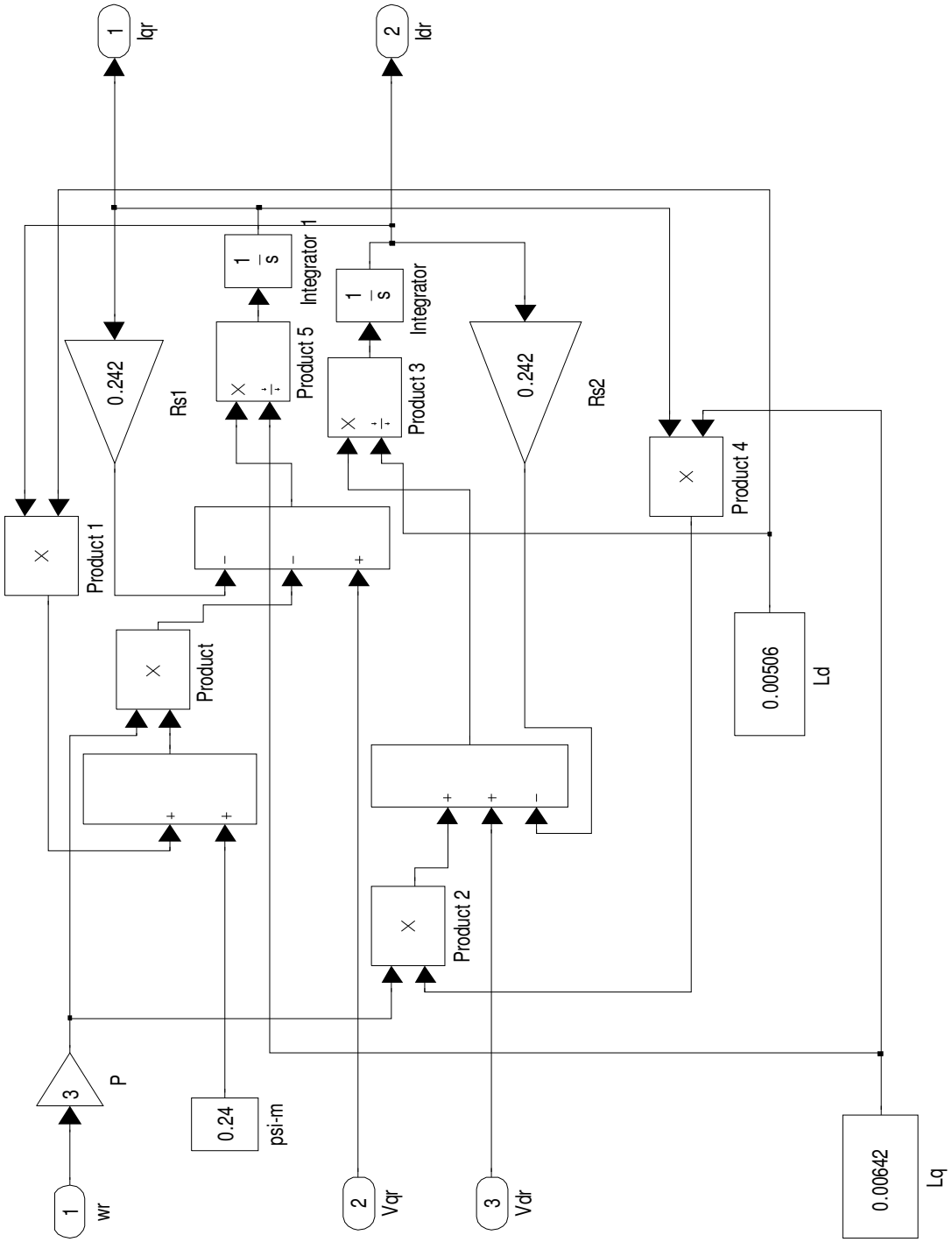

Figure B.8: Current Transformation subsystem.

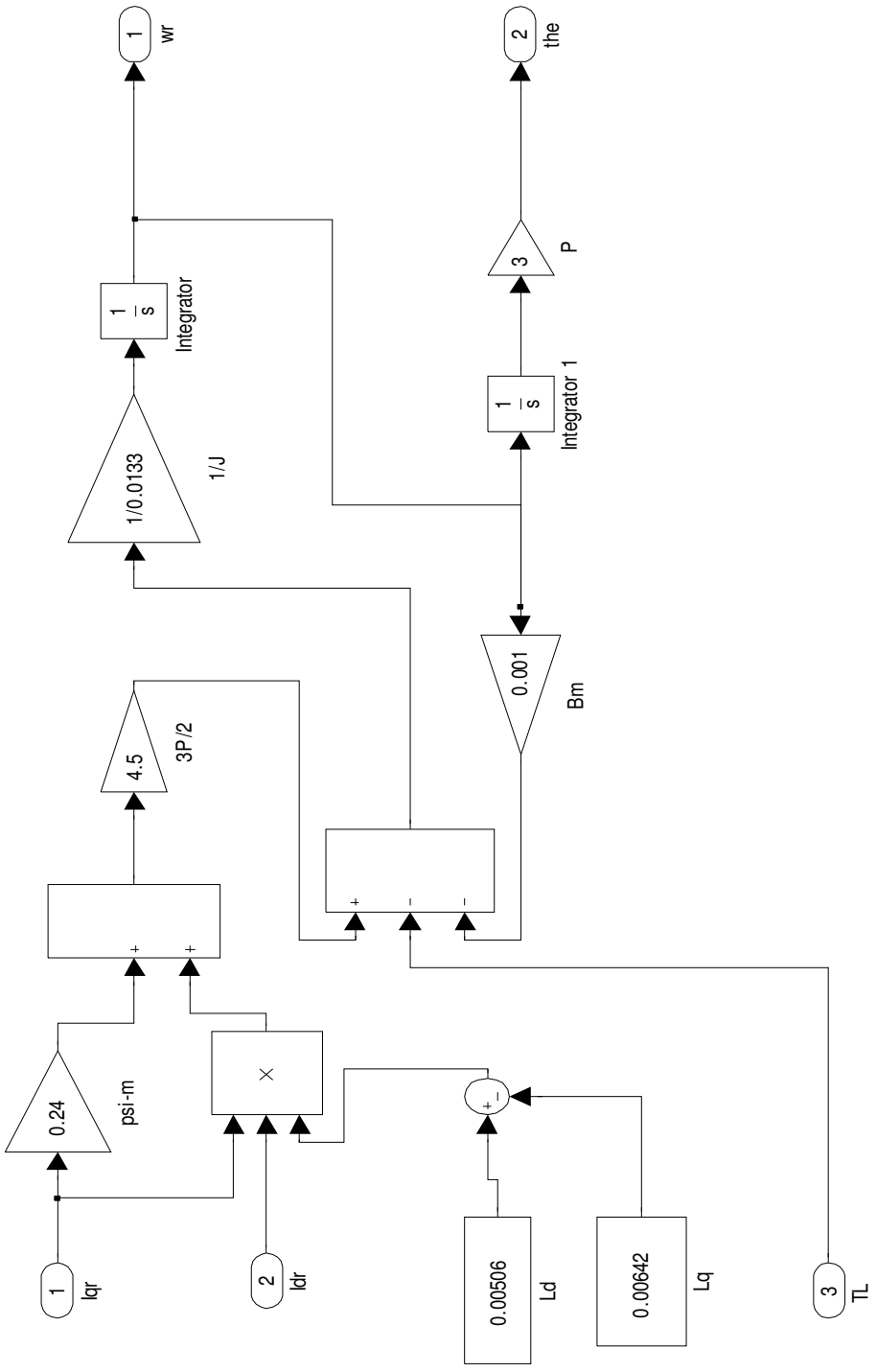

Figure B.9: Motor Output subsystem.

Appendix C

Interface circuits for inverter gate driver and current sensors:

Pull-up resistors, R1= R2 = R3 = R4 = R5 = R6 = 1.5 kΩ

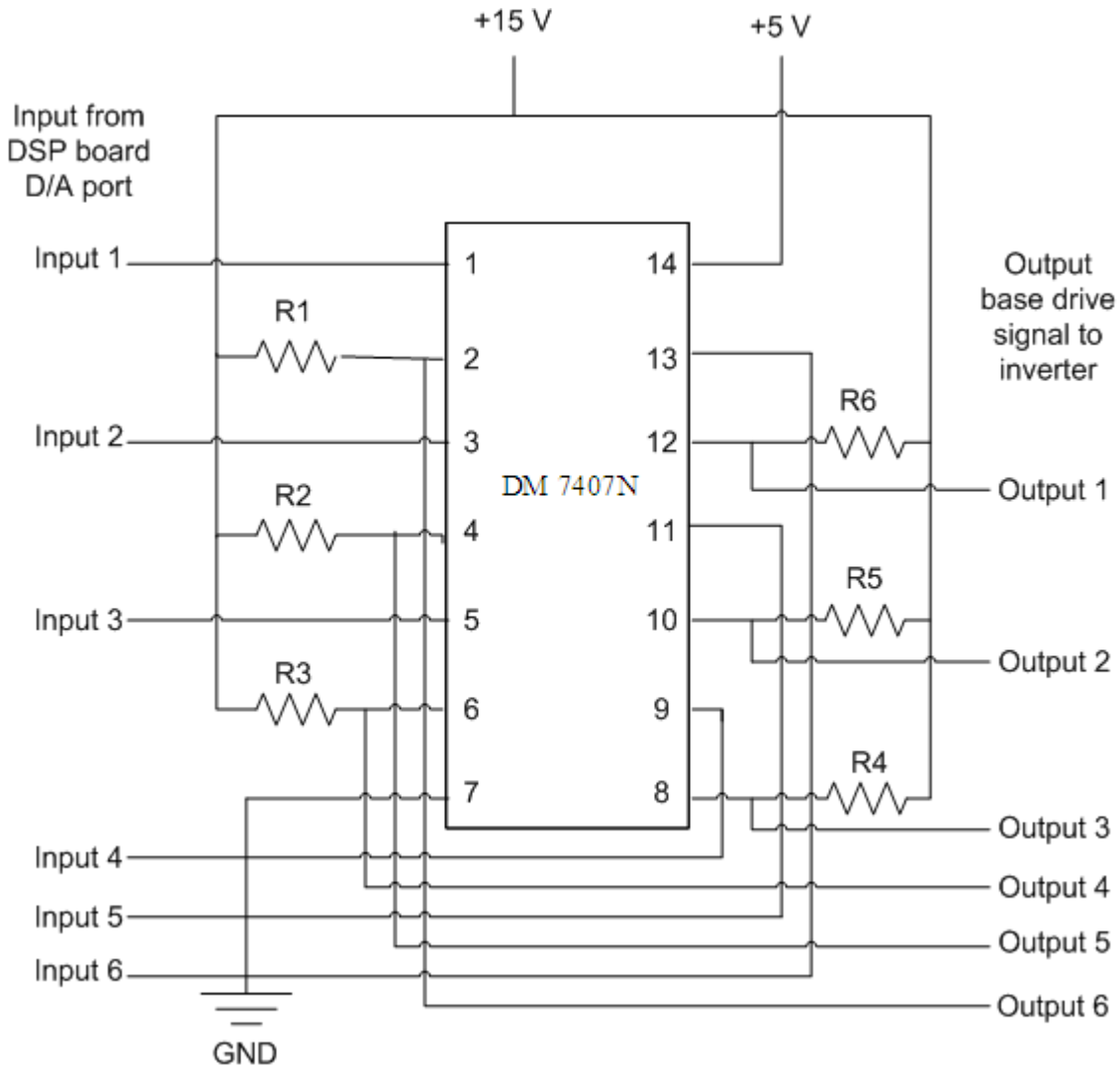

Figure C.1: Interface circuit for inverter gate driver.

Resistors used in the current sensors' interface circuit:

Resistor	Current sensor for phase-a	Current sensor for phase-b
R1	98.6 Ω	98.9 Ω
R2	1.8 kΩ	1.98 kΩ
R3	5.4 kΩ	5 kΩ
	phase-a gain = 4	*phase-b gain = 3.53*

(Op-Amp 741CN Gain = 1+R3/R2)

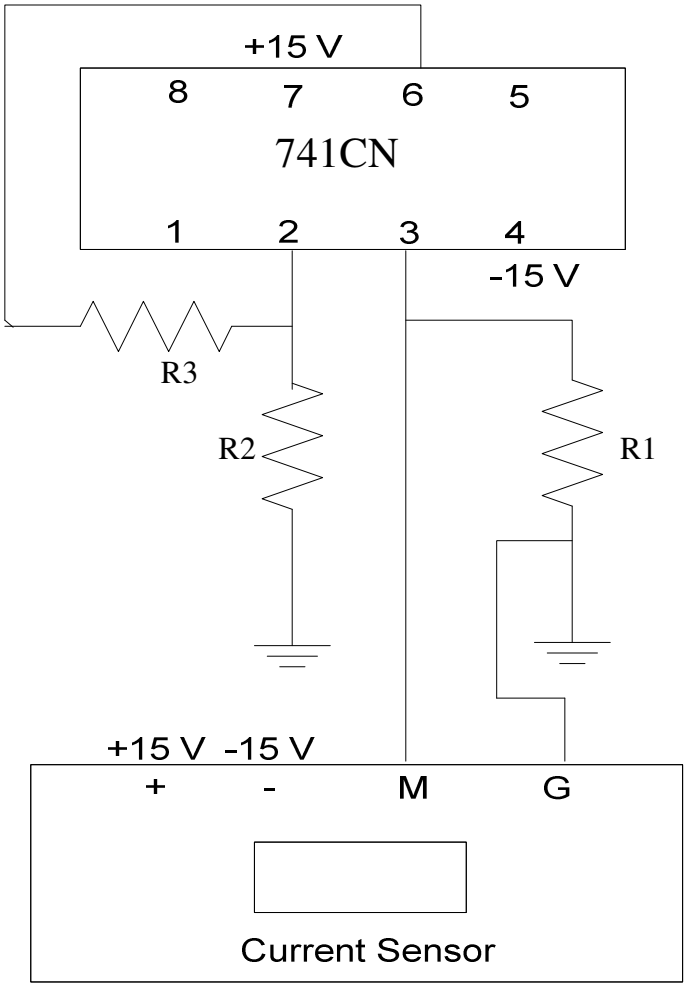

Figure C.2: Interface circuit for the two current sensors with external gains calculation.

Appendix D
Real-Time Simulink Model

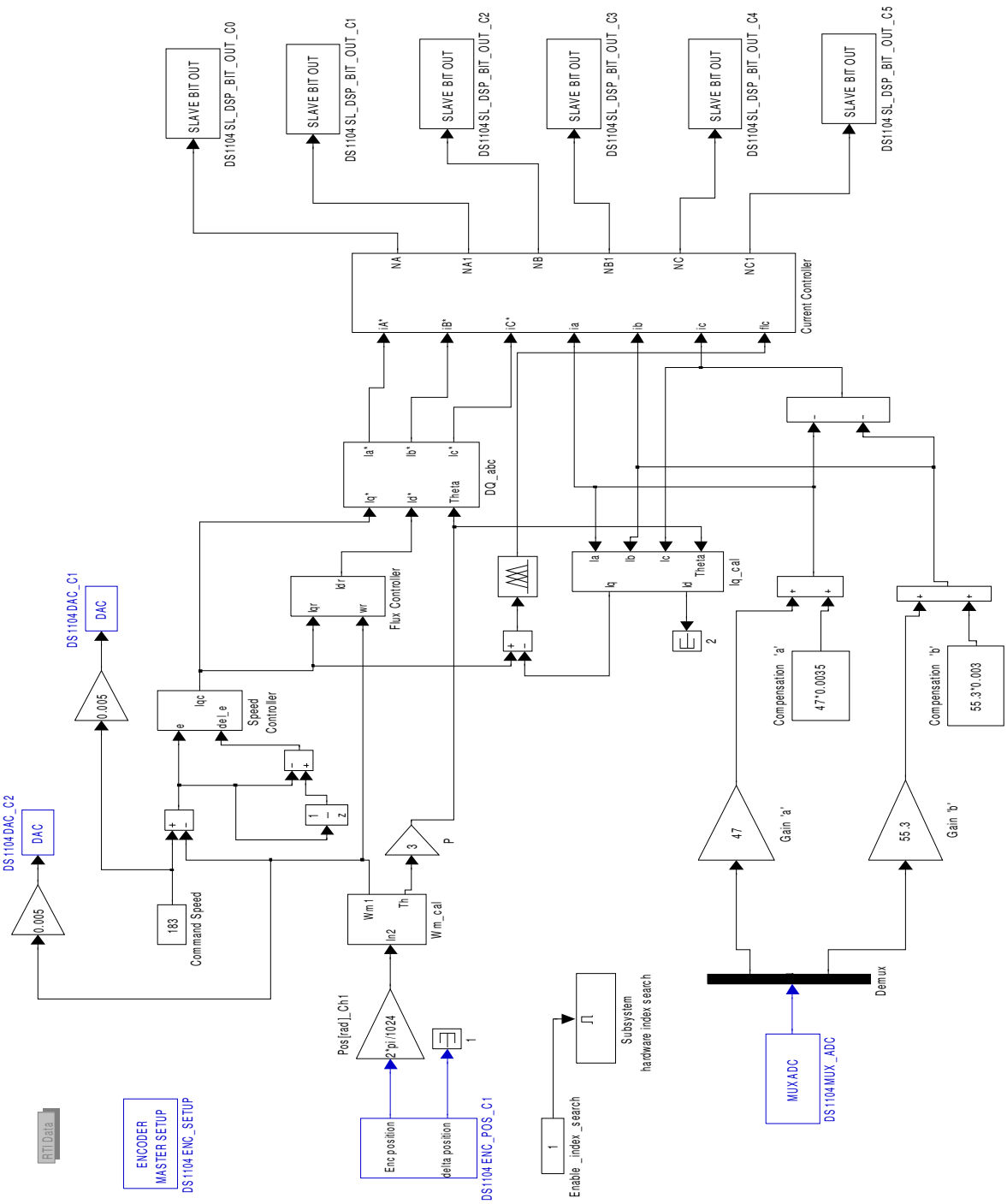

Figure D.1: Real-time Simulink model of the proposed IPMSM drive system.